Bridge Damage Identification Using Vehicle Response(Dissertation_全文)

AUTHOR(S):

Yamamoto, Kyosuke

Bridge Damage Identification Using Vehicle Response

Kyosuke Yamamoto

2012

BRIDGE DAMAGE IDENTIFICATION USING VEHICLE RESPONSE

BY

KYOSUKE YAMAMOTO

JULY, 2012

A dissertation submitted to Graduate school of engineering, Kyoto University
in partial fulfillment of requirements for the degree of Doctor of Engineering

Abstract

To perform efficient maintenance and assessment for a vast number of bridges at one time, bridge screening technology is required. A bridge which has damage with higher ratio should be given a priority for an inspection by screening than others. This study scopes bridge health monitoring (BHM) technologies only by using vehicle responses for damage identification. The bridge health can be evaluated roughly but quickly during the vehicle travelling through the bridge. Sensors are installed only on the vehicle. This dissertation calls this kind of methods only-Vehicle-data-Oriented BHM (VO-BHM) method. In this study, damage identification method based on new three VO-BHM methods are proposed and verified numerically and experimentally.

The first proposed method is curvature-based VO-BHM method. Wavelet coefficient of vehicle acceleration response is a non-linear function of the bridge curvature which is sensitive to local damage.

The second proposed method is indirect Mode-Shape-based VO-BHM method. This method insists in five steps: Estimation of input vibration of the vehicle, extracting of bridge response components, canceling of moving observer effect, mode decomposition and damage identification. In this method, the non-linear problem of vehicle-bridge interaction (VBI) system is handled by interpolation function matrix. In this method, to estimate the bridge mode shape, bridge vibrations are estimated, first. There are many uncertainties which affect the results in each step. However, the required estimation accuracy is always higher than obtained, because the bridge mode shape changes very slightly even after serious damage occurs.

The last proposed method is direct Mode-Shape-based VO-BHM method. In this method, interpolation is directly applied to vehicle acceleration responses. In this method, although the estimation accuracy of mode shape is still low, the performance for damage detection is superior to the other methods. To estimate mode shape, singular value decomposition is applied to preprocessed signals. Only this method can detect bridge damage from data measured in a field experiment.

To verify these three proposed methods, numerical simulation and laboratory and field experiments are performed. Numerical simulation uses rigid-spring model and one-dimensional finite element beam as the vehicle and bridge, respectively. By numerical simulation, the factors which affect estimation are cleared. The Curvature-based and direct Mode-Shape-based proposed methods are verified in laboratory experiment, but the uncertainties such as bumps and road unevenness decrease the damage identification accuracies as a result. On the other hand, only direct Mode-Shape-based VO-BHM method shows high feasibility for damage identification, even by using experimental data measured on the vehicle passing over the actual truss bridge. In the experiment, artificial damage is introduced. As a result, the changes of estimated mode shape due to bridge damage is larger than the variation of them caused by uncertainties.

For utilization of this method for actual damage identification, although there are still many

other uncertainties to be examined, it is first time that the efficient damage identification methods verified by data of actual bridge test are proposed.

Acknowledgements

This research work is conducted in Department of Civil and Earth Resources Engineering, Graduate School of Engineering, Kyoto University, with a help of a number of people.

My special thanks go to my supervisor, Professor Kunitomo Sugiura, for providing a great opportunity for researching this exciting topic in his laboratory. I appreciate all his guidance.

I also would like to show great gratitude my academic supervisor Associate Professor Yoshinobu Oshima, for continuous guidance and discipline through my dissertation. My study would not be nearly as successful without his supports.

My next thanks go to Professor Hirotaka Kawano for his excellent teaching, continuous support and guidance.

My research is strongly supported by Professor Toyoaki Miyagawa. I acknowledge many helpful advices from him. And I would like to show acknowledge to Professor Kim Chul-Woo for his many guidance. I learn a great deal in discussions with him about this study. I also thank Professor Hiromichi Shirato for his teaching. I also would like to thank Associate Professor Tomoaki Utsunomiya, Associate Professor Atsushi Hattori, Associate Professor Takashi Yamamoto, Assistant Professor Satoshi Takaya, Assistant Professor Kunitaro Hashimoto and Assistant Professor Toshiyuki Ishikawa for their support of providing comfortable environment for research. I am thankful to Professor Yukinori Koyama and Assistant Professor Tomohiro Kawanishi for giving me a research environment and supporting. I acknowledge the helpful advice from the members of Oshima-group in Kyoto University, especially, Mr. Hen Sal Pisoth, Mr. Norimitsu Kimata, Mr. Kim Jing-Young and Mr. Syohei Fukuda. I also wish to express appreciation to the members of research group of vibration monitoring in Kyoto University, especially Dr. Kai Chung Chang, Assistant Professor Patrick McGetrick and Mr. Ryo Isemoto for exciting research collaborations. I also wish to express appreciation to the all students in laboratories for encouragement to complete my dissertation.

My deep thanks also go to the members of research group in Kobe university, especially, Professor Mitsuo Kawatani and his student Mr. Tatsuaki Toshinami about a laboratory experiment in this dissertation.

I acknowledge to staffs, especially Mr. Higaki and Mr. Hiroto Arima for support of experiments, Ms. Sonomi Matsukawa, Ms. Namie Kawano and Ms. Kwon Rihae for support of paper works.

My thanks also go to Mr. Yuji Miyasaka, Mr. Yukinobu Ueda and Mr. Yasuhiro Miyasaka for their support of laboratory experiments in this study. The field experiment in this study is performed a part of research activities of Kansai affiliate of Japan Society of Civil Engineers. I appreciate the contribution of the member of the activity and Osaka Municipal Transportation Bureau for providing a truss bridge for investigation.

Lastly, I express my deepest appreciation to my father Fumio and mother Yoshiko, brothers Hiroyuki and Yohe for helping my life and giving the opportunity to continue the study.

Table of Contents

Chapter 1. Introduction

1.1. Background

1.1.1. Vibration-based BHM

Recently, to settle the problem on how to maintain a vast number of aging bridges beyond their lifetime, bridge health monitoring (BHM) based on vibration measurements has been intensively studied. BHM system is structural health monitoring (SHM) specialized in bridge. The structural state of mechanical and civil structures can be usually estimated by visual check [1], vibration, thermograph [2], tap-tone [3] and so on. Using vibration is efficient to obtain objective indices for structural health. Vibration-based SHM can be categorized into two methods [4]: using controlled excitation and using random excitation.

The methods using controlled excitations are often applied to SHM for mechanical structures such as industrial products [5] and members of civil structures [6]. The advantages of this method are the high accuracy and low difficulties in estimation for frequency response function (FRF). FRF involves all information of the structural characteristics in the spatial and frequency domain [7]. The changes of FRF show the effects of structural damage or abnormality, accurately. However, the application of this method to civil structures such as bridge is generally difficult due to their scales, even though there are some exceptions in which shakers are installed on short span bridges [8], [9] or truss members [6] to estimate their conditions.

SHM by using random excitation are applicable to general bridges. The random exciting loads acting on bridges are mainly wind loads [10], [11] and traffic loads [12]. One of the demerits of SHM based on random inputs lies in the difficulty to measure external force [4]. If the random inputs have stationary white characteristics, the FRF of bridge can be estimated as the pseudo-FRF only by using bridge vibration responses data [12] It is expected that wind load characteristics is generally stationary in proper short time [13], while traffic loads are not [14], [15]. If the monitored bridge is subjected to non-stationary loads more significantly than stationary loads, the frequency domain characteristics of the bridge vibrations change temporally [16] At this case, it is necessary to consider the applicability of analysis methods. For a short span bridge, a traffic load becomes a more significant factor than for a longer span bridge [15]. For utilization of vibration-based BHM, it is important to examine the applicability of the methods using traffic load excitation. BHM based on traffic vibration can be classified into three kinds mainly [4]: both vehicle and bridge responses oriented, only bridge response oriented and only vehicle response oriented.

The method using both vehicle and bridge data once can be often called model updating method [17]. In this method, the finite element models (FEM) of the bridge are optimized by bridge and vehicle vibration responses, to estimate the probable flexural stiffness. Although the high

accuracy of damage detection is reported in some previous studies based on a model updating method [18], there is still a technical issue that difficulties lie in optimization of many parameters by solving the equation of motion of vehicle-bridge interaction (VBI) system without divergence [19]. Moreover, during bridge system identification with both of the vehicle and bridge vibration data, the ill condition problem [19] is also often occurred. Feasibility of this method may be the highest in three kinds of BHM, while there are still many difficulties in measurement and algorithm.

BHM method only by using bridge vibration is a kind of output-only system identification [20]-[25]. This is only-bridge-data-oriented BHM (BO-BHM) method which is the most general in BHM methods based on traffic induced vibrations and it has been intensively studied, recently. The non-stationary characteristics of the traffic induced vibrations are often assumed as noise during an analysis for the bridge vibration data. Modal parameters can be estimated by taking bridge as a linear system in BO-BHM [25].

The last method is BHM method only by using vehicle responses, which is called only-vehicle-data-oriented BHM (VO-BHM) in this dissertation. It is a technology to evaluate bridge's state only by using vehicle responses indirectly, which is the method originally proposed by Yang et al [26], [27]. In VO-BHM, because it is not necessary to install sensors on the bridge directly, they are able to be performed quickly and in low cost. In spite of its advantages in time and cost, however, most of the available VO-BHM techniques must fail to detect damage if they are applied to existing bridges, mainly because of the low sensitivity of dynamic parameters to local damage [28], of the significant effects on vehicle responses from uncertainties such as road unevenness and of the poor capability of the data-processing techniques to deal with non-stationary and non-linear problems [16].

Both BO-BHM and VO-BHM are not capable to estimate the bridge flexural stiffness directly, while the model updating methods always focus on it [17], [19]. When you use them, the accuracy of bridge damage detection often depends on vibration index.

The ordinal vibration indices of BHM are modal parameters [29]. Nishimura et al [29] performs both numerical and experimental verifications in which the static and dynamic indices of the bridge models are observed before and after damage to evaluate damage sensitivities of those indices. As a result, it is confirmed that the damage sensitivity depends on characteristics of parameters. Deflection of the bridge model subjected to a static load shows high sensitivity to global damage even if the damage is minimal, while deflection shows lower sensitivity to local damage. The measured deflection varies widely because deflection is generally too small to measure accurately. Strain is sensitive static index to both global and local damages. However, it is necessary to setup many strain gauges on the bridge, because strain tends to become larger only around damage section. Thus, there is possibility to overlook the damage sign if sensors are installed on only far from damage section. On the other hand, dynamic parameters, such as frequency, mode shape and damping, are moderately sensitive to structural defects, and because dynamic parameters can be measured easier than static parameters, it is thought to be efficient to apply them to BHM. However,

the estimation accuracy of the eigen-frequency is not enough to detect bridge damage or abnormality due to the low accuracy of sensors and the low sensitivity of the eigen-frequency itself to local damage [16]. Because bridge damage is generally occurred locally, damage effects on time series signals of bridge are too minimal to detect from a global index [31]

Recently, the use of vibration measurements for BHM has been intensively studied to efficiently detect the changes due to damage. Existing studies show the feasibility of detecting bridge damages from changes of dynamic parameters such as eigen-frequency, damping and mode shape. However, vibration-based BHM could not still be applicable to actual bridges due to the low accuracy and reliability. Previous studies first apply frequency domain analysis to bridge vibration responses to evaluate bridge state roughly based on the estimated eigen-frequencies even though those frequencies are not sensitive to the local damage. Damping could be more sensitive to the damage [25]. But, because its estimation accuracy of damping depends on the amplitude of response, damping is too easy to be varied for reliable BHM. Mode shape is one of the spatial indices which are directly associated with flexural stiffness [30]. The accuracy of estimation for mode shape depends on the number of the sensors [32]

There are many methods to estimate mode shapes by analysis of measurements on the structure [12]. Mode shapes are usually estimated by cross power spectra method. The cross power spectrum often shows the bridge eigen-frequencies relatively more accurately than single power spectrum. Brinker et al [7] proposed frequency domain decomposition (FDD) methods for large structures. For large structures, the effects of ambient loads are more significant in the vibration responses than the effects of other live loads. At the time, the cross power spectrum matrix of measured signals can be transformed to pseudo-FRF under assumption that the ambient loads are white noises and their amplitudes are same regardless of locations. From existing studies, singular vectors and singular value spectra of pseudo-FRF indicate the mode shapes and eigen-frequencies accurately. Nagae et al [12] shows its detailed algorithm and the high accuracy of FDD verified in numerical simulations and laboratory experiments. While FDD uses singular value decomposition (SVD) to decompose the cross-power spectra, SVD itself can be also used for mode shape estimation only if the modal responses included in measurements are orthogonal like principle components [33]. SVD estimates the mixing matrix and principle components of the original signals as an orthogonal mixing matrix and orthogonal signals, respectively. SVD is an extended method of eigen value decomposition (EVD) and also one of principle component analysis (PCA) methods. They could be taken as mode shape matrix and modal responses approximately, if the modal responses are close to de-correlation. Independent component analysis (ICA) can also extract mode shapes in the same way of PCA [34]. All these modal analyses are based on extended methods of orthogonal signal decomposition. Theory basis of orthogonal decomposition methods is constructed by assumption of free vibration output, stationary outputs or outputs induced by random white noise [7]. Besides, the constant characteristics of the bridge system are also assumed at the same time. In vehicle-bridge interaction (VBI) system, the interaction degrees are changed by position of a travelling load [35].

Traffic-induced vibration of VBI system is, in other word, non-stationary vibration of a system of which parameters are varied temporary. Orthogonal decomposition system is not devised to deal with this kind problem. In BO-BHM and VO-BHM, it is thought that the non-stationary problem affect the accuracy of the estimation results.

Though spatial information is affected directly by the changes of flexural stiffness [16], mode shapes are not always sensitive to local damage because they are global parameters [30]. Some studies show that the mode shape curvature is more sensitive to local damages [36], [37]. Mode shape curvature shows peaks at the location of local damage such as cracks. However, the estimation accuracy is still low because the estimation of mode shape curvature is based on second order spatial differentiation of mode shape. The estimation accuracy depends on the accuracy of numerical differentiation method and sensor system.

To overcome this trade-off between damage sensitivity and estimation accuracy for BHM indices, recently, time-frequency domain analysis is applied to BHM. In existing studies, empirical mode decomposition (EMD) [16], continuous wavelet transform (CWT) [31] and short time Fourier's transform (STFT) [28] are applied to BHM. These time-frequency domain analyses succeed to provide positive results in finding damage sensitive indices. By EMD method, the predominant frequencies are calculated to spatial location. Roveri and Carcaterra [16] perform numerical verification in which acceleration responses of a simple beam subjected to travelling loads are decomposed by empirical function and in which it is confirmed that the predominant frequency of a decomposed signal changes due to damage. The merit of EMD method is the high probability of damage detection, though its demerit lies in the difficulties of describing the physical meanings of empirical components. The existing study about EMD [38] for civil structures just verifies its feasibility only in simple numerical simulations. Considered about an actual bridge, there could be many uncertainties included in traffic-induced vibrations. It has not been cleared that EMD can extract damage changes in the estimated frequencies in stable, when there are expectable uncertainties. For VO-BHM, Chang et al [39] try to extract the bridge first eigen-frequency from vehicle acceleration responses by EMD methods in numerical and experimental verifications. Zhu et al [31] try to explain the physical meanings of CWT results by the numerical and experimental verifications. The wavelet coefficient of displacement vibration response of the beam subjected to vehicular loads can be described as a convolution between window function and bridge curvature. The wavelet coefficient for damage case shows a larger peak at the time when the loads passing over the damage location than that for intact case does. Though it does not examine the effect of uncertainties such as road unevenness, when the vehicular model runs over the RC beam model, distinct peaks can be observed after a crack is introduced to the beam model in the laboratory experiments. Nguen et al [40] suggest application of CWT to vehicle acceleration responses to detect multi-cracks of beam-like structure. The high feasibility of CWT-based VO-BHM has been shown in numerical verification. But, their study has ignored the effect of road unevenness. Xiang et al [28] apply STFT to a vehicle response and find that the correlation of STFT's spectra of the vehicle acceleration response changes just only around the

damage location when their method is named Tap-scan method because the passing vehicle is taken as not only observer but also exciter for the bridge system. This method is based on damage detection by introducing excitation to the vehicle to generate stationary vibration in VBI system. Xiang's verification has been performed only in numerical simulation without considering road unevenness.

There are still new other approaches for vibration-based BHM in this field. Kim et al [41] propose new damage index based on autoregressive (AR) parameters. AR model is one of the linear system models [42]. In AR model, a time-series signal is described as summation of products of coefficients and time-delay data. AR coefficients are exactly related to dynamic parameters of the system including mass, damping and flexural stiffness [43]. In the existing studies, AR coefficients themselves show higher sensitivity performance than frequency or damping. Though this method sets same assumptions with FDD methods in which all system inputs are white noise, mode shapes and eigen-frequencies can be estimated in stable. However, Isemoto et al [44] obtain the same results from AR method and ARX method. ARX method can concern inputs like traffic-induced vibration by using vehicle responses. It could mean that the non-stationary and non-linear problems caused by inputs are negligible in BO-BHM, which also means the high feasibility of BHM only by using bridge vibration data.

There are some challenges to introduce a controlled excitation to a bridge for more accurate BHM. Naito et al [8] suggests the damage detection method based on the bridge antiresonance frequencies. For the verification of this method, excitation machine was set up on short and middle span bridges and acceleration responses ware measured. As a result, antiresonance frequency of the bridge can be detected for short span bridges [9], [45]. But, because verified damage model has been only global, it is unclear about the detection accuracy of local damage. Besides, the applicability depends on the performance of the shaker. Furukawa et al [6] developed a new investigation method for truss bridges. A micro excitation machine is applied to the focused member, and acceleration responses of the truss nodes are measured to calculate mode shapes in this method. The tendency of mode shapes changes around damage member when the damaged member is excited. One of the advantages of their methods is easy to perform.

Existing studies also emphasize that the accuracy of vibration-based BHM depends on the environmental conditions [46]. In other words, the changes in vibration properties resulted from temperatures, winds and traffic-load characteristics could be as significant as the changes caused by damage. Sakakibara et al [47] propose a management standard based on AR coefficients with considering temperature. It is noted that the environmental effects should be examined after developing damage indices.

Some researchers study about system identification methods using finite element model (FEM) updated by measurements both of vehicle and bridge [17], [19]. This model updating method shows the high sensitivity to the damage, while there are still challenges to improve the model updating algorithm. Yun et al [17] propose application of neural network method to the model

updating method. Lu and Liu [19] examined the effect of vehicular model error on the estimation results of damage. Both-vehicle-and-bridge-data-oriented BHM (VBO-BHM) such as model updating methods is based on direct concept to calculate bridge flexural stiffness by using input and output. Here, input is vehicle acceleration while output is bridge acceleration. Utilization of this idea costs much in aspect of time and budget.

On the other hand, the social issue which this dissertation attempts to resolve could lie in the development of a low cost maintenance system for bridges in wide area. The inspection method adopted in that system should be applicable for many bridges at one time, even if its accuracy is decreased. Based on this idea, screening by VO-BHM can take very important roll to ensure and to promote safety of bridges under the situation that there is no inspection or reporting about many bridges in local area.

1.1.2. Challenge for VO-BHM

Screening technology which is capable to assess a vast number of bridges roughly for early identification of their damages has been needed recently [48], [49]. The traditional investigation which is usually based on visual check has still been applied for all bridges, which could be time-consuming and laboring. Existing BO-BHM or VBO-BHM methods in the previous studies also could not satisfy the above demand. In the screening technologies, first, the health of all bridges is roughly but quickly evaluated. Next, detailed investigation such as BO-BHM or VBO-BHM is applied to the bridges which are judged to be "suspicious bridge" in the first stage. One of the screening technologies could be VO-BHM. It is the main motivation of this dissertation which attempts to develop VO-BHM methods.

The use of vibration measurements for BHM has been intensively studied to efficiently detect the changes induced by the damage. Existing studies show the feasibility of detecting bridge damages from changes of dynamic parameters such as eigen-frequency, damping and mode shape. However, vibration-based BHM could still be also time-consuming and costly like visual check. Instead of installing sensors on the bridge, Yang et al [26] proposed a new concept of extracting bridge frequencies from a passing vehicle. Its accuracy was not enough high to detect bridge damages, while it is feasible for rough screening. Both the theoretic basis and experimental verifications [50] of this method are presented. Recently, Yang and Chang succeeded identifying higher natural frequencies of the bridge by applying empirical mode decomposition (EMD) method for signal processing [39].

VO-BHM is a technology to estimate bridge's state only by using vehicle responses, which is so-called indirectly approach. In spite of its advantages in time and cost, however, most of the available VO-BHM techniques [28], [40] may fail detection of local bridge damage in enough accuracy when they are applied to existing bridges. The main reason is the poor capability to manage the problem of non-linearity. In VO-BHM, because sensors are installed on the vehicle, the measuring

points travel with the vehicle together [35]. Conventional vibration analyses for BHM could not be applied because they generally presuppose the sensors fixed on the structure.

Theoretically, VO-BHM faces two main technical issues: The problem of the balance between estimation accuracy and damage sensitivity, and the problem of non-linear system. The accuracy and sensitivity problem is caused by the effect of non-stationary traffic-induced vibration and by the low damage sensitivity of bridge vibration indices especially in frequency domain. Modal parameters such as eigen-frequency are changed very slightly due to probable local damage, because they are global parameters. On the other hand, conventional BHM analyses are generally based on output-only system identification which supposes stationary vibration, though the traffic-induced vibration is expected to be non-stationary. It could decrease the accuracy under required.

First, the preliminary studies of VO-BHM [26], [27], [39], [49] which focus on bridge eigen-frequency as an evaluation index are performed. Traditional Fourier spectrum analysis decomposes a signal of the bridge or vehicle in a summation of some components whose frequencies are averaged over the whole time. When applying the Fourier analysis to the VBI system [49] to analyze bridge responses, predominant frequencies do not change even though after a serious damage, because a local damage affects only local responses of the bridge. The reason of the low sensitivity could be in using of global parameters for detection of local damage. Recently, some researchers have developed more sensitive indices to bridge local damage. Xiang et al [28] proposes the tap-scan damage detection method which is based on a time-frequency domain analysis to estimate the change of local impedance of beam structure [12] In this method, a tapping-force is introduced to the passing vehicle and short time Fourier transform (STFT) is adapted to the vehicle responses. STFT results show a high sensitivity to the local damage although the accuracy depends on focused frequencies. For the detection of cracks of a beam-like structure, Nguen and Tran [40] applied CWT to compare wavelet coefficients between the cases of intact and damage. This verification result based on numerical simulation clears that the wavelet coefficient of the vehicle acceleration response in high scale is a sensitive index to the crack. In VO-BHM, time domain signals can be easily converted to spatial domain signals by referring vehicle position. The spatial information included in time-frequency indices such as STFT spectrum and wavelet coefficient is feasible to be used for damage detection of the bridge. The reason of the high sensitivity of spatial information is that they are directly related to the local impedance of the bridge [16] However, these studies verify their methods only by numerical simulation without considering the effects of road unevenness on the vehicle responses. It is true that there is probability to improve the sensitivity of vibration indices by using spatial characteristics as damage indices calculated by time-frequency domain analyses, but they should be examined in aspect of the relationship between the sensitivity to structural damages and robustness to probable uncertain effects.

Indeed, vibration response of a passing vehicle is affected more significantly by many uncertainties especially road unevenness than the bridge vibration itself or the microscopical damage signal [15], which means that uncertainties are not negligible. Besides, there are more other

uncertainties such as the low accuracy of sensors, the model errors, and the accidental impact to the vehicle, etc. Although this study focuses on rough screening, VO-BHM must handle these uncertainties to extract damage signals from the measured vehicle responses. The key of this study verification lies in consideration about uncertainty effects on the VO-BHM results.

The other technical issues are the problems of non-stationary signal and non-linear system [35]. It is generally difficult to handle these problems by conventional method. The measured responses for VO-BHM are limited during the vehicle passing on the bridge. Because of that, it is impossible, or at least very difficult, to measure the bridge free or stationary vibration. It means that measurements in VO-BHM are always non-stationary vibrations. Traditional estimation methods based on mode theory generally assume that measured vibrations are free, stationary or induced by white noise input, or that both output and input of the system are measured at the same time. However, VO-BHM cannot satisfy these preconditions supposedly. This is the problem of non-stationary signal in VO-BHM.

Moreover, the measured responses cannot be described as linear system, because the locations of sensors installed on the vehicles are not fixed and the spatial information of the measurements is converted to temporal data [35] Generally, bridge vibration data $\boldsymbol{y}(t) \in \mathrm{R}^n$ measured at fixed positions on the bridge can be described as

$$\boldsymbol{y}(t) = \mathbf{A}\boldsymbol{q}(t) \tag{1.1}$$

where $\mathbf{A} \in \mathrm{R}^{n\times m}$ and $\boldsymbol{q}(t) \in \mathrm{R}^m$ are spatial and temporal information of the system. Herein, n is the size of vector $\boldsymbol{y}(t)$ equals the number of measuring points and m is the size of modal responses vector $\boldsymbol{q}(t)$ which indicates the considered maximum order of mode. In BO-BHM, converting $\boldsymbol{q}(t)$ from time domain to frequency domain can be performed smoothly such as

$$\boldsymbol{Y}(\omega) = \mathbf{A}\boldsymbol{Q}(\omega) \tag{1.2}$$

The spatial information in each sensor does not change because the sensor is fixed spatially. Herein, the problem of Eq. (1.1) and Eq. (1.2) can be solved by conventional orthogonal decomposition such as SVD or FDD if $n > m$. But in VO-BHM, traditional frequency analysis should fail to extract both frequency and spatial domain information of the system, because the spatial information $\mathbf{A}$ becomes temporal signal matrix $\mathbf{A}(t)$, the problem is given by Eq. (1.3).

$$\boldsymbol{y}(t) = \mathbf{A}(t)\boldsymbol{q}(t) \tag{1.3}$$

And, Fourier's transform of Eq. (1.3) is given by Eq. (1.4).

$$\boldsymbol{Y}(\omega) = \mathbf{A}(\omega)\otimes\boldsymbol{q}(\omega) \tag{1.4}$$

where $\otimes$ indicates convolution. They cannot be solved by SVD.

These non-stationary and non-linear problems should be managed whenever analyzing vehicle responses for BHM.

1.1.3. Scopes

This study focuses just on the development of new VO-BHM which is a technology to detect changes in bridge structural system only by using vehicle responses. Because bridge damage is generally local, the proposed methods are designed to react with local impedance changes of beam-like structure. The efficiency of the adopted vibration indices are evaluated by the balance between damage changes and variation due to noise. Robustness to uncertainties is the most important performance of the method. This dissertation includes the challenge to resolve the problem of non-linear caused by moving observer's effect [35].

One of the advantages of VO-BHM is the capability of performing easily in many times. Thus, the methods are designed with considering about their extending for statistical approaches [41] in future.

VO-BHM in this dissertation is expected to be used for rough screening to secure the least enough safety of bridges. Although the feasibility to detect damage location [48], [51] and severity is confirmed in numerical and experimental verification, the main target of this dissertation is damage identification of serious local damage on bridge.

The efficiency and applicability of the proposed methods are verified by numerical simulation and experiment. Numerical simulation discusses the analytical basis of the proposed methods. The non-stationary vibration of VBI system affects the applicability of SVD method which presupposes stationary vibration. This applicability cannot be examined analytically because random road unevenness is the main factor. The road profile in numerical verification is based on actual data. Laboratory experiment mainly demonstrates the uncertainties' effects on the vehicle responses. Field experiment on an actual steel truss bridge is also carried out in this dissertation. Based on the experimental results, the feasibility of the proposed method is discussed.

1.2. The purpose of this study

The purpose of this study is to propose new VO-BHM method with considering the above technical issues shown, and to verify it analytically, numerically and experimentally. In this study, proposed VO-BHM methods mainly use vertical acceleration responses. But, one of them uses relative displacement between the vehicle body and bridge surface and the vehicle position, which could be

easily measured by sensors on the vehicle.

The first technical issue which should be managed is the problem of non-linearity because it affects the results of VO-BHM based on spatial information significantly. The proposed method introduces interpolation to solve this problem. Thus, the numerical simulation is also performed to confirm the efficiency of interpolation. A laboratory experiment and a field experiment are also carried out in aspect of the feasibility verification for the proposed methods under probable condition. The VO-BHM method applying wavelet transform is also proposed and examined because it is intensively studied in recent few years.

1.3. Composition of this thesis

In this study, new three VO-BHM method are proposed and verified by analytically, numerically and experimentally. For experimental verifications, laboratory and field experiments are performed. To examine the feasibility of the methods for damage identification, the changes of indices due to local damage are compared with the variation caused by uncertainties.

In Chapter 2, three proposed VO-BHM methods are proposed theoretically. First proposed method is Curvature-based method in which the wavelet coefficient of the vehicle acceleration response is used as a non-linear function of bridge curvature. Thus, when damage occurs, wavelet coefficient varies as the curvature changes. Herein, it is shown that the wavelet coefficient can be described as the function of bridge curvature, first. Then, the second is indirect Mode-Shape-based method, in which the bridge mode shape is indirectly estimated by the estimation of bridge vibration responses. This method is high theoretical consistency for mode analysis. In this method, there are five steps to estimate bridge vibrations from vehicle data and to extract the bridge mode shapes. Lastly, direct Mode-Shape-based method. This method is designed to overcome low robustness of other two methods, instead of theoretical consistency. Herein, basic theory of this method is explained.

In Chapter 3, the proposed methods are verified by numerical simulation. First, numerical simulation algorithm and basic assumptions are shown in this chapter. Then, verification for each method are performed. There are slightly changes in assumptions of numerical simulations between the methods. Thus, at the beginning of each section, the basic assumptions and properties of numerical simulation for each proposed method is shown. Then, the feature of dynamic behaviors of the VBI system and verification results are shown. In the verification of Curvature-based method, acceleration responses and Fourier's spectra are examined. Wavelet coefficients of the vehicle responses are compared between intact and damage cases. In the verification of second method, each factors of the proposed method such as ill condition, de-correlation assumption and curve fitting performance are examined. For indirect Mode-Shape-based VO-BHM method, the de-correlation of

the decomposed bridge vibration components and error terms are calculated and discussed.

In Chapter 4, the proposed methods are verified by laboratory experiment. Herein, two proposed methods which are Curvature-based and Mode-Shape-based methods are verified in the aspect of the uncertainty effects.

In Chapter 5, the proposed methods are verified by field experiment. The two proposed methods are verified by using data measured on the actual bridge and passing vehicle. In this chapter, first, experimental settings are explained. Then, the feature of bridge modal parameters are confirmed by existing techniques [7]. The application results of the proposed methods are shown and discussed about.

In Chapter 6, the results are concluded.

In this dissertation, appendixes about changes of correct modal parameters due to damage, FDD method and examination of statistics are shown in Appendix A, B and C, respectively

Reference

[1] Yamada, K.: What is cleared from the accident of member fracture of Kiso River Bridge, Journal of JSCE, Vol.93, No.1, pp.29-30, 2008.

[2] Myriounis, D.P., Kordatos, E.Z., Hasan, S.T. and Matikas, T.E.: Crack-tip stress field and fatigue crack growth monitoring using infrared Lock-In thermography in A359/SiCp composites, Strain, Vol.47, pp.e619-e627, 2011.

[3] Miyoshi, A., Sonoda, Y., Nakayama, A. and Yoshida, N.: An analysis study on the deterioration diagnosis of the RC structures using the rotary hammering test, Proc. of JCI annual confference, Vol.30, No.3, pp.1723-1728, 2008.

[4] Kim, C.W.: Challenges of on-going bridge health monitoring, Newsletter of Kyodokai, No49, pp.76-78, 2011.

[5] Ono, T. and Ishihara, T.: Design of disturbance observers using a priori information on unknown inputs, Trans. Jpn. Soc. Mech. Eng., Vol.75-760, No.09-0417, pp.81-87, 2009.

[6] Furukawa, A., Otsuka, H. and Umebayashi, F.: Damage identification of steel truss bridge by vibration testing using micro shaker, Journal of Applied Mechanics, JSCE, Vol.9, pp.1103-1110, 2006. (in Japanese)

[7] Brinker, R., Zhang, L. and Andersen, P.: Modal identification of output-only systems using frequency domain decomposition, Smart Materials and Structures, Vol.10, pp.441-445, 2001.

[8] Naito, H., Otake, Y., Saito, T. and Suzuki, M.: Basis examination of damage identification of concrete member based on vibration test, Journal of JCI Annual Convention, Vol. 33, No.2, pp.949-954, 2011. (in Japanese)

[9] Naito, H., Otake, Y., Watanabe, T., Suzuki, M., Nakano, S., Iwaki, I. and Kisara, N.: Study on damage identification of beam on anti-resonance frequency, Journal of Structural Engineering, JSCE, Vol.58A, pp.150-161, 2012.

[10] Minato, J. and Sawada, Y.: Real-time estimation of dynamic wind load on a structure, Journal of Structural Engineering, JSCE, Vol.58A, pp.170-179, 2012.

[11] Abe, M. and Fujino, Y.: Maximum displacement response estimation from acceleration record for random excitation, Journal of JSCE, ser.A1 (Journal of Structural Engineering & Earthquake Engineering), Vol.66, No.3, pp.477-490, 2010.

[12] Nagae, N., Watase, M. and Tamaki, T.: Operational modal analysis using cross correlation function, Journal of Structural Engineering. A, JSCE, Vol.57A, pp.232-241, 2011.

[13] Minato, J., Ohsumi, A. and Sawada, Y.: Generation of artificial wind and estimation of load from structural response, Int. J. of Innovative Computing, Information and Control, Vol.6, No.10, pp.4615-4629, 2010.

[14] Okabayashi, T. and Yamaguchi, Z.: Mean square response analysis of highway bridge under a series of moving vehicles, Proc. of the JSCE, Vol.1983, No.334, pp.1-11, 1983.

[15] Yamamoto, K., Isemoto, R., Oshima, Y., Kim, C.W. and Sugiura, K.: Evaluation of acceleration responses in a steel truss bridge and passing vehicle before and after member's breakage, Journal of Structural Engineering, JSCE, Vol.58A, pp.180-193, 2012. (in Japanese)

[16] Roveri, N. and Carcaterra A.: Damage detection in structures under traveling loads by Hilbert-Huang transform, Mechanical Systems and Signal Processing, Vol.28, pp.128-144, 2012.

[17] Lee, J.W., Kim, J.D., Yun, C.B., Yi, J.H. and Shim, J.M.: Health-monitoring method for bridges under ordinary traffic laodings, Journal of Sound and Vibration , Vol.257(2), pp.247-264, 2002.

[18] Kim, C.W., Isemoto, R., Kawatani, M. and Sugiura, K.: Structural diagnosis of bridge using output-only vibration in moving vehicle laboratory experiment, JSCE J. of Applied Mechanics, Vol.[], pp.[][][]-[][][], 2011.

[19] Lu, Z.R. and Liu, J.K.: Identification of both structural damages in bridge deck and vehicular parameters using measured dynamic responses, computers and Structures, Vol.89, pp1397-1405, 2011.

[20] Doebling, S.W.: Damage identification and health monitoring of structural and mechanical systems from changes in their vibration characteristics: a literature review, Los Alamos National Laboratory Report, LA-3070-MS, 1996.

[21] Salawu, O.S.: Detection of structural damage through changes in frequency: a review, Journal of Engineering Structures, Vol.19, No.9, pp.718-723, 2005.

[22] Freiswell, M.I. and Mottershead, J.E.: Finite Element model updating in structural dynamics, Dordrecht:Kluwer Academic Publishers, pp.56-77, 1995.

[23] He, X. and De Roeck, G.: System identification of mechanical structures by a high-order multivariate autoregressive model, Computers and Structures, Vol. 64(1-4), pp.341-351, 1997.

[24] Toshinami, T., Kawatani, M. and Kim, C.W. : Feasibility investigation for identifying bridges fundamental frequencies from vehicle vibrations, Bridge maintenance, safety, management and life-cycle optimization, IABMAS 2010, pp.317-322, 2010.

[25] Kim, C.W. and Kawatani, M.: A damage identification procedure for girder bridges based on coupling vibration with moving vehicles, Advances in Reliability and Optimization of Structural Systems, (ISBN 0 425 39901 7), 2006.

[26] Yang, Y.B., Lin, C.W., and Yau, J.D.: Extracting bridge frequency from the dynamic response of a passing vehicle, Journal of Sound and Vibration, Vol.272, pp.471-493, 2004.

[27] Yang, Y.B. and Chang, K.C.: Extracting the bridge frequencies indirectly from a passing vehicle, Parametric study, Engineering Structures, 31, pp.2448-2459, 2009.

[28] Xiang, Z., Dai, X., Zhang, Y. and Lu, Q.: The Tap-Scan Damage Detection Method for Beam Structures, Advances Interaction & Multiscale Mechanics, pp.541-553, 2010.

[29] Kim, C.W., Kawatani, M. and Ozaki, R.: Modal identification of short and medium span bridges under moving

loads, Proc. of 10th ICOSSAR, pp.2446-2452, 2009.

[30] Nishimura A., Fujii, M., Miyamoto, A. and Kagayama, T.: Sensitivity of mechanical behavior of bridges for their damage assessment, Doboku Gakkai Ronbunsyu, JSCE, Vol.1987, No.380, pp.355-364, 1987.

[31] Zhu, X.Q. and Law, S.S.: Wavelet-based crack identification of bridge beam from operational deflection time history, International Journal of Solids and Structures, 43, pp.2299-2317, 2006.

[32] Masuda, A., Sone, A. and Morita, S.: Continuous monitoring of changes in mode shapes based on time-frequency analysis, Proc. of JSME Symposium, Vol.2002, No.2, pp.66-70, 2002.

[33] Kerschen, G. and Golinval, J.G.: Physical interpretation of the proper orthogonal modes using the singular value 13ecomposition, Journal of Sound and Vibration, Vol.249(5), pp.849-865, 2002.

[34] Takaki, K., Nagase, K., Hayakawa, K. and Kawasaki, T.: An estimation method of mode shapes by independent component analysis and its application to fault diagnosis, Transactions of the Japan Society of Mechanical Engineers Series C, Vol.70, No.698, pp.2847-2853, 2004.

[35] Yamamoto, K., Oshima, Y., Sugiura. K. and Kawano, H.: Estimation of bridge mode shapes based on vehicle responses,Journal of Japan Society of Civil Engineers, Ser. A1 (Structural Engineering & Earthquake Engineering), Vol.67, No.2, pp.242-257, 2011. (in Japanese)

[36] Pandey, A.K., Biswas, M. and Samman, M.M.: damage detection from changes in curvature mode shapes, Journal of Sound and Vibration, Vol.145, No.2, pp.321-332, 1991.

[37] Chance, J., Thomlinson, G.R., Worden, K.: A simplified approach to the numerical experimental modeling of the synamics of cracked beam, The 12th International Model Analysis Conference, pp.778-785, 1994.

[38] Xu, Y.L., Asce, M. and Chen, J.: structural damage detection using empirical mode decomposition: experimental investigation, Journal of Engineering Mechanics, Vol.130, No.11, pp.1279-1288, 2004.

[39] Y.B. Yang, K.C. Chang: Extraction of bridge frequencies from the dynamic response of a passing vehicle enhanced by the EMD technique, Journal of Sound and Vibration, 322, pp.718-739, 2009.

[40] Nguyen, K.V. and Tran, H.T.: Multi-cracks detection of a beam-like structure based on the on-vehicle vibration signal and wavelet analysis, Journal of Sound and Vibration, Vol.329, pp.4455-4465, 2010.

[41] Kim, C.W., Isemoto, R., Toshinami, T., Kawatani, M., McGetrick, P.J. and Obrien, E.J.: Experimental investigation of drive-by bridge inspection, 5th Int. Conf. on Structural Health Monitoring of Intelligent Infrastructure (SHMII-5), pp.1-10, 2011.

[42] Gersch, W., Nielsen, N.N. and Akaike, H.: Maximum likelihood estimation of structural parameters from random vibration data, J. of Sound and Vibration, Vol.31, No.3, pp.295-308, 1973.

[43] Kim, C. W., Kawatani, M., and Hao, J.: Model parameter identification of short span bridges under a moving vehicle by means of multivariate AR model, Structure and Infrastructure Engineering, (DOI: 10.108/15732479.2010.539061), 2010.

[44] Isemoto, R., Kim, C.W. and Sugiura, K.: Health monitoring of short span bridge using vibration characteristics estimated by ARX model, The 24th KKCNN symposium on Civil Engineering, pp.201-204,2011.

[45] Kashiwa, H., Otake, Y., Naito, H., Nakano, S., Kisara, N. and Suzuki, T.: Excitation experiment of existing bridges by small shaker, Proc. of the 66th Annual conference of the JSCE, I-315, pp.629-630, 2011.

[46] Peeters, B. and De Roeck, G.: One-year monitoring of the Z24-Bridge: environmental effects versus damage events,

Earthquake Engineering and Structural dynamics, Vol.30, pp.149-171, 2001.

[47] (Sakakibara)

[48] Yamamoto, K., Oshima, Y., Kim, C.W. and Sugiura, K.: Damage detection of bridges based on time frequency analysis of responces of a passing vehicle, Journal of Structural Engineering. A, JSCE, Vol.57A, pp.637-645, 2011. (in Japanese)

[49] Sugiura, K., Kitagaki, K., Yamaguchi, T., Kitada, T. and Hashimoto, K.: Laboratory experiment for estimation of bridge eigen-frequency based on moving vehicle's responses, Proceedings of the 64th Annual conference of the JSCE, I-291, pp.581-582, 2009.

[50] Ling, C.W. and Yang, Y.B.: Use of a passing vehicle to scan the fundamental bridge frequencies: An experimental verification, Engineering Structures, Vol.27, pp.1865-1878, 2005.

[51] Yamamoto, K., Toshinami, T., Oshima, Y., Kim, C.W., Sugiura, K. and Kawatani, M.: Bridge assessment based on statistical analysis of the response of a vehicle passing over the bridge, Journal of JSCE, Ser.A2, (Applied Mechanics), Vol.67, No.2, pp.I_855-I_864, 2011.

Chapter 2. Proposed Methods

2.1. General Remarks

This study proposes three different damage identification methods for only-vehicle-data-oriented BHM (VO-BHM). In the proposed methods, spatial characteristics such as bridge curvature and mode shape are estimated only by using vehicle response and location as damage evaluation indices. Three proposed methods are curvature-based method and indirect and direct mode shape estimation methods.

VO-BHM method based on bridge curvature uses continuous wavelet transform (CWT) [1]. According to previous studies [2], [3], wavelet coefficient calculated by applying CWT to the vehicle response can be described as a form of non-linear function of bridge curvature. Thus, changes of the wavelet coefficient of vehicle response can be taken as changes of the bridge curvature due to damage. In this study, first, the relation between wavelet coefficient of vehicle response and bridge curvature is shown analytically.

Next, two kinds of VO-BHM methods based on bridge mode shape are proposed in this study: Indirect and direct mode shape estimation methods. Because position of each sensor installed on the travelling vehicle is changed temporary, the bridge mode shape becomes a function of time from that of space. Both indirect and direct methods use interpolation matrix to convert the mode shape from a form of time function to function of position.

The damage identification based on the indirect estimation of bridge mode shape [4] consists in five steps: (1) Input estimation of vehicle vibration system, (2) extracting of bridge vibration components, (3) canceling of moving observation effect, (4) mode decomposition by singular value decomposition (SVD) [5], (5) damage identification based on mode shape, in which bridge mode shape is indirectly estimated after estimation of bridge vibrations. The merit of this method lies in the theoretical consistency exactly based on mode theory. The inverse interpolation matrix is applied to bridge vibration components estimated in Step (2). However, uncertain factors in each step may affect the result.

The last proposed method is the damage identification based on the direct estimation of bridge mode shape. In the direct method, although the same interpolation matrix is used as the indirect method, the interpolation matrix is applied not to estimated bridge vibrations but to the measured vehicle responses directly. This method can be categorized into two methods which use inverse and transpose matrix of the interpolation matrix, respectively. The mode shape estimation both in these methods always include errors caused by road unevenness. However, if the other conditions except bridge state are identical between before and after damage introduced, changes of estimated bridge mode shape can be taken as changes due to damage.

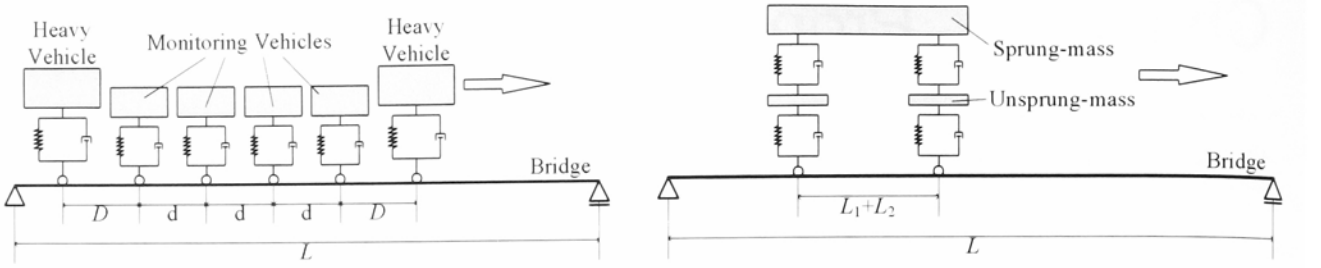

(a) Trailer system (b) Half-car model

Fig. 2.1.1 Vehicle-bridge interaction models

Herein, the vehicle-bridge interaction (VBI) system is modeled by using rigid-body spring model as vehicle and one-dimension simple supported finite element (FE) beam as bridge. Fig. 2.1.1 shows the example of the VBI system models. Only in the indirect bridge mode shape estimation, a trailer system shown in Fig. 2.1.1 (a) is assumed, while a half-car model shown in Fig. 2.1.1 (b) is assumed in the other proposed methods with considering practical use. The assumed condition of inspection is that a monitoring vehicle runs at the legal speed on the objective bridge in several times both before and after damage occurs. The bridge damage is local decreasing of flexural stiffness and mass.

The curvature-based VO-BHM only uses vehicle acceleration response which is the merit over the other methods. One sensor should be installed on the sprung-mass or unsprung-mass in this method. On the other hand, in both the indirect and direct mode-shape-based VO-BHM methods, not only an acceleration response of each vehicle body but also a relative displacement between each vehicle body and road surface should be measured. Besides, it is necessary to know the vehicle positions to make basis functions of interpolation matrix. The advantages in using the indirect and direct mode-shape-based VO-BHM lie in theoretical consistency and robustness, respectively.

2.2. Curvature-based VO-BHM

2.2.1. Preliminary Analysis

Zhu and Law [2] show relationship between bridge curvature and wavelet coefficient of bridge displacement. Bridge curvature is sensitive index to local damage because it is associated directly with flexural stiffness of the bridge. On the other hand, according to the previous study [3], wavelet coefficient of vehicle acceleration can be also used for damage detection of beam-like structure. However, analytical basis of application to vehicle responses is not shown.

Herein, for damage identification, it is shown that wavelet coefficient of vehicle response is a non-linear function of bridge curvature. First, the relationship between bridge curvature and wavelet coefficient of displacement response of the bridge subjected to travelling loads is described

according to the method of Zhu and Law [2]. Then, this relationship is extended to acceleration response of the monitoring vehicle.

The equation of motion of the vehicle-bridge interaction (VBI) system which is modeled as continuous beam subject to n moving loads $P_i(t)$ $(i = 1, \dots, n)$ can be described as Eq. (2.1).

$$\rho A(x)\frac{\partial^2 y(x,t)}{\partial t^2} + C(x)\frac{\partial y(x,t)}{\partial t} + \frac{\partial^2}{\partial x^2}\left(EI(x)\frac{\partial^2 y(x,t)}{\partial x^2}\right) = \sum_{i=1}^{n} P_i(t)\delta\big(x - x_i(t)\big) \tag{2.1}$$

where $y(x,t)$ is bridge displacement at the location of x and time of t and $\rho A(x)$, $C(x)$, $EI(x)$ are the mass per unit length, the damping and flexural stiffness of the bridge. $P_i(t)$ is the i-th load and $x_i(t)$ is the location of P_i at the time of t. n is the number of loads. $\delta(x)$ is the Dirac delta function. The bridge displacement $y(x,t)$ can be given by using k-th order mode shape function $\phi_k(x)$ and modal response $q_k(t)$ in the form of

$$y(x,t) = \sum_{k=1}^{\infty} \phi_k(x)\, q_k(t). \tag{2.2}$$

By substituting Eq. (2.2) to Eq. (2.1), multiplying by $\phi_j(x)$ and integrating with respect to x between 0 and L with considering the orthogonality conditions, Eq. (2.53) is described as follows:

$$\ddot{q}_k(t) + 2\xi_k\omega_k\dot{q}_k(t) + \omega_k^2 q_k(t) = \frac{1}{M_k}\sum_{i=1}^{n} P_i(t)\phi_k\big(x_i(t)\big) \tag{2.3}$$

where M_k, ξ_k and ω_k are the k-th order modal mass, damping ratio and undamped eigen angular frequency, respectively. M_k is

$$M_k = \int_0^L \rho A \phi_k(x)\mathrm{d}x. \tag{2.4}$$

On the other hand, impulse response function (IRF) of the system expressed by Eq. (2.3) can be given as a solution of $q_k(t)$ when $P_i(t) = 0$, as follows:

$$h_k(t) = \frac{\mathrm{e}^{-\xi_k\omega_k t}}{\omega_k'}\sin(\omega_k' t) \tag{2.5}$$

$$\omega_k' = \omega_k\sqrt{1-\xi_k^2} \tag{2.6}$$

where $h_k(t)$ is IRF of k-th mode of the bridge system, and ω_k' is k-th order eigen angular frequency. By using IRF, the solution of Eq. (2.3) is

$$q_k(t) = h_k(t)\otimes\left(\frac{1}{M_k}\sum_{i=1}^{n} P_i(t)\phi_k(x_i(t))\right). \tag{2.7}$$

Thus, the bridge displacement response $y(x,t)$ can be expressed by

$$y(x,t) = \sum_{k=1}^{\infty}\left[\frac{\phi_k(x)}{M_k}\left\{h_k(t)\otimes\left(\sum_{i=1}^{n} P_i(t)\phi_k(x_i(t))\right)\right\}\right]. \tag{2.8}$$

Observing $y(x,t)$ at a fixed location x_m, Eq. (2.8) can be described as follows:

$$y(x_m,t) = \sum_{k=1}^{\infty}\left[\frac{\phi_k(x_m)}{M_k}\left\{h_k(t)\otimes\left(\sum_{i=1}^{n} P_i(t)\phi_k(x_i(t))\right)\right\}\right]. \tag{2.9}$$

The second derivation of the displacement with x_j which is position of the one vehicular load P_j can be described as follows:

$$\frac{\partial^2 y(x_m,t)}{\partial x_j^2} = \sum_{k=1}^{\infty}\left[\frac{\phi_k(x_m)}{M_k}\left\{h_k(t)\otimes\left(\sum_{i=1}^{n} P_i(t)\frac{\partial^2\phi_k(x_i(t))}{\partial x_j(t)^2}\right)\right\}\right] \tag{2.10}$$

where $\partial^2\phi_k(x_j)/\partial {x_j}^2$ is the second order derivation of the k-th mode which is a component of the bridge curvature.

CWT of an integrable function $f(x)$ is defined as

$$Wf(x,s) \equiv f(x)\otimes\theta_s(x) = \int_{-\infty}^{\infty} f(x)\,\theta^*\left(\frac{x-u}{s}\right)\mathrm{d}u \tag{2.11}$$

where $\theta_s(x)$ is so-called mother wavelet which is the dilation of window function $\theta(x)$ by the scale s. u is the translation indicating the locality. $(\ )^*$ denotes the complex conjugate. W is

wavelet transform of the function behind.

Zhu and Law [2] apply CWT to Eq. (2.9) to derive Eq. (2.12) only when $n = 1$.

$$
\begin{aligned}
Wy(x_m, s) &= y(x_m, t) \otimes \frac{\partial^2 \theta_s\left(x_j(t)\right)}{\partial x_j(t)^2} \\
&= \sum_{k=1}^{\infty}\left[\frac{\phi_k(x_m)}{M_k}\left\{h_k(t) \otimes \left(\sum_{i=1}^{n} P_i(t)\phi_k\left(x_i(t)\right)\right) \otimes \frac{\partial^2 \theta_s\left(x_j(t)\right)}{\partial x_j(t)^2}\right\}\right] \\
&= \sum_{k=1}^{\infty}\left[\frac{\phi_k(x_m)}{M_k}\left\{h_k(t) \otimes \left(\sum_{i=1}^{n} P_i(t)\frac{\partial^2 \phi_k\left(x_i(t)\right)}{\partial x_j(t)^2}\right) \otimes \theta_s\left(x_j(t)\right)\right\}\right] \\
&= \frac{\partial^2 y(x_m, t)}{\partial x_j(t)^2} \otimes \theta_s\left(x_j(t)\right)
\end{aligned}
\tag{2.12}
$$

where s is the scale of mother wavelet θ_s. If the Gaussian function is applied as θ_s, the second order derivative of Gaussian function $\partial^2\theta_s(x_i)/\partial x_i{}^2$ is well known as the Mexican Hat wavelet that has the following explicit expression:

$$
\frac{\partial^2 \theta(x)}{\partial x^2} = \frac{2}{\sqrt{3}}\pi^{-\frac{1}{4}}(x^2 - 1)\mathrm{e}^{-x^2}. \tag{2.13}
$$

$Wy(x_m, s)$ for one fixed scale is called wavelet coefficient. The wavelet coefficient calculated by Eq. (2.12) is proportional to the second derivative of $y(x_m, t)$ smoothed by the Gaussian window. Thus, The wavelet coefficient of bridge displacement response can be regarded as the curvature that can be obtained directly differentiation of displacement. The contact force of the vehicular load $P_i(t)$ can be associated with $x_i(t)$. $P_i(t)$ can be converted to the function x_i. Then, Eq. (2.14) is obtained as

$$
\begin{aligned}
&Wy(x_m, s) = \\
&\sum_{k=1}^{\infty}\left[\frac{\phi_k(x_m)}{M_k}\left\{h_k(t) \otimes \left(\sum_{i=1}^{n} P_i(t)\frac{\partial^2 \phi_k\left(x_i(t)\right)}{\partial x_j(t)^2} + \frac{\partial^2 P_i(t)}{\partial x_j(t)^2}\phi_k\left(x_i(t)\right)\right) \otimes \theta_s\left(x_j(t)\right)\right\}\right].
\end{aligned}
\tag{2.14}
$$

Because $P_i(t)$ could be strongly associated with vehicle acceleration responses, the dynamic response effect should be considered. From the results of verification by Zhu and Law [2], instead of this dynamic effect problem, wavelet coefficient of the displacement of the beam-like structure shows peaks at the time when the vehicular loads are located immediately above the crack. It means the damage detection feasibility in application of CWT.

For acceleration responses of the bridge, letting us assume that the run speed of i-th travelling load is constant ($= v_j$), the wavelet coefficient of bridge acceleration response can be described as Eq. (2.15) in the same form of Eq. (2.13).

$$W\ddot{y}(x_m, s) = \frac{\partial^2 y(x_m,t)}{\partial x_j(t)^2} \otimes \frac{\mathrm{d}^2}{\mathrm{d}t^2}\left(\theta_s\left(x_j(t)\right)\right) = \frac{\partial^2 y(x_m,t)}{\partial x_j(t)^2} \otimes \left(v_j^2 \theta_s''\left(x_j(t)\right)\right) \tag{2.15}$$

where $\theta_s''(x)$ is the second differentiation of $\theta_s(x)$ in respect of x. Although the window function is changed, wavelet coefficient of acceleration response $W\ddot{y}(x_m, s)$ is still also proportional to the second derivative of $y(x_m, t)$ which indicates bridge curvature.

2.2.2. Curvature Estimation based on Vehicle Acceleration Response

On the other hand, Nguen and Tran [3] also apply CWT to vehicle acceleration response to detect multi-cracks on beam-like structure. Although Eq. (2.14) is just only applicable for BHM, their method is capable to be applied to VO-BHM, in which the scale is set in high which corresponds to low frequency. However, because road profile has dominant component in low frequency, CWT should be applied with low scale, for deduction of road profile. The high frequency component is also expected to be relatively sensitive to the bridge local damage.

Now, the forced displacement input of i-th axle (or vehicle) $u\left(x_i(t)\right)$ can be described as follows:

$$u\left(x_i(t)\right) = y(x_i(t), t) + r\left(x_i(t)\right) \tag{2.16}$$

where $y(x,t)$ and $r(x)$ are bridge displacement and road unevenness, respectively. Letting the output of i-th axle (or vehicle) $z_i(t)$, the equation of motion of vehicle vibration system is given by IRF $h_{\mathrm{V}_i}(t)$ in the form of

$$z_i(t) = h_{\mathrm{V}_i}(t) \otimes u\left(x_i(t)\right). \tag{2.17}$$

It is easy to extend Eq. (2.17) to multiple dimension.

$$\boldsymbol{z}(t) = \mathbf{h}_{\mathrm{V}}(t) \otimes u\left(\boldsymbol{x}(t)\right). \tag{2.18}$$

Then, acceleration response of i-th axle (or vehicle) can be described as follows:

$$\ddot{z}_i(t) = \ddot{h}_{\mathrm{V}_i}(t) \otimes \left(y(x_i(t), t) + r\left(x_i(t)\right)\right). \tag{2.19}$$

The wavelet coefficient of $\ddot{z}_i(t)$ can be obtained as

$$W\ddot{z}_j(x_j,s) = \ddot{z}_j(t) \otimes \frac{\partial^2 \theta_s\left(x_j(t)\right)}{\partial x_j(t)^2} = D_1(t) + D_2(t) + D_3(t) \tag{2.20}$$

where

$$D_1(t) = \ddot{h}_{V_j}(t) \otimes \sum_{k=1}^{\infty} \left[\frac{\phi_k(x_j)}{M_k} \left\{ \ddot{h}_k(t) \otimes \left(\sum_{i=1}^{n} P_i(t) \frac{\partial^2 \phi_k(x_i(t))}{\partial x_j(t)^2} \right) \otimes \theta_s\left(x_j(t)\right) \right\} \right] \tag{2.21}$$

$$D_2(t) = \ddot{h}_{V_j}(t) \otimes \sum_{k=1}^{\infty} \left[\frac{1}{M_k} \frac{\partial^2 \phi_k\left(x_j(t)\right)}{\partial x_j(t)^2} \left\{ \ddot{h}_k(t) \otimes \left(\sum_{i=1}^{n} P_i(t) \phi_k(x_i(t)) \right) \otimes \theta_s\left(x_j(t)\right) \right\} \right] \tag{2.22}$$

$$D_3(t) = \ddot{h}_{V_j}(t) \otimes r(x_j) \otimes \frac{\partial^2 \theta_s\left(x_j(t)\right)}{\partial x_j(t)^2} \tag{2.23}$$

$D_1(t)$, $D_2(t)$ and $D_3(t)$ are vehicle acceleration response induced by bridge displacement mode shape, bridge curvature mode shape and road profile, respectively. Herein, $D_1(t)$ and $D_2(t)$ change as bridge curvature and mode shape change after damage occurs. $D_3(t)$ is proportional to road unevenness.

Eq. (2.20) means that wavelet coefficient of vehicle acceleration response can be expressed in a form of non-linear function of bridge curvature. According to previous studies [2], [6], [7], bridge curvature is a sensitive index which changes distinctively when bridge damage occurs. Damage identification in curvature-based VO-BHM method can be performed by focusing on changes of wavelet coefficient of vehicle acceleration responses between before and after damage.

2.3. Indirect Mode-Shape-based VO-BHM

2.3.1. Preliminary Assumptions

In this method, several monitoring vehicles (or axles) and, if necessary for excitation, excitation vehicles are assumed. Bridge is also assumed to be one-dimensional beam with a length of L. Vehicle acceleration response, relative displacement between the vehicle body and road surface and vehicle location should be measured in each monitoring vehicle (or axle). In estimation of bridge mode shape, it is necessary to obtain bridge vibration components estimated only by vehicle

Table 2.3.1 Main flow of VRA's bridge mode shape estimation

Step		Remarks
1	Input estimation of the vehicle system	Inverse System Estimation Frequency Response Function
2	Deduction of road unevenness (Extracting bridge vibration component)	Spatial Synchronization
3	Moving observation effect canceling	Lagrange function Cardinal sine function Trigonometrical function
4	Mode shape estimation	Singular Value Decomposition
5	Damage detection	Mode Accuracy Criteria

responses, which is input estimation of the vehicle vibration system. The measuring points of bridge vibration change as the vehicle travels. Thus, it is necessary to consider about input estimation problem and moving effect canceling. In this study, the proposed method based on mode shape insists in 5 steps shown in Table 2.3.1.

In description of the proposed indirect VO-BHM based on bridge mode shape, monitoring vehicles are assumed as several simple spring-mass models at regular intervals shown in Fig. 2.1.1 (a). It is necessary to use more than three monitoring vehicles, at least, in this method, because of deduction of road unevenness.

Herein, the damage identification flow of this method is shown, first. In the flow, there are five steps which affect the damage identification accuracy. In this study, mode decomposition is performed by SVD [5] under assumption that amplitudes of mode shapes included in each applied signal are constant, while the amplitudes of mode shapes measured by each sensor are changed temporary due to vehicle run. Thus, this method includes a step converting mode shape measured in moving observation from a form of time function to a function of position by interpolation. The mode shape in a form of time function can be approximated by interpolation as the summation of the products of coefficients and basis functions. These coefficients correspond to discrete mode shape.

2.3.2. Damage Identification Flow

In VO-BHM based on bridge mode shape estimation, the signals measured on the vehicle should be

transformed to bridge vibration components. In this study, the proposed method insists in 5 steps shown in Table 2.3.1.

The bridge vibration components are contained in the forced displacement of the vehicle. In first step of the proposed method, the forced displacement of the vehicle is estimated as input of the system. Herein, inverse system estimation (ISE) [8], [9] and frequency response function (FRF) are applied to vehicle vibration data for the input estimation. The difference between these two methods lies in measurements. Both vehicle acceleration response and relative displacement between vehicle and road are used in ISE, while only acceleration is used in FRF. The forced displacement of the vehicle contains not only the bridge vibration response components but also the road unevenness. In the next step, to extract only the bridge responses components, deduction of road unevenness from the forced displacement should be performed. Simple idea to extract the bridge components from the estimated forced displacement is to calculate difference between the signals measured on the different vehicles (or axles) after spatially synchronized. Then, the obtained bridge response components in second step are signals measured at moving positions, not at fixed positions. In traditional method [10], [11], [12] to estimate bridge mode shapes, sensors are assumed to be fixed on the bridge. The signals of VO-BHM cannot be used for mode shape estimation due to this moving measuring point effect. In the third step, by interpolation function to appropriate the mode shape by known basis function, the moving effect can be canceled. It also means that the moving effect canceling is one solution for the non-linearity of VBI system and that the estimated signals could be taken as measurements at the assumed fixed points. Mainly adopted interpolation is Lagrange's basis function [13]. The objective bridge responses which can be decomposed by SVD are obtained through three steps. For forth step, SVD are applied to estimated bridge responses like only-bridge-data-oriented BHM (BO-BHM). SVD assumes the de-correlation between the modal responses. This assumptions are always satisfied by signals of free vibration, stationary vibration and output vibration of the system subjected to random white noise input. But, here, the objective vibration is output due to traffic non-stationary input. Thus, their de-correlation should be examined.

STEP 1: Input estimation of vehicle system

In VO-BHM, measured signal is only output of the vehicle vibration system, but the signal to be obtained is the bridge vibration. The bridge vibration component is contained in the input of the vehicle system. To estimate input of the system, generally, frequency response function (FRF) is used in frequency domain. But, the accuracy of this method is often decreased due to the improperness of the Fourier transform [14]. Thus, the estimation results in this step should be affected by this improperness when using FRF. Inverse system estimation (ISE) [8], [9] based on the state space equation of the vehicle system is also applied to the vehicle responses. A demerit of ISE method is that not only vehicle acceleration but also relative displacement between vehicle body and road surface must be measured, while it is necessary to measure only vehicle acceleration in FRF. On the

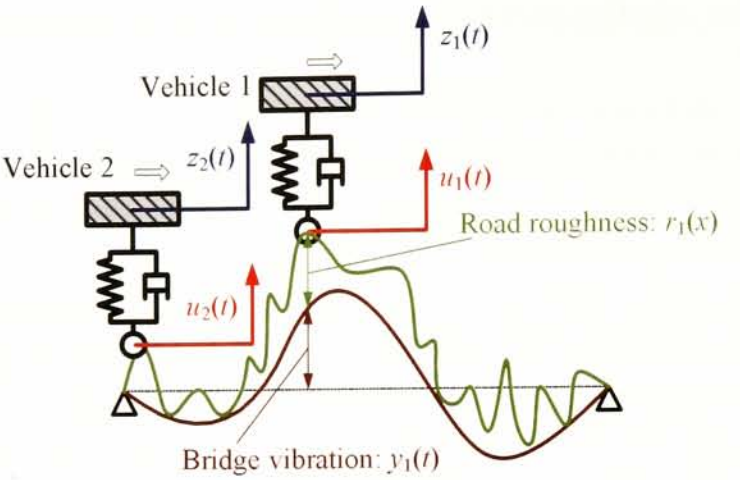

Fig. 2.3.1 Input and output of vehicle system model

contrary, FRF which is a parameter of the vehicle vibration system must be calibrated before inspection. In ISE method, it is not necessary to perform calibration of the vehicle.

(a) Frequency Response Function

One of the merits of FRF is the capability of being easily obtained. The relation between the forced displacements vector for each axles $\boldsymbol{U}(\omega) \in \mathrm{C}^{n+1}$ and the vehicle responses vector $\boldsymbol{Z}(\omega) \in \mathrm{C}^{n+1}$ in frequency domain can be described as Eq. (2.1) by FRF $\mathbf{H}(\omega) \in \mathrm{C}^{(n+1)\times(n+1)}$.

$$\boldsymbol{Z}(\omega) = \mathbf{H}(\omega)\boldsymbol{U}(\omega) \tag{2.24}$$

where it is assumed that $(n+1)$ vehicles (or axles) are applied to measure their own vibrations. To estimate $\mathbf{H}(\omega)$, it is necessary to input controlled displacement vibrations to the vehicle before actual inspection.

However, for example, letting us assume that the vehicle system is a simple spring mass model shown in Fig. 2.3.1, FRF of the vehicle vibration system is

$$H_{ii}(\omega) = \frac{j\omega c_i + k_i}{-\omega^2 m_i + j\omega c_i + k_i} \tag{2.25}$$

where m_i, c_i and k_i are mass, damping and stiffness of the i-th vehicle. j indicates imaginary unit. The input to be obtained is given by Eq. (2.24) as follows:

$$\boldsymbol{U}(\omega) = \mathbf{H}(\omega)^{-1}\boldsymbol{Z}(\omega). \tag{2.26}$$

Let us $Z_i(\omega)$ and $U_i(\omega)$ be the i-th elements of $\boldsymbol{Z}(\omega)$ and $\boldsymbol{U}(\omega)$, respectively. Then, because the order of the FRF is less than zero, estimation of output $Z_i(\omega)$ can be calculated accurately using

input $U_i(\omega)$ and $H_i(\omega)$ based on Eq. (2.24), which is a proper problem. On the other hand, for inverse estimation for input $U_i(\omega)$, because the inverse of FRF $(= \mathbf{H}(\omega)^{-1})$ has larger order than zero, the problem becomes improper and input $U_i(\omega)$ cannot be calculated from $Z_i(\omega)$ frequently.

(b) Inverse System Estimation

To overcome the improper problem of input estimation, the inverse system estimation method is sometimes proposed in existing studies [8] However, the substance of this method is twice numerical integration. Thus, indeed, the estimation accuracy depends on the sensor performance.

To apply ISE to the first step of this method, both the vehicle acceleration responses and the relative displacement between the vehicle body and the road surface must be measured. The equations of state and observation for the vehicle system can be described as Eq. (2.25) and (2.26), respectively.

$$\begin{Bmatrix} \dot{\boldsymbol{z}}(t) \\ \ddot{\boldsymbol{z}}(t) \end{Bmatrix} = \begin{bmatrix} \mathbf{O} & \mathbf{I} \\ -\mathbf{M_V}^{-1}\mathbf{K_V} & -\mathbf{M_V}^{-1}\mathbf{C_V} \end{bmatrix} \begin{Bmatrix} \boldsymbol{z}(t) \\ \dot{\boldsymbol{z}}(t) \end{Bmatrix} + \begin{bmatrix} \mathbf{O} & \mathbf{O} \\ \mathbf{M_V}^{-1}\mathbf{K_V} & \mathbf{M_V}^{-1}\mathbf{C_V} \end{bmatrix} \begin{Bmatrix} \boldsymbol{u}(t) \\ \dot{\boldsymbol{u}}(t) \end{Bmatrix} \tag{2.25}$$

$$\begin{Bmatrix} \boldsymbol{z}(t) - \boldsymbol{u}(t) \\ \ddot{\boldsymbol{z}}(t) \end{Bmatrix} = \begin{bmatrix} \mathbf{I} & \mathbf{O} \\ -\mathbf{M_V}^{-1}\mathbf{K_V} & -\mathbf{M_V}^{-1}\mathbf{C_V} \end{bmatrix} \begin{Bmatrix} \boldsymbol{z}(t) \\ \dot{\boldsymbol{z}}(t) \end{Bmatrix} + \begin{bmatrix} -\mathbf{I} & \mathbf{O} \\ \mathbf{M_V}^{-1}\mathbf{K_V} & \mathbf{M_V}^{-1}\mathbf{C_V} \end{bmatrix} \begin{Bmatrix} \boldsymbol{u}(t) \\ \dot{\boldsymbol{u}}(t) \end{Bmatrix} \tag{2.26}$$

where $\mathbf{z}(t) \in \mathrm{R}^{n+1}$, $\boldsymbol{u}(t) \in \mathrm{R}^{n+1}$, $\mathbf{M_V} \in \mathrm{R}^{(n+1)\times(n+1)}$, $\mathbf{C_V} \in \mathrm{R}^{(n+1)\times(n+1)}$, and $\mathbf{K_V} \in \mathrm{R}^{(n+1)\times(n+1)}$ are the response, input, mass matrix, damping matrix and spring stiffness matrix of the vehicle system, respectively. Relative displacement between the vehicle and the road surface equals the relative displacement $\mathbf{z}(t) - \boldsymbol{u}(t)$. $\dot{(\ )}$ and $\ddot{(\ )}$ denote first and second order derivation in time domain. Then, the inverse system equation of this state space system can be solved by using changes of a time-series signal $\boldsymbol{x}(t)$ which can be described as

$$\dot{\boldsymbol{x}}(t + \Delta t) = \frac{\boldsymbol{x}(t + \Delta t) - \boldsymbol{x}(t)}{\Delta \mathrm{t}}. \tag{2.27}$$

By substitution of Eq. (2.27), the inverse system can be rewritten as

$$\begin{Bmatrix} \mathbf{z}(t + \Delta t) \\ \dot{\mathbf{z}}(t + \Delta t) \end{Bmatrix} = \begin{bmatrix} \mathbf{I} & \Delta t\mathbf{I} \\ \mathbf{O} & \mathbf{I} \end{bmatrix} \begin{Bmatrix} \mathbf{z}(t) \\ \dot{\mathbf{z}}(t) \end{Bmatrix} + \begin{bmatrix} \mathbf{O} & \Delta t^2\mathbf{I} \\ \mathbf{O} & \Delta t\mathbf{I} \end{bmatrix} \begin{Bmatrix} \mathbf{z}(t) - \boldsymbol{u}(t) \\ \ddot{\mathbf{z}}(t) \end{Bmatrix} \tag{2.28}$$

$$\begin{Bmatrix} \boldsymbol{u}(t + \Delta t) \\ \dot{\boldsymbol{u}}(t + \Delta t) \end{Bmatrix} = \begin{Bmatrix} \mathbf{z}(t) \\ \dot{\mathbf{z}}(t) \end{Bmatrix} + \begin{bmatrix} -\mathbf{I} & \mathbf{O} \\ \mathbf{C_V}^{-1}\mathbf{K_V} & \mathbf{C_V}^{-1}\mathbf{M_V} \end{bmatrix} \begin{Bmatrix} \mathbf{z}(t + \Delta t) - \boldsymbol{u}(t + \Delta t) \\ \ddot{\mathbf{z}}(t + \Delta t) \end{Bmatrix}. \tag{2.29}$$

The system parameters $\mathbf{M_V}$, $\mathbf{C_V}$, and $\mathbf{K_V}$ are difficult to be measured. However, even if these parameters are unknown, at least, $\boldsymbol{u}(t)$ can be estimated by based on Eq. (2.28) and Eq. (2.29) while $\dot{\boldsymbol{u}}(t)$ cannot. If the system parameters can be obtained, $\dot{\boldsymbol{u}}(t)$ can be estimated to improve the

estimation accuracy of $\boldsymbol{u}(t)$. When the initial values of the state variables $\begin{Bmatrix}\mathbf{z}(0)\\ \dot{\mathbf{z}}(0)\end{Bmatrix}$ is set, by substitution of the state variables $\begin{Bmatrix}\mathbf{z}(t)\\ \dot{\mathbf{z}}(t)\end{Bmatrix}$ and the observed variables $\begin{Bmatrix}\mathbf{z}(t)-\boldsymbol{u}(t)\\ \ddot{\mathbf{z}}(t)\end{Bmatrix}$ to Eq. (2.28), the state variables for the next step time $\begin{Bmatrix}\mathbf{z}(t+\Delta t)\\ \dot{\mathbf{z}}(t+\Delta t)\end{Bmatrix}$ can be estimated. As the results, the input values $\begin{Bmatrix}\boldsymbol{u}(t+\Delta t)\\ \dot{\boldsymbol{u}}(t+\Delta t)\end{Bmatrix}$ are calculated by Eq. (2.29).

STEP 2: Deduction of road unevenness (Extracting bridge vibration component)

The estimated input $\boldsymbol{u}(t) \in \mathrm{R}^{n+1}$ in time domain, or $\boldsymbol{U}(\omega) \in \mathrm{C}^{n+1}$ in frequency domain contains both the bridge response $\boldsymbol{y}_{\mathrm{V}}(t) \in \mathrm{R}^{n+1}$ measured at moving points and the road unevenness $\boldsymbol{r}(t)$.

$$\boldsymbol{u}(t) = \boldsymbol{y}_{\mathrm{V}}(t) + \boldsymbol{r}(t) \tag{2.30}$$

where $\boldsymbol{r}(t) \in \mathrm{R}^{n+1}$ is the road unevenness directly under the measuring points on the vehicles (or axles). In the second step of the proposed method, the road unevenness should be deducted to estimate the bridge modal parameters.

When $(n+1)$ vehicles (or axles) are assumed to measure their own vibrations, the maximum order of the bridge mode to be considered in this method is n.

Now, by following the superposition principle of vibration theory, bridge vibration can be given by using bridge mode shapes of k-th order $\phi_k(x)$ and modal responses $q_k(t)$ in the form.

$$y(x,t) = \sum_{k=1}^{n} \phi_k(x)\, q_k(t) \tag{2.31}$$

where x and t denote position and time, respectively. Here, bridge is modeled as one-dimensional beam. The bridge length is L.

Then, letting us assume the difference of two displacements at different positions corresponding to two vehicles. The difference can be expressed as

$$\tilde{y}_i(t) \equiv y(\tilde{x}_i, t) - y(\tilde{x}_{i+1}, t + s\Delta t) = \sum_{k=1}^{n} \phi_k(\tilde{x}_i)\,\{q_k(t) - q_k(t+\Delta t)\} \tag{2.32}$$

where $\tilde{x}_i$ denotes the position of the moving vehicle or axle i. In this case, the positions of the

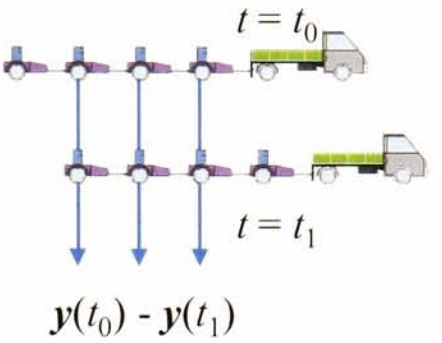

Fig. 2.2.2 Spatial synchronization for deduction of road profile by a trailer system

vehicles must satisfy the following condition:

$$\tilde{x}_{i+1}(t + \Delta t) = \tilde{x}_i(t) \tag{2.33}$$

where Δt is time difference determined by the vehicle speed and intervals. To satisfy this assumption, the vehicles must run over the exactly same pathway with equal intervals in this method. When the measuring vehicle is assumed to be a trailer system such as shown in Fig. 2.2.2, the assumption could be easier to be satisfied. Eq. (2.32) can be rewritten as

$$\begin{aligned} \tilde{\boldsymbol{y}}(t) &= \boldsymbol{\Phi}(t)\tilde{\boldsymbol{q}}(t) \\ &= \boldsymbol{\Phi}(t)\{\boldsymbol{q}(t) - \boldsymbol{q}(t + \Delta t)\} \end{aligned} \tag{2.34}$$

where $\tilde{\boldsymbol{y}}(t) \in \mathrm{R}^n$, $\boldsymbol{q}(t) \in \mathrm{R}^n$ and $\tilde{\boldsymbol{q}}(t) \in \mathrm{R}^n$ are bridge response component vector, modal response vector and modal response component vector, respectively. The (i, j) element of $\boldsymbol{\Phi}(t)$ is the i-th order mode shape at the location of $\tilde{x}_j(t)$.

Now, letting $u_i(t)$ be i-th element of vector $\tilde{\boldsymbol{u}}(t)$, the bridge response component $\tilde{\boldsymbol{y}}(t)$ can be also obtained by subtraction $u_i(t)$ from $u_{i+1}(t + \Delta t)$ asfollows:

$$\begin{aligned} \tilde{u}_i(t) &\equiv u_i(t) - u_{i+1}(t + \Delta t) \\ &= \{y(x_i(t), t) + r(x_i(t))\} - \{y(x_{i+1}(t + \Delta t), t + \Delta t) + r(x_{i+1}(t + \Delta t))\} \\ &= \{y(x_i(t), t) + r(x_i(t))\} - \{y(x_i(t), t + \Delta t) + r(x_i(t))\} \\ &= \{y(x_i(t), t) - y(x_i(t), t + \Delta t)\} + \{r(x_i(t)) - r(x_i(t))\} \\ &= y(x_i(t), t) - y(x_i(t), t + \Delta t) = \tilde{y}_i(t) \end{aligned} \tag{2.35}$$

where $\tilde{y}_i(t)$ and $r(x_i(t))$ are i-th elements of $\tilde{\boldsymbol{y}}(t)$ and $\boldsymbol{r}(t)$, respectively.

For example, when $n = 3$, $\boldsymbol{\Phi}(t)$ is described as

$$\boldsymbol{\Phi}(t) = \begin{bmatrix} \phi_1(\tilde{x}_1(t)) & \phi_2(\tilde{x}_1(t)) & \phi_3(\tilde{x}_1(t)) \\ \phi_1(\tilde{x}_2(t)) & \phi_2(\tilde{x}_2(t)) & \phi_3(\tilde{x}_2(t)) \\ \phi_1(\tilde{x}_3(t)) & \phi_2(\tilde{x}_3(t)) & \phi_3(\tilde{x}_3(t)) \end{bmatrix}. \tag{2.36}$$

STEP 3: Moving observation effect canceling

The estimated bridge response components $\tilde{\boldsymbol{y}}(t)$ contain the information of bridge mode shape. The form of the information is different from the measurements at the fixed points on the bridge. Here, the bridge response components measured at the fixed points on the bridge $\hat{\boldsymbol{y}}(t) \in \mathrm{R}^n$, which is the difference of the bridge displacement responses between at the time of t and $t + \Delta t$, can be described as

$$\hat{\boldsymbol{y}}(t) = \mathbf{A}\tilde{\boldsymbol{q}}(t) \tag{2.37}$$

where $\mathbf{A} \in \mathrm{R}^{n \times n}$ is the discrete mode shape matrix. The (i, j) element of $\mathbf{A} \in \mathrm{R}^{n \times n}$ is the i-th mode shape amplitude at the j-th measuring point. The number of the assumed measuring points are n. Then, mode shape function $\phi_k(x)$ can be approximated by n basis functions $\bar{\boldsymbol{N}}(x) \in \mathrm{R}^n$.

$$\phi_k(x) = \bar{\boldsymbol{N}}(x)\boldsymbol{A}_k \tag{2.38}$$

where $\boldsymbol{A}_k \in \mathrm{R}^n$ is the k-th column of the discrete mode shape matrix $\mathbf{A}$. The summation of basis functions matrix $\bar{\boldsymbol{N}}(x)$ should always be 1.

$$\sum_{j=1}^{n} N_j(x) = 1 \tag{2.39}$$

where $N_j(x)$ is the j-th element of the basis function vector $\bar{\boldsymbol{N}}(x)$. And, $\bar{\boldsymbol{N}}(x)$ must also satisfy below

$$N_j(\hat{x}_l) = \begin{cases} 1 \ldots (l = j) \\ 0 \ldots (l \neq j) \end{cases} \tag{2.40}$$

where $\hat{x}_l$ means the l-th measuring points. We can find many basis functions satisfying these conditions. For example, Lagrange interpolation exactly satisfy Eq. (2.39) and Eq. (2.40). On the other hand, while Cardinal sine function satisfy Eq. (2.39) but does not satisfy Eq. (2.40), its interpolation gives good results in stable. If these conditions are not satisfied, the assumed $\mathbf{A}$ is not same with the mode shape matrix.

The (i, j) element of the interpolation matrix $\mathbf{N}(t)$ is defined as

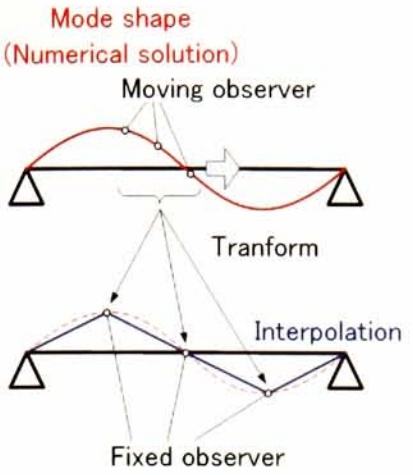

Fig. 2.2.3 Basic concept of interpolation in mode-shape-based VO-BHM

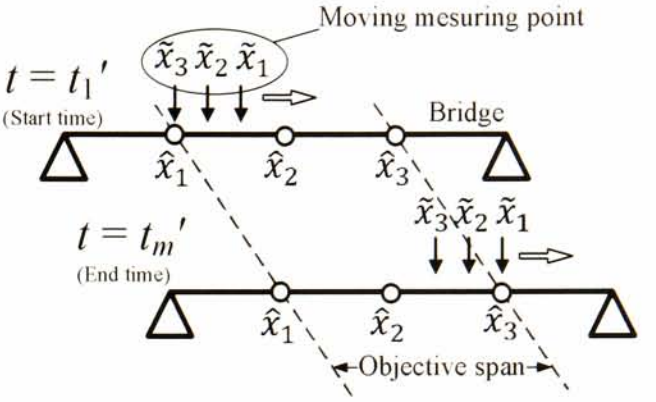

Fig. 2.2.4 Objective time

$$\mathrm{N}_{ij}(t) = N_j\big(\tilde{x}_i(t)\big) \tag{2.41}$$

where $\tilde{x}_i$ is the function of time which indicates the position of the i-th measuring points. By using the interpolation matrix $\mathbf{N}(t)$, the mode shape information matrix $\boldsymbol{\Phi}(t)$ can be rewritten as

$$\boldsymbol{\Phi}(t) = \mathbf{N}(t)\mathbf{A} \tag{2.42}$$

By applying this approximate expression to the estimated signals, the measurements at the moving points can be transformed to the measurements at the fixed points. The estimated bridge response components at the moving points $\tilde{\boldsymbol{y}}(t)$ can be described as

$$\tilde{\boldsymbol{y}}(t) = \boldsymbol{\Phi}(t)\tilde{\boldsymbol{q}}(t) = \mathbf{N}(t)\mathbf{A}\tilde{\boldsymbol{q}}(t) \tag{2.43}$$

The bridge response components at the assumed fixed points $\hat{\boldsymbol{y}}(t)$ can be calculated by the follows:

$$\hat{\boldsymbol{y}}(t) = \mathbf{N}(t)^{-1}\tilde{\boldsymbol{y}}(t) = \mathbf{A}\tilde{\boldsymbol{q}}(t) \tag{2.44}$$

where $[\ \ ]^{-1}$ indicates inverse matrix. This relational expression can be calculated only during the vehicles passing inside between the first and last assumed measuring points. In other words, the objective time range is from the time when the last vehicle or axle enters the first fixed point $\hat{x}_1$ to the time when the first vehicle or axle reaches the last fixed points $\hat{x}_n$, such as shown in Fig. 2.2.4.

(a) Lagrange interpolation

Then, Lagrange interpolation [14] can be described as

$$N_j(x) = \left(\frac{n+1}{L}\right)^{n-1} \prod_{\substack{l=1 \\ (l \neq j)}}^{n} \frac{x - \hat{x}_l}{j - l}. \tag{2.45}$$

where $\prod(\ \ )$ means the multiplication of all elements. For example, $\prod_{k=1}^{n} a_k = a_1 \times a_2 \times \ldots \times a_n$. And, $\hat{x}_l$ is the assumed fixed points and should be set at equal interval on the bridge.

(b) Cardinal sine interpolation

For interpolation, you can use any basis function. Although Cardinal sine function [15] cannot satisfy the condition of Eq. (2.39), it is stable and easy to be installed. The basis function based on the Cardinal sine function can be described as

$$N_j(x) = \mathrm{sinc}\left(\frac{x - x_l}{L}\right) = \frac{\sin\left(\frac{\pi(x - x_l)}{L}\right)}{\frac{\pi(x - x_l)}{L}}. \tag{2.46}$$

(c) Trigonometrical functions interpolation

Because mode shapes are generally almost same even after serious damage, basis function can be assumed mode shape itself such as Trigonometrical functions. Eq. (2.47) can be applied for the basis function of interpolation.

$$N_j(x) = \begin{cases} \sin\left(\frac{j\pi}{L}\right) & \ldots \quad j = 2m + 1 \\ \cos\left(\frac{j\pi}{L}\right) & \ldots \quad j = 2m \end{cases} \tag{2.47}$$

where m is a counting number. When Eq. (3.26) is applied to this method, estimated $\mathbf{A}$ is not mode shape matrix any more. However, it could be a damage index because it has still the information of the mode shape.

STEP 4: Mode shape estimation

To estimate bridge mode shape in VRA, the available signals are just only bridge system outputs. Because of that, an output-only identification method must be applied. One of the methods is Singular Value Decomposition (SVD) method.

SVD itself is one of the orthogonal decomposition methods. Optional matrix $\widetilde{\mathbf{Y}} \in R^{n \times m}$ can be decomposed such as

$$\widehat{\mathbf{Y}} = \mathbf{U}\boldsymbol{\Sigma}\mathbf{V}^{\mathrm{T}} \tag{2.48}$$

where $\mathbf{U} \in R^{n\times n}$ and $\mathbf{V} \in R^{n\times m}$ are orthogonal matrices, and $\mathbf{\Sigma} \in R^{n\times n}$ is a diagonal matrix. n and m are the number of measurements and data number, respectively. When $\hat{\mathbf{Y}}$ is the bridge response component data matrix estimated by step 3, $\mathbf{U}$ and $\mathbf{\Sigma V}^{\mathrm{T}}$ are estimated mode shape matrix and modal response components as normalization of the maximum of each column of $\mathbf{U}$. SVD assumes that the modal response components are de-correlation with each other. In brief, the following condition equation is assumed to be satisfied.

$$\hat{\mathbf{y}}(t)\hat{\mathbf{y}}(t)^{\mathrm{T}} = \mathbf{A}\{\tilde{\boldsymbol{q}}(t)\tilde{\boldsymbol{q}}(t)^{\mathrm{T}}\}\mathbf{A}^{\mathrm{T}} \tag{2.49}$$

where $\tilde{\boldsymbol{q}}(t)\tilde{\boldsymbol{q}}(t)^{\mathrm{T}}$ is assumed to be a diagonal matrix.

STEP 5: Damage identification based on mode shape

Finally, damage is identified on a basis of estimated mode shape of the bridge. Herein, mode accuracy criteria (MAC) [16] value is applied to evaluate the change of estimated mode shape. MAC value denotes the cross correlation between two mode shape matrices. MAC can be described as

$$\mathrm{MAC}_{kl} = \frac{\left(\sum_j \{\mathbf{A}_0\}_{jk}\{\mathbf{A}_1\}_{jl}\right)^2}{\left(\sum_j \{\mathbf{A}_0\}_{jk}^2\right)\left(\sum_j \{\mathbf{A}_1\}_{jl}^2\right)} \tag{2.50}$$

where $\mathbf{A}_0$ and $\mathbf{A}_1$ is basis and estimated mode shape matrices. When $\mathbf{A}_0$ and $\mathbf{A}_1$ are similar in shape, MAC value is close to 1. If MAC value decreases, it indicates the changes of mode shapes which may be occurred by bridge damage.

2.4. Direct Mode-Shape-based VO-BHM

2.4.1. Concept Basis

In this study, direct mode-shape-based VO-BHM method is also proposed in which the interpolation matrix directly is applied to the vehicle acceleration responses to estimate the bridge mode shape.

The accuracy of VO-BHM based on bridge mode shape depends on the characteristics of non-stationary signals and non-linear interaction between vehicle and bridge. In the previous study about vibration-based BHM [17], [18], [19], improvement of estimation accuracy is intensively studied. On the other hand, there is limitation in the estimation accuracy of bridge mode shape by VO-BHM method. Because bridge mode shape changes very slightly due to local damage, it has been difficult

to reach the required accuracy enough to identify the bridge damage, generally. The main factor decreasing the accuracy is the non-linearity due to the moving observation effect. However, this effect can be managed by the interpolation shown in the former section. While the indirect mode-shape-based VO-BHM method applies the interpolation approximation to the estimated bridge vibration, the same interpolation matrix is applied directly to measured vehicle acceleration responses in the direct mode-shape-based VO-BHM method.

This direct approach can be categorized into two methods mainly: the method using inverse interpolation matrix to solve the equation of motion of vehicle system and the method using transposed interpolation matrix to extract bridge mode shape based on the equation of motion of bridge mode system.

In both of the direct mode-shape-based VO-BHM methods, it is not necessary to know the road unevenness. Just applying interpolation matrix to vehicle response directly, bridge mode shape can be estimated. In this method, damage identification is performed by comparing the estimated mode shapes before and after damage introduced.

2.4.2. Inverse Interpolation Method

The equation of motion of the vehicle can be described as

$$\mathbf{M}_V\ddot{\boldsymbol{z}}(t) + \mathbf{C}_V\dot{\boldsymbol{z}}(t) + \mathbf{K}_V\boldsymbol{z}(t) = \mathbf{C}_P\dot{\boldsymbol{u}}(t) + \mathbf{K}_P\boldsymbol{u}(t) \tag{2.51}$$

where $\mathbf{M}_V \in R^{n\times n}$, $\mathbf{C}_V \in R^{n\times n}$ and $\mathbf{K}_V \in R^{n\times n}$ are mass, damping and spring stiffness matrices of the vehicles, and $\mathbf{C}_P \in R^{n\times n}$ and $\mathbf{K}_P \in R^{n\times n}$ are damping and spring stiffness of the vehicle for external force, respectively. When the assumed vehicle model is a simple mass-spring model, $\mathbf{C}_V$ and $\mathbf{K}_V$ are same as $\mathbf{C}_P$ and $\mathbf{K}_P$, respectively. Then, $\boldsymbol{z}(t) \in R^n$ and $\boldsymbol{u}(t) \in R^n$ are vehicle responses and forced displacement. For a half-car model, these parameters are shown in Table 2.4.1.

The input of the vehicle system $\boldsymbol{u}(t)$ can be described as

$$\boldsymbol{u}(t) = \boldsymbol{\Phi}(t)\boldsymbol{q}(t) \tag{2.52}$$

where $\boldsymbol{\Phi}(t)$ and $\boldsymbol{q}(t)$ are the bridge mode shape matrix and modal response vector. $(i,\ j)$ element of $\boldsymbol{\Phi}(t)$ can be described as

$$\Phi_{ij}(t) = \phi_j\big(x_i(t)\big) \tag{2.53}$$

where $\phi_j(x)$ is j-th mode shape and $x_i(t)$ is the position of the vehicle axle which corresponds to $z_i(t)$.

Letting us assume that the unsprung physical characteristics of the front and rear axles are

Table 2.4.1 Parameters of a half-car model

	$[\ ]_V$	$[\ ]_P$
Mass	$\begin{bmatrix} \frac{L_2 m_s}{L_1+L_2} & 0 & \frac{L_1 m_s}{L_1+L_2} & 0 \\ \frac{I_s}{L_1+L_2} & 0 & -\frac{I_s}{L_1+L_2} & 0 \\ 0 & m_{u1} & 0 & 0 \\ 0 & 0 & 0 & m_{u2} \end{bmatrix}$	$\begin{bmatrix} \frac{L_2 m_s}{L_1+L_2} & 0 & 0 & 0 \\ 0 & m_{u1} & 0 & 0 \\ 0 & 0 & \frac{L_1 m_s}{L_1+L_2} & 0 \\ 0 & 0 & 0 & m_{u2} \end{bmatrix}$
Damping	$\begin{bmatrix} c_{s1} & -c_{s1} & c_{s2} & -c_{s2} \\ L_1 c_{s1} & -L_1 c_{s1} & -L_2 c_{s1} & L_2 c_{s2} \\ -c_{s1} & c_{s1}+c_{u1} & 0 & 0 \\ 0 & 0 & -c_{s2} & c_{s2}+c_{u2} \end{bmatrix}$	$\begin{bmatrix} 0 & 0 & 0 & 0 \\ 0 & 0 & 0 & 0 \\ 0 & c_{u1} & 0 & 0 \\ 0 & 0 & 0 & c_{u2} \end{bmatrix}$
Stiffness	$\begin{bmatrix} k_{s1} & -k_{s1} & k_{s2} & -k_{s2} \\ L_1 k_{s1} & -L_1 k_{s1} & -L_2 k_{s1} & L_2 k_{s2} \\ -k_{s1} & k_{s1}+k_{u1} & 0 & 0 \\ 0 & 0 & -k_{s2} & k_{s2}+k_{u2} \end{bmatrix}$	$\begin{bmatrix} 0 & 0 & 0 & 0 \\ 0 & 0 & 0 & 0 \\ 0 & k_{u1} & 0 & 0 \\ 0 & 0 & 0 & k_{u2} \end{bmatrix}$

*) $\boldsymbol{z}(t) = \{z_{s1}(t) \quad z_{u1}(t) \quad z_{s2}(t) \quad z_{u2}(t)\}^{\mathrm{T}}$

identical, Eq. (2.51) becomes

$$\begin{Bmatrix} \ddot{z}_{u1}(t) \\ \ddot{z}_{u2}(t) \end{Bmatrix} = \boldsymbol{\Phi}(t)\boldsymbol{\sigma}(t) - \bar{\boldsymbol{\varepsilon}}(t) \tag{2.54}$$

where,

$$\boldsymbol{\sigma}(t) = \frac{c_u}{m_u}\dot{\boldsymbol{q}}(t) + \frac{k_u}{m_u}\boldsymbol{q}(t) \tag{2.55}$$

$$\begin{aligned} \bar{\boldsymbol{\varepsilon}}(t) = {} & \frac{1}{m_u}\begin{bmatrix} -c_{s1} & c_{s1}+c_u & 0 & 0 \\ 0 & 0 & -c_{s2} & c_{s2}+c_u \end{bmatrix}\dot{\boldsymbol{z}}(t) - \frac{c_u}{m_u}\dot{\boldsymbol{r}}(t) \\ & + \frac{1}{m_u}\begin{bmatrix} -k_{s1} & k_{s1}+k_u & 0 & 0 \\ 0 & 0 & -k_{s2} & k_{s2}+k_u \end{bmatrix}\boldsymbol{z}(t) - \frac{k_u}{m_u}\boldsymbol{r}(t). \end{aligned} \tag{2.56}$$

Here, m_u, c_u and k_u are unsprung-mass, damping and stiffness.

by applying the $\mathbf{N}(t)$ to the $\boldsymbol{\Phi}(t)$ for approximation, the directly estimation equation for VBI can be obtained as follows:

$$\mathbf{N}^{-1}(t)\begin{Bmatrix} \ddot{z}_{u1}(t) \\ \ddot{z}_{u2}(t) \end{Bmatrix} = \mathbf{A}\boldsymbol{\sigma}(t) - \boldsymbol{\varepsilon}(t) \tag{2.57}$$

where the error term is

$$\boldsymbol{\varepsilon}(t) = \mathbf{N}^{-1}(t)\bar{\boldsymbol{\varepsilon}}(t) \tag{2.58}$$

In this method, $\boldsymbol{\sigma}(t)$ and $\boldsymbol{\varepsilon}(t)$ denote bridge mode response components and error term, respectively. If $\boldsymbol{\sigma}(t)$ and $\boldsymbol{\varepsilon}(t)$ are de-correlation signals, $\mathbf{A}$ can be estimated by SVD of $\mathbf{N}^{-1}(t)\begin{Bmatrix}\ddot{z}_{u1}(t)\\ \ddot{z}_{u2}(t)\end{Bmatrix}$. In this study, damage changes of $\mathbf{A}$ is examined in aspect of the de-correlation of $\boldsymbol{\sigma}(t)$.

2.4.3. Transposed Interpolation Method

In the finite element method (FEM) model whose degree of freedom (DOF) is d for bridge, the equation of motion of the bridge is given by the displacement vector $\boldsymbol{y}(t) \in \mathrm{R}^d$, the mass matrix $\mathbf{M}_\mathrm{B} \in \mathrm{R}^{d\times d}$, the damping matrix $\mathbf{C}_\mathrm{B} \in \mathrm{R}^{d\times d}$ and the stiffness matrix $\mathbf{K}_\mathrm{B} \in \mathrm{R}^{d\times d}$ in the form as.

$$\mathbf{M}_\mathrm{B}\ddot{\boldsymbol{y}}(t) + \mathbf{C}_\mathrm{B}\dot{\boldsymbol{y}}(t) + \mathbf{K}_\mathrm{B}\boldsymbol{y}(t) = \mathbf{L}(t)\boldsymbol{P}(t) \tag{2.59}$$

where $\boldsymbol{P}(t) \in \mathrm{R}^n$ is the contact force vector and $\mathbf{L}(t) \in \mathrm{R}^{m\times n}$ is the equivalent load matrix. $\dot{(\ )}$ and $\ddot{(\ )}$ mean the first and second order temporal derivative, respectively. The each element of $\boldsymbol{y}(t)$ corresponds to the displacement of each node.

On the other hand, the displacement $\boldsymbol{y}(t)$ of the bridge can be described as the summation of the products of spatial functions and temporary functions as follows:

$$\boldsymbol{y}(t) = \mathbf{X}\boldsymbol{q}(t) \tag{2.60}$$

where $\mathbf{X} \in \mathrm{R}^{d\times m}$ and $\boldsymbol{q} \in \mathrm{R}^m$ are mode shape matrix and modal response vector, respectively. The k-th column of the mode shape matrix $\mathbf{X}$ corresponds to the k-th mode shape. Then, Eq. (2.59) can be rewritten by substitution of Eq. (2.60) and by multiplied $\mathbf{X}^\mathrm{T}$ from the left side as follows:

$$\mathbf{M}_\mathrm{X}\ddot{\boldsymbol{q}}(t) + \mathbf{C}_\mathrm{X}\dot{\boldsymbol{q}}(t) + \mathbf{K}_\mathrm{X}\boldsymbol{q}(t) = \mathbf{X}^\mathrm{T}\mathbf{L}(t)\boldsymbol{P}(t) \tag{2.61}$$

where $\mathbf{M}_\mathrm{X} = \mathbf{X}^\mathrm{T}\mathbf{M}_\mathrm{B}\mathbf{X}$, $\mathbf{C}_\mathrm{X} = \mathbf{X}^\mathrm{T}\mathbf{C}_\mathrm{B}\mathbf{X}$ and $\mathbf{K}_\mathrm{X} = \mathbf{X}^\mathrm{T}\mathbf{K}_\mathrm{B}\mathbf{X}$ are modal mass, damping, stiffness matrices. Then, bridge damping is generally very small and negligible. Herein, $\mathbf{X}^\mathrm{T}\mathbf{L}(t)$ can be approximated as $\mathbf{A}^\mathrm{T}\mathbf{N}^\mathrm{T}(t)$ of which size may be smaller. The contact force can be described as Eq. (2.62).

$$\boldsymbol{P}(t) = \mathbf{M}_\mathrm{P}\big(\boldsymbol{g} - \ddot{\boldsymbol{z}}(t)\big) \tag{2.62}$$

where $\mathbf{M}_\mathrm{P} \in \mathrm{R}^{n\times n}$ is the mass matrix of the vehicles for calculation of the contact forces, and $\boldsymbol{g}$

and $\ddot{\boldsymbol{z}}(t)$ are vectors of gravity acceleration and acceleration responses of the vehicle, respectively. $\mathbf{M}_{\mathrm{P}}$ is shown in Table 2.4.1 for a half-car model. By substitution of Eq. (2.62) to Eq. (2.61) and letting us assume that $\mathbf{X}^{\mathrm{T}}\mathbf{L}(t)$ can be approximated as $\mathbf{A}^{\mathrm{T}}\mathbf{N}(t)$, the equation of motion of the bridge becomes

$$\mathbf{A}\left(\mathbf{M}_{\mathrm{X}}\ddot{\boldsymbol{q}}(t)+\mathbf{C}_{\mathrm{X}}\dot{\boldsymbol{q}}(t)+\mathbf{K}_{\mathrm{X}}\boldsymbol{q}(t)\right)=\mathbf{N}^{\mathrm{T}}(t)\mathbf{M}_{\mathrm{P}}\left(\boldsymbol{g}-\ddot{\boldsymbol{z}}(t)\right). \tag{2.63}$$

Divided by m_u, Eq. (2.63) becomes

$$\mathbf{N}^{\mathrm{T}}(t)\begin{Bmatrix}\ddot{z}_{u1}(t)\\ \ddot{z}_{u2}(t)\end{Bmatrix}=\mathbf{A}\boldsymbol{\tau}(t)+\boldsymbol{\epsilon}(t) \tag{2.64}$$

where

$$\boldsymbol{\tau}(t)=-\frac{1}{m_u}\left(\mathbf{M}_{\mathrm{X}}\ddot{\boldsymbol{q}}(t)+\mathbf{C}_{\mathrm{X}}\dot{\boldsymbol{q}}(t)+\mathbf{K}_{\mathrm{X}}\boldsymbol{q}(t)\right) \tag{2.65}$$

$$\boldsymbol{\epsilon}(t)=\mathbf{N}^{\mathrm{T}}(t)\left(\left(1+\frac{1}{2}\frac{m_{\mathrm{s}}}{m_{\mathrm{u}}}\right)\begin{Bmatrix}g\\ g\end{Bmatrix}-\frac{1}{2}\frac{m_{\mathrm{s}}}{m_{\mathrm{u}}}\begin{Bmatrix}\ddot{z}_{\mathrm{s}1}\\ \ddot{z}_{\mathrm{s}2}\end{Bmatrix}\right). \tag{2.66}$$

Based on Eq. (2.64), $\mathbf{A}$ can be estimated by SVD of $\mathbf{N}^{\mathrm{T}}(t)\begin{Bmatrix}\ddot{z}_{u1}(t)\\ \ddot{z}_{u2}(t)\end{Bmatrix}$. The uncertain factors which affect the estimation accuracy can be evaluated by the correlation degree of $\boldsymbol{\tau}(t)$ and $\boldsymbol{\epsilon}(t)$. If de-correlation both of $\boldsymbol{\tau}(t)$ and $\boldsymbol{\epsilon}(t)$ can be assumed, SVD method gives $\mathbf{A}$ as bridge mode shape matrix. When the observer is a half car, the orthogonal matrix of SVD of $\mathbf{N}^{\mathrm{T}}(t)\begin{Bmatrix}g\\ g\end{Bmatrix}$ is $\frac{1}{2}\begin{bmatrix}1 & 1\\ 1 & -1\end{bmatrix}$, which indicates the intact bridge mode shape.

2.5. Summary of this chapter

In this chapter, the three methods for bridge damage identification based on VO-BHM are proposed.

The first method is based on wavelet coefficient of the vehicle acceleration response which is non-linear function of the bridge curvature. The curvature-based VO-BHM method uses CWT to calculate wavelet coefficient of the vehicle acceleration response. This wavelet coefficient can be given in a form of non-linear function of the bridge curvature. Thus, as the bridge curvature changes due to damage, the wavelet coefficient is varied at the damage position. However, the equation of the proposed method includes a term of road profile effect. It means that the accuracy of damage identification may depend on road profile.

Next, the second proposed method is VO-BHM in which bridge mode shapes are indirectly estimated by way of estimation of bridge vibration. The second method consists in five steps to estimate the bridge response exactly based on the mode theory. To cancel the effect of moving observation, interpolation is applied to the estimated bridge responses, indirectly. The second proposed method which is damage identification by indirect mode-shape-based VO-BHM consists in five steps: Input estimation, road unevenness deduction, canceling of moving observation effect by interpolation, mode decomposition and damage identification based on estimated mode shapes. Thus, there are many uncertainties which affect the results in five steps.

On the other hand, the third method applies interpolation directly to the vehicle acceleration responses. Third method can be categorized in two methods, mainly: Methods using inverse and transposed interpolation. Both the second and third proposed methods are damage identification based on bridge mode shapes.

Reference

[1] Hester, D. and González, A.: Wavelet-based crack identification of bridge beam from operational deflection time history, Journal of Mechanical Systems and Signal Processing, Vol.28, pp.145-166, 2012.

[2] Zhu, X.Q. and Law, S.S.: Wavelet-based crack identification of bridge beam from operational deflection time history, International Journal of Solids and Structures, 43, pp.2299-2317, 2006.

[3] Nguyen, K.V. and Tran, H.T.: Multi-cracks detection of a beam-like structure based on the on-vehicle vibration signal and wavelet analysis, Journal of Sound and Vibration, Vol.329, pp.4455-4465, 2010.

[4] Yamamoto, K., Oshima, Y., Sugiura. K. and Kawano, H.: Estimation of bridge mode shapes based on vehicle responses,Journal of Japan Society of Civil Engineers, Ser. A1 (Structural Engineering & Earthquake Engineering), Vol.67, No.2, pp.242-257, 2011. (in Japanese)

[5] Kerschen, G. and Golinval, J.G.: Physical interpretation of the proper orthogonal modes using the singular value decompostion, Journal of Sound and Vibration, Vol.249(5), pp.849-865, 2002.

[6] Roveri, N. and Carcaterra A.: Damage detection in structures under traveling loads by Hilbert-Huang transform, Mechanical Systems and Signal Processing, Vol.28, pp.128-144, 2012.

[7] Pandey, A.K., Biswas, M. and Samman, M.M.: damage detection from changes in curvature mode shapes, Journal of Sound and Vibration, Vol.145(2), pp.321-332, 1991.

[8] Sasa, s. and Nagayasu, M.: Kalman filter input estimation, Technical Report of National Aerospace Laboratory, JAXA, No.1182, 1992.

[9] Silverman, L.M.: IEEE Trans Autom. Control, 14-3,270,1969

[10] Brinker, R., Zhang, L. and Andersen, P.: Modal identification of output-only systems using frequency domain decomposition, Smart Materials and Structures, Vol.10, pp.441-445, 2001.

[11] Mehrjoo, M., Khaji, N., Moharrami, H. and Bahreininejad, A.:Damage detection of truss bridge joints using Artificial Neural Networks, Journal of Expert Systems with Applications, Vol.35, pp.1122–1131, 2008.

[12] Leea,J.J. and Yunb, C.B.: Damage diagnosis of steel girder bridges using ambient vibration data, Journal of Engineering Structures, Vol.28, pp.912–925, 2006.

[13] Chakrabarti, A. and Hamsapriye: Derivation of the errors involved in interpolation and their application to numerical quadrature formulae, Journal of Computational and Applied Mathematics, Vol.98, pp.59-68, 1998.

[14] Ohkoshi, K., Kawamura, A., Shirakawa, T. and Gotoh, K.: Study on road surface measuring system by use of frequency response characteristics of a vehicle, Trans. of JSCE Hokkaido Affiliate, Vol.59, pp.734-737, 2002.

[15] Chena, Q., Wangb, Y. and Wangc, Y.: A sampling theorem for non-bandlimited signals using generalized Sinc functions, Journal of Computers and Mathematics with Applications, Vol.56, pp.1650-1661, 2008.

[16] Freiswell, M.I. and Mottershead, J.E.: Finite Element model updating in structural dynamics, Dordrecht:Kluwer Academic Publishers, pp.56-77, 1995.

[17] Yang, Y.B. and Chang, K.C.: Extracting the bridge frequencies indirectly from a passing vehicle, Parametric study, Engineering Structures, 31, pp.2448-2459, 2009.

[18] Yamamoto, K., Oshima, Y., Kim, C.W. and Sugiura, K.: Damage detection of bridges based on time frequency analysis of responces of a passing vehicle, Journal of Structural Engineering. A, JSCE, Vol.57A, pp.637-645, 2011.

[19] Kim, C.W., Isemoto, R., Kawatani, M. and Sugiura, K.: Structural diagnosis of bridge using output-only vibration in moving vehicle laboratory experiment, Journal of JSCE, Ser.A2, Vol.67, No.2 (Applied Mechanics), pp.I-833-842, 2011.

Chapter 3. Numerical Verification

3.1. General Remarks

This study presents a numerical simulation. The aim of the numerical simulation is verification about the proposed only-vehicle-data-oriented BHM (VO-BHM) methods. The each proposed method assumes that road profile must be managed. In the first method based on bridge curvature, uncertainty caused by road profile is decreased by focusing on the high frequency domain. On the other hand, the second and third methods based on mode shape assume de-correlation of signals. By comparison in changes of the vibration indices due to damage and uncertain factors numerically, the mechanism of the influential factors in the VO-BHM can be examined. Several vehicles travel over the bridge under ideal measuring condition in the numerical simulation.

Herein, in the numerical simulation, rigid-body spring systems [1] are used for passing vehicles, while the one-dimensional beam [2] is modeled by finite element method (FEM) as the bridge. To calculate the dynamic behavior of the vehicle-bridge interaction (VBI) system, Newmark-β method [3] is adopted. In this chapter, first, the way of the numerical simulation based on modal analysis and Newmark-β method is explained. Then, the verification results are presented for each methods.

3.2. Numerical Simulation

3.2.1. Modal analysis based on FEM

In this study, modal analysis is used to calculate the bridge eigen-frequencies and mode shapes.

Bridge is modeled as continuous beam in the mode analysis theory. The equation of motion can be written as

$$\rho A \frac{\partial^2 y(x,t)}{\partial t^2} + C \frac{\partial y(x,t)}{\partial t} + \frac{\partial^2}{\partial x^2}\left(EI(x) \frac{\partial^2 y(x,t)}{\partial x^2} \right) = 0 \tag{3.1}$$

where ρA and C are mass and damping per unit length and $EI(x)$ is flexural stiffness of Euler-Bernoulli beam, and $y(x,t)$ is the displacement which is a function of the position x and time t. By applying FEM model with the degree of freedom (DOF) of d, the displacement, mass, damping and flexural stiffness can be expressed by the displacement vector $\boldsymbol{y}(t) \in \mathrm{R}^d$, the mass matrix $\mathbf{M}_\mathbf{B} \in \mathrm{R}^{d \times d}$, the damping matrix $\mathbf{C}_\mathbf{B} \in \mathrm{R}^{d \times d}$ and the total stiffness matrix $\mathbf{K}_\mathbf{B} \in \mathrm{R}^{d \times d}$,

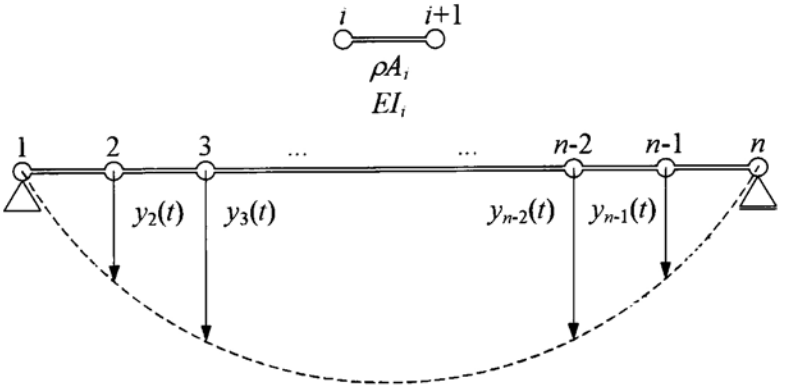

Fig. 3.2.1 Bridge model

respectively. The each component of $\boldsymbol{y}(t)$ corresponds to the displacement of each node. Eq. (3.1) can be rewritten by these vectors and matrices as

$$\mathbf{M}_{\mathrm{B}}\ddot{\boldsymbol{y}}(t) + \mathbf{C}_{\mathrm{B}}\dot{\boldsymbol{y}}(t) + \mathbf{K}_{\mathrm{B}}\boldsymbol{y}(t) = \mathbf{0} \tag{3.2}$$

where $\ddot{(\ )}$ and $\dot{(\ )}$ denote the first and second order temporal derivative, respectively. FEM model of bridge is shown in Fig. 3.2.1.

On the other hand, the displacement $y(x,t)$ of the bridge can be expressed by the summation of the products of spatial functions and temporary functions such as

$$y(x,t) = \sum_{k=1}^{m} \phi_k(x) q_k(t) = \boldsymbol{\phi}^{\mathrm{T}}(x)\boldsymbol{q}(t) \tag{3.3}$$

where the spatial function $\phi_k(x)$ is k-th mode shape which is a component of mode shape vector $\boldsymbol{\phi}^{\mathrm{T}}(x) = \{\phi_1(x), \phi_2(x), \ldots, \phi_{m-1}(x), \phi_m(x)\}^{\mathrm{T}}$, and the temporary function $q_k(t)$ is the k-th modal displacement responses which is a component of modal response vector $\boldsymbol{q}(t) = \{q_1(t), q_2(t), \ldots, q_{m-1}(t), q_m(t)\}^{\mathrm{T}}$. This equation can be also expressed by using the mode shape matrix $\mathbf{X} \in \mathrm{R}^{d\times m}$ and modal response vector $\boldsymbol{q} \in \mathrm{R}^{m}$ as

$$\boldsymbol{y}(t) = \mathbf{X}\boldsymbol{q}(t) \tag{3.4}$$

where the k-th column of the mode shape matrix $\mathbf{X}$ corresponds to the k-th mode shape $\phi_k(x)$. The maximum of the modal order considered is m. Then, the equation of motion of FEM model of the bridge [2] can be given by substitution of Eq. (3.4) and by multiplied $\mathbf{X}^{\mathrm{T}}$ from the left side in the form of

$$\mathbf{M}_X\ddot{\boldsymbol{q}}(t) + \mathbf{C}_X\dot{\boldsymbol{q}}(t) + \mathbf{K}_X\boldsymbol{q}(t) = \mathbf{0} \tag{3.5}$$

where $\mathbf{M}_X = \mathbf{X}^T\mathbf{M}_B\mathbf{X}$, $\mathbf{C}_X = \mathbf{X}^T\mathbf{C}_B\mathbf{X}$ and $\mathbf{K}_X = \mathbf{X}^T\mathbf{K}_B\mathbf{X}$ are modal mass, damping, stiffness matrices. Because bridge damping is generally very small, the second term in Eq. (3.5) can be negligible. Free vibration $\boldsymbol{q}(t) = a\exp(j\boldsymbol{\omega}t)$ is one of the solutions, and because mode shape $\mathbf{X}$ is orthogonal matrix, Eq. (3.5) becomes

$$(-\mathbf{X}^T\mathbf{M}_B\mathbf{X}\,\mathrm{diag}(\boldsymbol{\omega}^2) + \mathbf{X}^T\mathbf{K}_B\mathbf{X})a\exp(j\boldsymbol{\omega}t) = \mathbf{0} \tag{3.6}$$

In order to have a solution of Eq. (3.5) over $\boldsymbol{q}(t)$, the following equation is given by Eq. (3.6) in the form of

$$\mathbf{M}_B^{-1}\mathbf{K}_B = \mathbf{X}\,\mathrm{diag}(\boldsymbol{\omega}^2)\,\mathbf{X}^T \tag{3.7}$$

where $\boldsymbol{\omega} \in \mathrm{R}^m$ is modal angular frequency vector and diag( ) means a diagonal matrix of which elements correspond to input vector. $\mathbf{X}$ and $\boldsymbol{\omega}$ can be calculated by singular value decomposition (SVD) of $\mathbf{M}_B^{-1}\mathbf{K}_B$.

3.2.2. The equation of motion of VBI system

The equation of motion for bridge subjecting to several loads can be expressed as

$$\rho A\frac{\partial^2 y(x,t)}{\partial t^2} + C\frac{\partial y(x,t)}{\partial t} + \frac{\partial^2}{\partial x^2}\left(EI(x)\frac{\partial^2 y(x,t)}{\partial x^2}\right) = \sum_{i=1}^{n} P_i(t)\delta(x-\tilde{x}_i) \tag{3.8}$$

where $\tilde{x}_i$ is the position of the i-th loads $P_i(t)$ and n is the number of the loads. $\delta(x)$ is the Dirac delta function. In the same way, the equation of motion of VBI system can be given by substitution of $\mathbf{X}$ and $\boldsymbol{q}(t)$ to Eq. (3.8) in the form of

$$\mathbf{M}_X\ddot{\boldsymbol{q}}(t) + \mathbf{C}_X\dot{\boldsymbol{q}}(t) + \mathbf{K}_X\boldsymbol{q}(t) = \mathbf{X}^T\mathbf{L}(t)\boldsymbol{P}(t) \tag{3.9}$$

where $\boldsymbol{P}(t) \in \mathrm{R}^n$ is the contact force vector and $\mathbf{L}(t) \in \mathrm{R}^{m\times n}$ is the equivalent load matrix. This equivalent load matrix $\mathbf{L}(t)$ transforms a concentric load $P_i(t)$ at $\tilde{x}_i$ to two loads and two moments applying to nodes under the same deflections and slope-deflections of the nodes.

On the other hand, the equation of motion of "n" vehicles can be expressed as

$$\mathbf{M}_V\ddot{\boldsymbol{z}}(t) + \mathbf{C}_V\dot{\boldsymbol{z}}(t) + \mathbf{K}_V\boldsymbol{z}(t) = \mathbf{C}_P\dot{\boldsymbol{u}}(t) + \mathbf{K}_P\boldsymbol{u}(t) \tag{3.10}$$

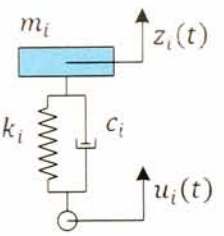

(a) Simple mass spring model

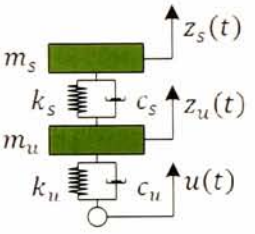

(b) Quarter-car model

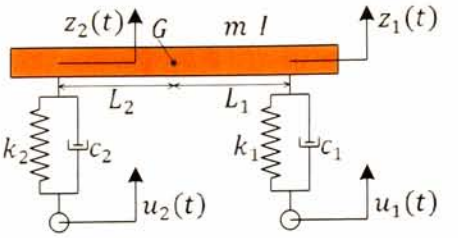

(c) Simple 2 Axles model

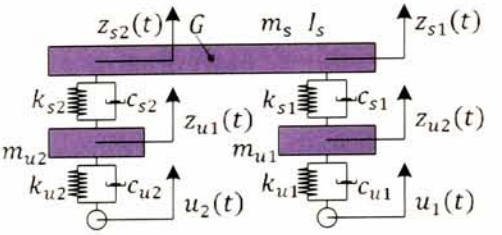

(d) Half-car model

Fig. 3.2.2 Vehicle model

where $\boldsymbol{z}(t) \in \mathrm{R}^n$ and $\boldsymbol{u}(t) \in \mathrm{R}^n$ are vehicle responses and forced displacement, and $\mathbf{M}_\mathrm{V} \in \mathrm{R}^{n\times n}$, $\mathbf{C}_\mathrm{V} \in \mathrm{R}^{n\times n}$ and $\mathbf{K}_\mathrm{V} \in \mathrm{R}^{n\times n}$ are the mass, damping and spring stiffness matrices of the vehicles, and $\mathbf{C}_\mathrm{P} \in \mathrm{R}^{n\times n}$ and $\mathbf{K}_\mathrm{P} \in \mathrm{R}^{n\times n}$ are damping and spring stiffness of the vehicle for external force, respectively. $\mathbf{M}_\mathrm{V}$, $\mathbf{C}_\mathrm{V}$ and $\mathbf{K}_\mathrm{V}$ are shown in Table 3.2.1. The equation of motion for vehicle is different depending on the vehicle model. When the assumed vehicle model is a simple mass-spring model, $\mathbf{C}_\mathrm{V}$ and $\mathbf{K}_\mathrm{V}$ are the same as $\mathbf{C}_\mathrm{P}$ and $\mathbf{K}_\mathrm{P}$, respectively.

The contact force vector $\boldsymbol{P}(t)$ can be given by vehicle response $\ddot{\boldsymbol{z}}(t)$ in the form of

$$\boldsymbol{P}(t) = \mathbf{M}_\mathrm{P}\big(\boldsymbol{g} - \ddot{\boldsymbol{z}}(t)\big) \tag{3.11}$$

where $\mathbf{M}_\mathrm{P} \in \mathrm{R}^{n\times n}$ is the mass matrix of the vehicles for calculation of the contact forces which is also shown in Table 3.2.1, and $\boldsymbol{g}$ is a constant vector of gravity acceleration.

For example, when the vehicles are modeled as simple mass-spring model shown in Fig. 3.2.2 (a), the equation of motion of the i-th vehicle is

$$m_i\ddot{z}_i(t) + c_i\dot{z}_i(t) + k_i z_i(t) = c_i\dot{u}_i + k_i u_i \tag{3.12}$$

where m_i, c_i, k_i, z_i and u_i are the mass, damping, spring stiffness, response and forced displacement of the vehicle, respectively. The forced displacement is the summation of the bridge responses component $y(\tilde{x}_i, t)$ and the road unevenness $r(x)$.

$$u_i(t) = y(\tilde{x}_i, t) + r\big(\tilde{x}_i(t)\big) \tag{3.13}$$

The contact force is the weight of each vehicle axles. When the vehicles are modeled as

Table 3.2.1 Vehicle properties for each model

(a) Simple mass spring model

	$[\ ]_V$	$[\ ]_P$
Mass	$\begin{bmatrix} \ddots & & \\ & m_i & \\ & & \ddots \end{bmatrix}$	$\begin{bmatrix} \ddots & & \\ & m_i & \\ & & \ddots \end{bmatrix}$
Damping	$\begin{bmatrix} \ddots & & \\ & c_i & \\ & & \ddots \end{bmatrix}$	$\begin{bmatrix} \ddots & & \\ & c_i & \\ & & \ddots \end{bmatrix}$
Stiffness	$\begin{bmatrix} \ddots & & \\ & k_i & \\ & & \ddots \end{bmatrix}$	$\begin{bmatrix} \ddots & & \\ & k_i & \\ & & \ddots \end{bmatrix}$

(b) Quarter-car model

	$[\ ]_V$	$[\ ]_P$
Mass	$\begin{bmatrix} m_s & 0 \\ 0 & m_u \end{bmatrix}$	$\begin{bmatrix} m_s & 0 \\ 0 & m_u \end{bmatrix}$
Damping	$\begin{bmatrix} c_s & -c_s \\ -c_s & c_s + c_u \end{bmatrix}$	$\begin{bmatrix} 0 & 0 \\ 0 & c_u \end{bmatrix}$
Stiffness	$\begin{bmatrix} k_s & -k_s \\ -k_s & k_s + k_u \end{bmatrix}$	$\begin{bmatrix} 0 & 0 \\ 0 & k_u \end{bmatrix}$

(c) Simple 2 Axles model

	$[\ ]_V$	$[\ ]_P$
Mass	$\begin{bmatrix} \frac{L_2 m_s}{L_1 + L_2} & \frac{L_1 m_s}{L_1 + L_2} \\ \frac{I_s}{L_1 + L_2} & -\frac{I_s}{L_1 + L_2} \end{bmatrix}$	$\begin{bmatrix} \frac{L_2 m_s}{L_1 + L_2} & 0 \\ 0 & \frac{L_1 m_s}{L_1 + L_2} \end{bmatrix}$
Damping	$\begin{bmatrix} c_1 & c_2 \\ L_1 c_1 & -L_1 c_2 \end{bmatrix}$	$\begin{bmatrix} c_1 & c_2 \\ L_1 c_1 & -L_1 c_2 \end{bmatrix}$
Stiffness	$\begin{bmatrix} k_1 & k_2 \\ L_1 k_1 & -L_1 k_2 \end{bmatrix}$	$\begin{bmatrix} k_1 & k_2 \\ L_1 k_1 & -L_1 k_2 \end{bmatrix}$

(d) Half-car model

	$[\ ]_V$	$[\ ]_P$
Mass	$\begin{bmatrix} \frac{L_2 m_s}{L_1 + L_2} & 0 & \frac{L_1 m_s}{L_1 + L_2} & 0 \\ \frac{I_s}{L_1 + L_2} & 0 & -\frac{I_s}{L_1 + L_2} & 0 \\ 0 & m_{u1} & 0 & 0 \\ 0 & 0 & 0 & m_{u2} \end{bmatrix}$	$\begin{bmatrix} \frac{L_2 m_s}{L_1 + L_2} & 0 & 0 & 0 \\ 0 & m_{u1} & 0 & 0 \\ 0 & 0 & \frac{L_1 m_s}{L_1 + L_2} & 0 \\ 0 & 0 & 0 & m_{u2} \end{bmatrix}$
Damping	$\begin{bmatrix} c_{s1} & -c_{s1} & c_{s2} & -c_{s2} \\ L_1 c_{s1} & -L_1 c_{s1} & -L_2 c_{s1} & L_2 c_{s2} \\ -c_{s1} & c_{s1} + c_{u1} & 0 & 0 \\ 0 & 0 & -c_{s2} & c_{s2} + c_{u2} \end{bmatrix}$	$\begin{bmatrix} 0 & 0 & 0 & 0 \\ 0 & 0 & 0 & 0 \\ 0 & c_{u1} & 0 & 0 \\ 0 & 0 & 0 & c_{u2} \end{bmatrix}$
Stiffness	$\begin{bmatrix} k_{s1} & -k_{s1} & k_{s2} & -k_{s2} \\ L_1 k_{s1} & -L_1 k_{s1} & -L_2 k_{s1} & L_2 k_{s2} \\ -k_{s1} & k_{s1} + k_{u1} & 0 & 0 \\ 0 & 0 & -k_{s2} & k_{s2} + k_{u2} \end{bmatrix}$	$\begin{bmatrix} 0 & 0 & 0 & 0 \\ 0 & 0 & 0 & 0 \\ 0 & k_{u1} & 0 & 0 \\ 0 & 0 & 0 & k_{u2} \end{bmatrix}$

*) For (d) half-car model, $\boldsymbol{z}(t) = \{z_{s1}(t) \quad z_{u1}(t) \quad z_{s2}(t) \quad z_{u2}(t)\}^T$

simple mass-spring model shown in Fig. 3.2.2 (a), the element of the vector $\boldsymbol{P}(t)$ is $P_i(t)$ and it can be described as

$$P_i(t) = m_i\big(g - \ddot{z}_i(t)\big) \tag{3.14}$$

where m_i, g and $\ddot{z}_i(t)$ are the mass of the i-th vehicle, gravitational acceleration and the acceleration responses of the i-th vehicle, respectively. When a vehicle is modeled as the quarter-car model shown in Fig. 3.2.2 (b), the equation of motion of the vehicle can be expressed by

$$m_s\ddot{z}_s(t) + c_s\dot{z}_s(t) + k_s z_s(t) = c_s\dot{z}_u(t) + k_s z_u(t) \tag{3.15}$$

$$\begin{aligned} m_u\ddot{z}_u(t) + c_u\dot{z}_u(t) + k_u z_u(t) \\ = c_s\big(\dot{z}_s(t) - \dot{z}_u(t)\big) + k_s\big(z_s(t) - z_u(t)\big) + c_u\dot{u}(t) + k_u u(t). \end{aligned} \tag{3.16}$$

The equation of motion for quarter-car model can be given by Eq. (3.15) and Eq. (3.16) in the form of

$$\begin{aligned} &\begin{bmatrix} m_s & 0 \\ 0 & m_u \end{bmatrix}\begin{Bmatrix} \ddot{z}_s(t) \\ \ddot{z}_u(t) \end{Bmatrix} + \begin{bmatrix} c_s & -c_s \\ -c_s & c_s + c_u \end{bmatrix}\begin{Bmatrix} \dot{z}_s(t) \\ \dot{z}_u(t) \end{Bmatrix} + \begin{bmatrix} k_s & -k_s \\ -k_s & k_s + k_u \end{bmatrix}\begin{Bmatrix} z_s(t) \\ z_u(t) \end{Bmatrix} \\ &\qquad = \begin{bmatrix} 0 & 0 \\ 0 & c_u \end{bmatrix}\begin{Bmatrix} \dot{u}_s(t) \\ \dot{u}_u(t) \end{Bmatrix} + \begin{bmatrix} 0 & 0 \\ 0 & k_u \end{bmatrix}\begin{Bmatrix} u_s(t) \\ u_u(t) \end{Bmatrix} \end{aligned} \tag{3.17}$$

where the subscript s and u denote sprung and unsprung. In Eq. (3.15), it can be confirmed that $[\ ]_V$ and $[\ ]_P$ are different. The length of $\boldsymbol{u}(t)$ is the same as the DOF of the vehicle. Letting us assuming that $u_s(t) = u_u(t)$, the forced displacement of the sprung mass $u_s(t)$ is always multiplied by zero in order to describe the vehicle system comprehensively.

For the quarter-car model, the contact force becomes

$$\begin{Bmatrix} P_s(t) \\ P_u(t) \end{Bmatrix} = \begin{bmatrix} m_s & 0 \\ 0 & m_u \end{bmatrix}\left(\begin{Bmatrix} g \\ g \end{Bmatrix} - \begin{Bmatrix} \ddot{z}_s(t) \\ \ddot{z}_u(t) \end{Bmatrix}\right). \tag{3.18}$$

The matrices of the vehicle property depending on the model type are shown in Table 3.2.1. The forced displacement vector $\boldsymbol{u}(t)$ can be given by using mode shape matrix $\mathbf{X}$ and the equivalent loading matrix $\mathbf{L}(t)$ in the form of

$$\boldsymbol{u}(t) = \mathbf{L}^{\mathrm{T}}(t)\mathbf{X}\boldsymbol{q}(t) + \boldsymbol{r}(t) \tag{2.19}$$

By using Eq. (3.9), Eq. (3.10), Eq. (3.11) and Eq. (3.19), the equation of motion of "VBI system" can be described as

$$\begin{bmatrix} \mathbf{M}_X & \mathbf{X}^T\mathbf{L}(t)\mathbf{M}_P \\ \mathbf{0} & \mathbf{M}_V \end{bmatrix} \begin{Bmatrix} \ddot{\boldsymbol{q}}(t) \\ \ddot{\boldsymbol{z}}(t) \end{Bmatrix} + \begin{bmatrix} \mathbf{C}_X & \mathbf{0} \\ -\mathbf{C}_P\mathbf{L}^T(t)\mathbf{X} & \mathbf{C}_V \end{bmatrix} \begin{Bmatrix} \dot{\boldsymbol{q}}(t) \\ \dot{\boldsymbol{z}}(t) \end{Bmatrix} + \begin{bmatrix} \mathbf{K}_X & \mathbf{0} \\ -\mathbf{K}_P\mathbf{L}^T(t) & \mathbf{K}_V \end{bmatrix} \begin{Bmatrix} \boldsymbol{q}(t) \\ \boldsymbol{z}(t) \end{Bmatrix} = \begin{Bmatrix} \mathbf{X}^T\mathbf{L}(t)\mathbf{M}_P\boldsymbol{g} \\ \mathbf{C}_P\dot{\boldsymbol{r}}(t) + \mathbf{K}_P\boldsymbol{r}(t) \end{Bmatrix}. \tag{3.20}$$

3.2.3. Dynamic simulation algorithm

In this study, the Newmark-β method [3] is adopted to VBI system for calculation of the responses of the vehicles and bridge. Eq.(3.20) can be rewritten as

$$\mathbf{M}(t)\ddot{\boldsymbol{x}}(t) + \mathbf{C}(t)\dot{\boldsymbol{x}}(t) + \mathbf{K}(t)\boldsymbol{x}(t) = \boldsymbol{b}(t) \tag{3.21}$$

where $\boldsymbol{x}(t) = \{\boldsymbol{q}^T(t) \quad \boldsymbol{z}^T(t)\}^T$ and $\boldsymbol{b}(t) = \{\mathbf{X}^T\mathbf{L}(t)\mathbf{M}_P\boldsymbol{g} \quad \mathbf{C}_P\dot{\boldsymbol{r}}(t) + \mathbf{K}_P\boldsymbol{r}(t)\}^T$ are output and input of VBI system, and $\mathbf{M} \in R^{(m+n)\times(m+n)}$, $\mathbf{C} \in R^{(m+n)\times(m+n)}$ and $\mathbf{K} \in R^{(m+n)\times(m+n)}$ are VBI system mass, damping and stiffness, respectively. Now, the velocity and displacement of VBI output can be described as

$$\dot{\boldsymbol{x}}\big((k+1)\Delta t\big) = \dot{\boldsymbol{x}}(k\Delta t) + \Delta t\left(\gamma\ddot{\boldsymbol{x}}\big((k+1)\Delta t\big) + (1-\gamma)\ddot{\boldsymbol{x}}(k\Delta t)\right) \tag{3.22}$$

$$\boldsymbol{x}\big((k+1)\Delta t\big) = \boldsymbol{x}(k\Delta t) + \Delta t\,\dot{\boldsymbol{x}}(k\Delta t) + \Delta t^2\left(\beta\ddot{\boldsymbol{x}}\big((k+1)\Delta t\big) + \left(\frac{1}{2}-\beta\right)\ddot{\boldsymbol{x}}(k\Delta t)\right) \tag{3.23}$$

where k is the step number and Δt is the discrete time rate. β and γ are the coefficient of the Newmark-β method, which is usually set in $\beta = 1/6$ and $\gamma = 1/2$. Then, when $t = (k+1)\Delta t$, a linear relational expression between $k\Delta t$ and $(k+1)\Delta t$ can be given by substitution of Eq. (3.22) and Eq. (3.23) to Eq. (3.21) in the form of

$$\begin{aligned} &\Big(\mathbf{M}\big((k+1)\Delta t\big) + \Delta t\gamma\mathbf{C}\big((k+1)\Delta t\big) + \Delta t^2\beta\mathbf{K}\big((k+1)\Delta t\big)\Big)\ddot{\boldsymbol{x}}\big((k+1)\Delta t\big) \\ &\quad = \boldsymbol{b}\big((k+1)\Delta t\big) - \mathbf{C}\big((k+1)\Delta t\big)\{\dot{\boldsymbol{x}}(k\Delta t) + \Delta t\big((1-\gamma)\ddot{\boldsymbol{x}}(k\Delta t)\big)\} \\ &\quad - \mathbf{K}\big((k+1)\Delta t\big)\left\{\boldsymbol{x}(k\Delta t) + \Delta t\,\dot{\boldsymbol{x}}(k\Delta t) + \Delta t^2\left(\left(\frac{1}{2}-\beta\right)\ddot{\boldsymbol{x}}(k\Delta t)\right)\right\}. \end{aligned} \tag{3.24}$$

Because the all output of the k-th step, external force $\boldsymbol{b}\big((k+1)\Delta t\big)$ and the properties of the $(k+1)$-th step are known, Eq. (3.24) can be solved easily. The solution of Eq. (3.24) is

$$\ddot{\boldsymbol{x}}\big((k+1)\Delta t\big) = \mathbf{A}^{-1}\big((k+1)\Delta t\big)\boldsymbol{f}(k\Delta t) \tag{3.25}$$

where $\mathbf{A}$ and $\boldsymbol{f}$ are

$$\mathbf{A}\big((k+1)\Delta t\big) = \mathbf{M}\big((k+1)\Delta t\big) + \Delta t\gamma\mathbf{C}\big((k+1)\Delta t\big) + \Delta t^2\beta\mathbf{K}\big((k+1)\Delta t\big) \tag{3.26}$$

$$\begin{aligned}\boldsymbol{f}(k\Delta t) = {} & \boldsymbol{b}\big((k+1)\Delta t\big) \\ & -\mathbf{C}\big((k+1)\Delta t\big)\{\dot{\boldsymbol{x}}(k\Delta t) + \Delta t\big((1-\gamma)\ddot{\boldsymbol{x}}(k\Delta t)\big)\} \\ & -\mathbf{K}\big((k+1)\Delta t\big)\left\{\boldsymbol{x}(k\Delta t) + \Delta t\,\dot{\boldsymbol{x}}(k\Delta t) + \Delta t^2\left(\left(\frac{1}{2}-\beta\right)\ddot{\boldsymbol{x}}(k\Delta t)\right)\right\}.\end{aligned} \tag{3.27}$$

In this study, for numerical simulations of VBI system, Eq. (3.25) is adopted to calculate the responses of the vehicles and bridge.

3.3. Verification of Curvature-based VO-BHM

3.3.1. Properties of Numerical Simulations

The previous studies show feasibility of VO-BHM methods directly applying time-frequency domain analyses such as short-time Fourier's transform [4] and CWT [5] to vehicle acceleration response. The wavelet coefficient of the vehicle responses has a peak around local damage. However, those previous studies have ignored the effect of road profile. In this study, applicability of CWT to VO-BHM method is confirmed even if road profile is not negligible. From Eq. (2.20), wavelet coefficient is a non-linear function of bridge curvature which is a sensitive damage index. However, road profile effect D_3 in Eq. (2.20) should make the detection of damage changes of wavelet coefficient difficult. Since road profile has low frequencies in predominant components, in this study, small scales of wavelet coefficient which correspond to high frequency components are focused on.

The numerical simulation models of vehicle [1] and bridge are shown in Fig. 3.3.1. Herein, introduced damage is modeled as local decreasing of flexural stiffness and mass. The properties of numerical models are shown in Table 3.3.1. The profiles of road unevenness generated by Monte Carlo simulation based on ISO standards [6], [7] are shown in Table 3.3.1 (c). Spatial frequency

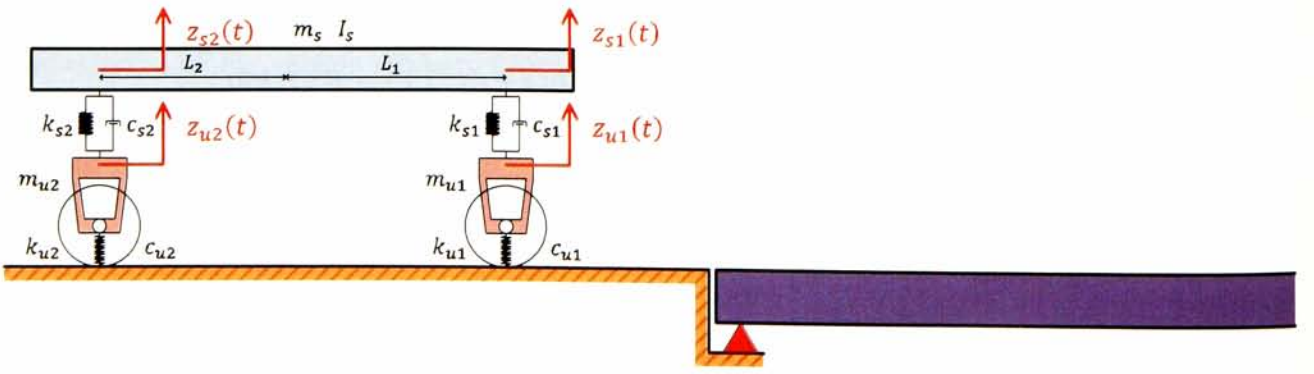

Fig. 3.3.1 Vehicle and bridge model

Table 3.3.1 Model setup of the numerical simulation for curvature estimation verification

(a) Vehicle properties

Sprung-mass	Mass	(kg)	m_s	18000
	Damping	(kg/s)	c_{s1}, c_{s2}	10000
	Spring Stiffness	(kg/s^2)	k_{s1}, k_{s2}	1000000
	Inertia		I	65000
	Length	(m)	L_1, L_2	1.875
Unsprung-mass	Mass	(kg)	m_{u1}, m_{u2}	1100
	Damping	(kg/s)	c_{u1}, c_{u2}	30000
	Spring Stiffness	(kg/s^2)	k_{u1}, k_{u2}	3500000
	Run Speed	(m/s)	v	10.0

(b) Bridge properties

Physical parameters			Eigen-frequency for the intact case				
Length	Mass per length	Flexural Stiffness	1st	2nd	3rd	4th	5th
(m)	(kg/m)	(Nm)	(Hz)	(Hz)	(Hz)	(Hz)	(Hz)
L	ρA	EI	f_1	f_2	f_3	f_4	f_5
30.0	3000	1.56×10^{10}	3.96	15.75	34.98	61.15	93.64

(c) Road profile

Name	ISO standard	a	b	ξ
5-Extra Good	Extra Good	0.001	0.05	2.00
6-Good	Good	0.003	0.02	2.50
7-Standard	Standard	0.0098	0.08	1.92

(d) Bridge state

Name	Decreasing Ratio	
	Flexural Stiffness E	Mass per unit length ρA
Intact	0 %	0 %
Damage -20%	20 %	2 %
Damage -40%	40 %	4 %
Damage -60%	60 %	6 %
Damage -80%	80 %	8 %

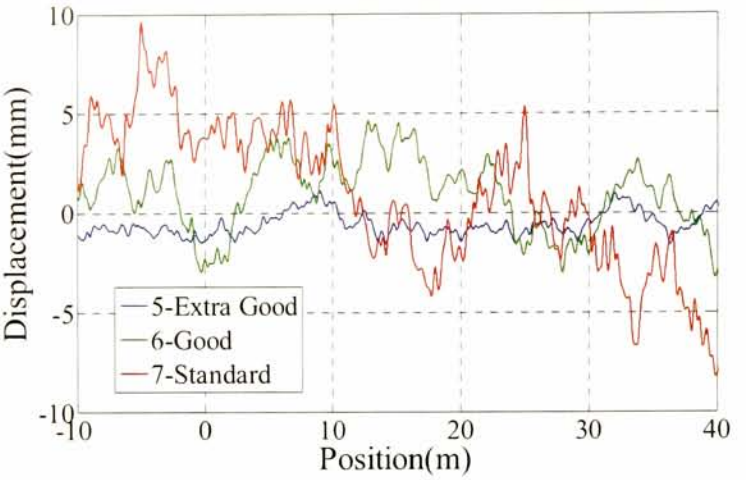

Fig. 3.3.2 Road unevenness

function of road unevenness is given by

$$S = \frac{a}{\Omega^{\xi} + b^{\xi}}. \tag{3.28}$$

In this study, complex Gaussian is adopted for mother wavelet because time-frequency spectrogram by complex mother wavelet becomes much smoother than that by the others, and it is ensured that damage recognition becomes easier. The complex Gaussian mother wavelet $\psi(t)$ can be described as Eq. (3.28)

$$\psi(t) = \frac{\mathrm{d}^4}{\mathrm{d}t^4} C_4 e^{-t^2 - it} \tag{3.29}$$

where C_4 is a coefficient which is decided to satisfy $\psi(t)\psi^*(t) = 1$. In this verification, scale and time shift correspond to frequency and vehicle position, respectively. The scale s can be transformed to the pseudo frequency f by center frequency F_c of mother wavelet ψ and sampling rate F_s in the form of

$$f = \frac{F_c}{sF_s}. \tag{3.30}$$

The complex wavelet coefficient $\boldsymbol{Z}(t, f)$ can be described as

$$\boldsymbol{Z}(t, f) = \ddot{\boldsymbol{z}}(t) \otimes \psi^* \left(f \frac{F_s}{F_c} t \right) \tag{3.31}$$

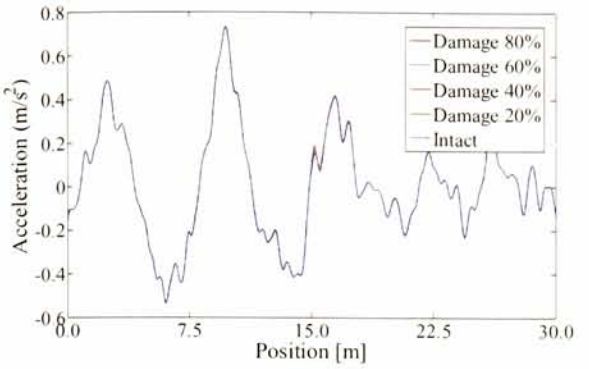

(a) Sprung-mass at the front axle

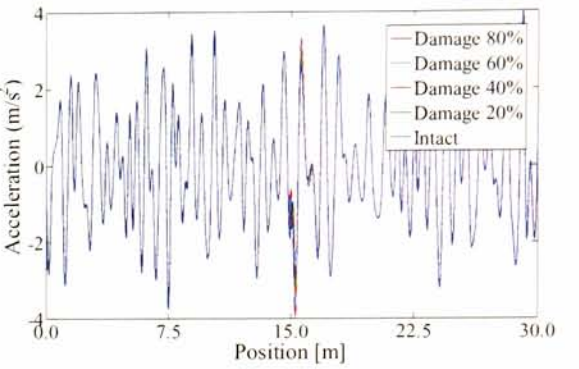

(b) Unsprung-mass at the front axle

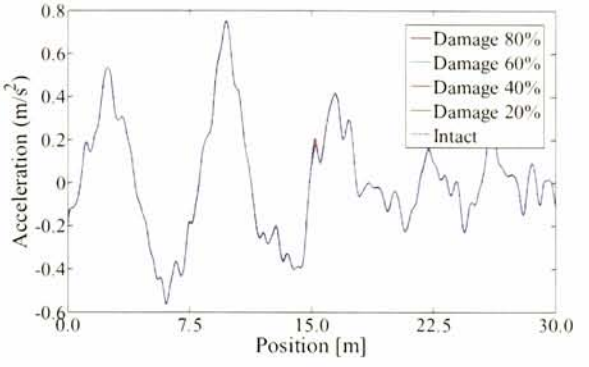

(c) Sprung-mass at the rear axle

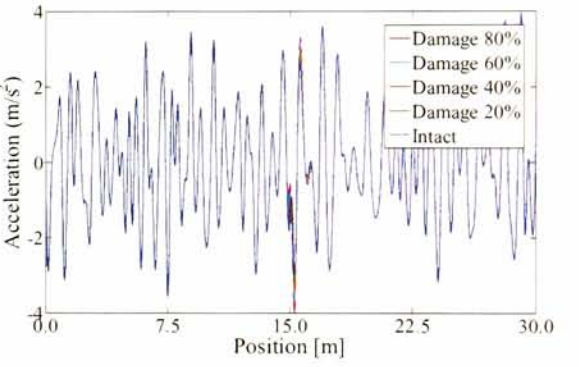

(d) Unsprung-mass at the rear axle

Fig. 3.3.3 Vehicle acceleration responses (Damage width: 20 (cm), Damage location: $L/2$, Road profile: Standard)

The power spectrogram $\boldsymbol{P}(t,f)$ of the vehicle acceleration response $\ddot{\boldsymbol{z}}(t)$ is described as

$$\boldsymbol{P}(t,f) \equiv \boldsymbol{Z}(t,f)\boldsymbol{Z}^{*}(t,f). \tag{3.32}$$

3.3.2. Results and Discussions

Fig. 3.3.3 shows comparison between the vehicle responses for intact and damage cases. Blue line denotes the vehicle acceleration response in the intact case, and other colored lines denote those in the damage cases. Fig. 3.3.3 (a) and Fig. 3.3.3 (b) show sprung-mass and unsprung-mass acceleration responses at the front axle, and Fig. 3.3.3 (c) and Fig. 3.3.3 (d) show those at the rear axle. The horizontal lines denote the position of the corresponding axle. The edges of the bridge are located in $x = 0$ (m) and $x = 30$ (m). Herein, the bridge damage is introduced in the center of the span. The width of the damage is 20 (cm) which is $L/150$. It is very difficult to detect different between them in time domain, especially in aspect of sprung-mass acceleration responses.

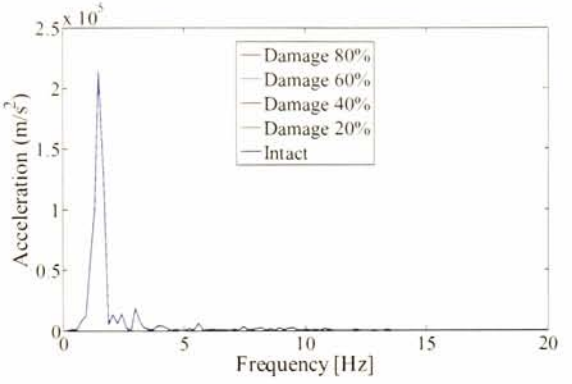

(a) Sprung-mass at the front axle

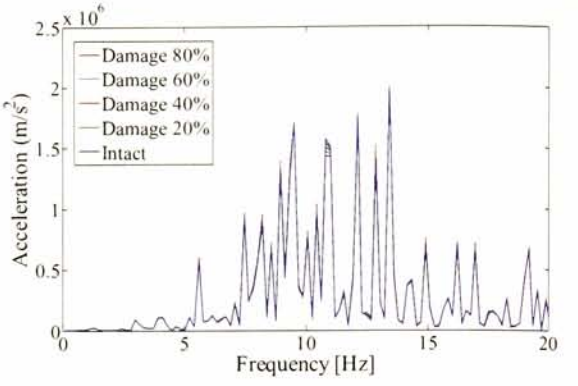

(b) Unsprung-mass at the front axle

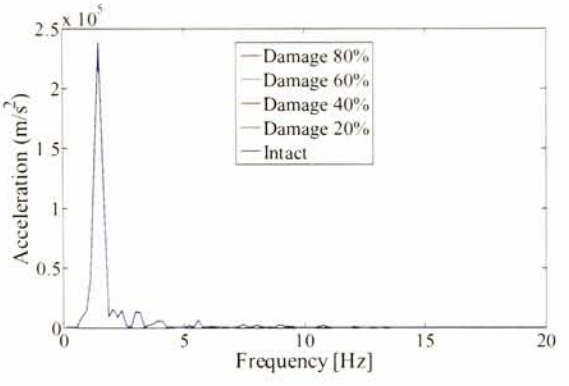

(c) Sprung-mass at the rear axle

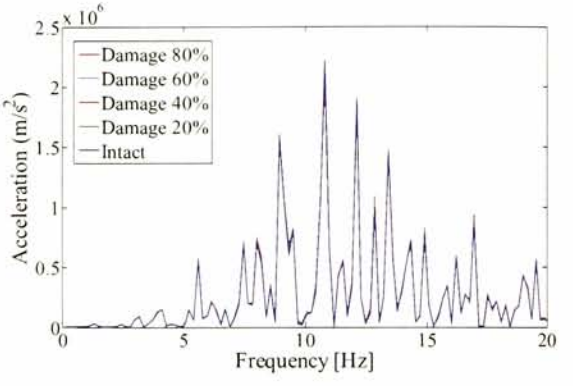

(d) Unsprung-mass at the rear axle

Fig. 3.3.4 Fourier's spectra of the vehicle acceleration responses (Damage width: 20 (cm), Damage location: $L/2$, Road profile: Standard)

Fig. 3.3.4 shows power spectra of vehicle responses in the same cases. In the same way as Fig. 3.3.3, blue and other colored lines denote the power spectra in intact and damage cases, respectively. It is also very difficult to recognize difference between them in frequency domain. Because bridge damage occurs in local, the damage effect on the vibration signals of travelling vehicle is also limited in local. However, Fourier's transform decomposes a signal of the vehicle in a summation of several components whose frequencies are averaged over the whole time. In this process, the local changes of vehicle vibration in a damage case are also averaged.

To overcome this problem about sensitivity in frequency, the previous studies [7], [8] focus on wavelet coefficient in time-frequency domain. According to those studies, wavelet coefficient of vehicle acceleration response is very sensitive. But, those studies ignore road profile. In this study, on the other hand, the effect of road unevenness is considered. Fig. 3.3.5 shows the spectrogram of the wavelet coefficient of vehicle acceleration response measured in the unsprung-mass at the rear axle based on Eq. (3.31). The horizontal line denotes the position of the rear axle of the travelling

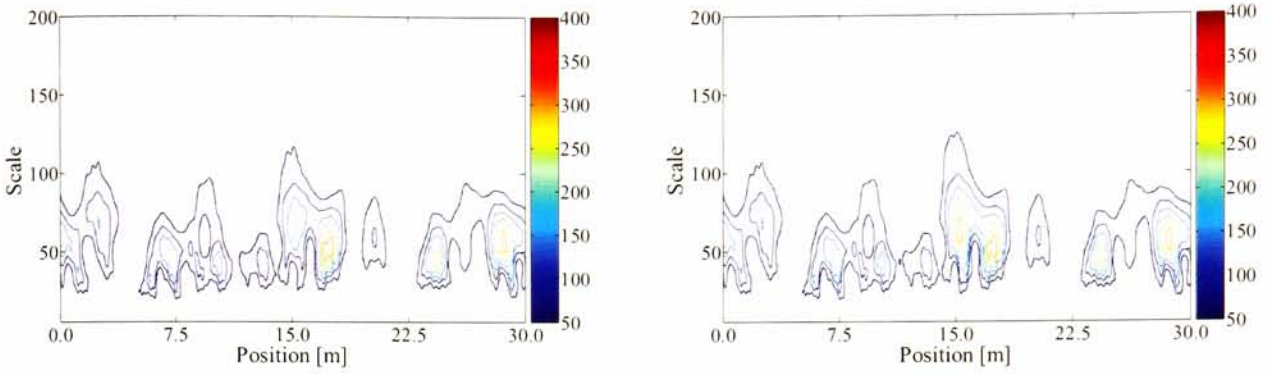

(a) Intact (b) Damage: -80%

Fig. 3.3.5 Power spectrogram of the wavelet coefficient (Unsprung-mass at the rear axle)

vehicle. Fig. 3.3.5 (a) and Fig. 3.3.5 (b) show those in intact and damage cases, respectively. In the damage case, local decreasing of the bridge flexural stiffness and mass is introduced. The damage width is 20 (cm) and the damage location is the center of span. From comparison in the powers of wavelet coefficients between intact and damage cases, it is revealed that the power amplitude tends to larger only around the damage location.

The time histories of powers at specific frequencies are shown in Fig. 3.3.6 in the same cases as Fig. 3.3.5. The horizontal line denotes the position of the vehicle, in the same way. The blue and other colored lines denote the power of wavelet coefficient of the unsprung-mass acceleration responses at the rear axle in the intact and damage cases, respectively. Fig. 3.3.6 (a-1) and Fig. 3.3.6 (a-2) show the wavelet coefficient powers of sprung-mass acceleration at the scale of 100 and 5, which correspond to 5 (Hz) and 100 (Hz), respectively. From Fig. 3.3.6 (a-1), based on low frequency component of sprung-mass response, it is still difficult to detect difference between the intact and damage cases, even for the severest damage. On the other hand, from Fig. 3.3.6 (a-2), peaks can be observed at the location of local damage. The height of damage peak tends to increase according to damage severity. However, the heights of the damage peaks are not distinctive from the other peaks due to uncertainties such as road profile. Fig. 3.3.5 (b-1) and Fig. 3.3.5 (b-2) also show the wavelet coefficient power of the unsprung-mass acceleration based on Eq. (3.31). In both Fig. 3.3.5 (b-1) and Fig. 3.3.5 (b-2), peaks can be observed at the location of local damage, especially in Fig. 3.3.5 (b-2). It means high feasibility for VO-BHM including identification of bridge local damage based on the wavelet coefficient of unsprung-mass in high frequency domain. Fig. 3.3.7 shows wavelet coefficient power of the unsprung acceleration at the scale of 5, which corresponds to 100 (Hz), in the different damage cases. Fig. 3.3.7 (a) and Fig. 3.3.7 (b) show the powers in the cases of local damage introduced in $L/2$ and $L/10$. From these figures, it is confirmed that the power of the wavelet coefficient of unsprung-mass acceleration in high frequency domain increases steeply only at the damage location. It also means that the wavelet transform may provide a sensitive index by which the damage location can be identified.

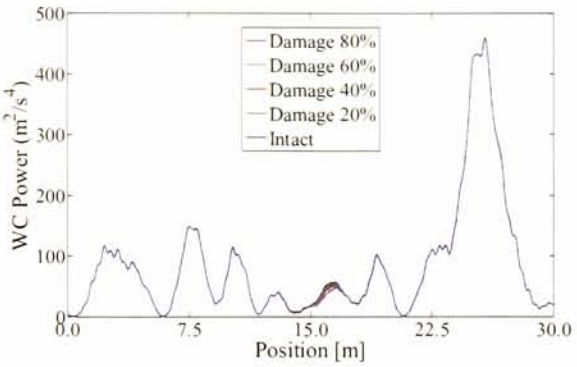

(a-1) Sprung-mass at the front axle
Scale = 100 (5Hz)

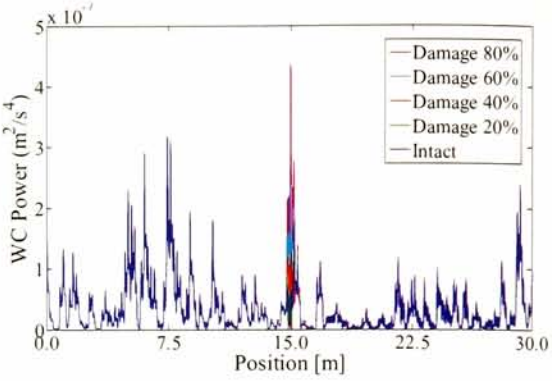

(a-2) Sprung-mass at the front axle
Scale = 5 (100Hz)

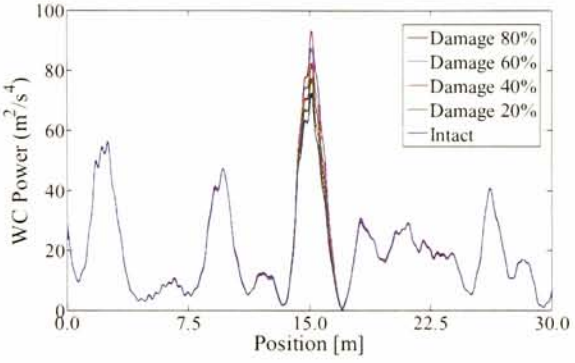

(b-1) Unsprung-mass at the front axle
Scale = 100 (5Hz)

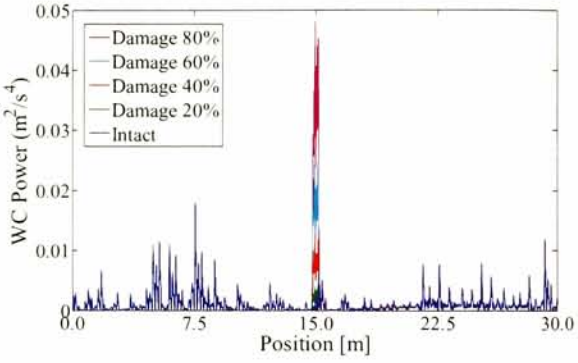

(b-2) Unsprung-mass at the front axle
Scale = 5 (100Hz)

Fig. 3.3.6 Power time histories calculated by CWT (Damage width: 20 (cm), Damage location: $L/2$, Road profile: Standard)

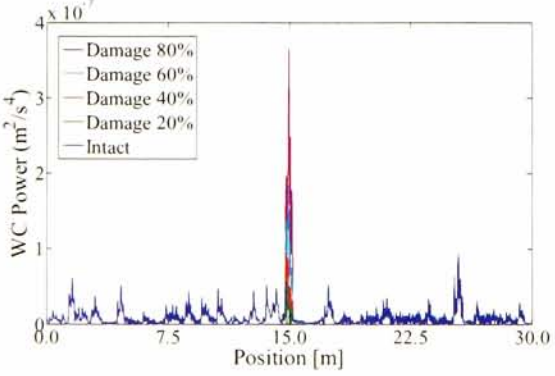

(a) Damage location : $L/2$

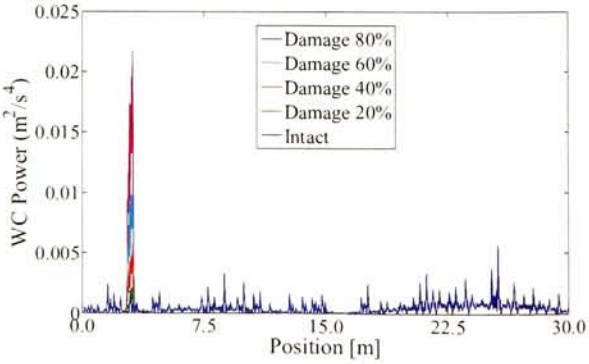

(b) Damage location : $L/10$

Fig. 3.3.7 CWT results when varying damage location (Unsprung-mass at the front axle, Scale = 100 (5Hz), Road Profile: Extra Good)

3.4. Verification of Indirect VO-BHM based on Bridge Mode Shapes

3.4.1. Properties of Numerical Simulation

Vehicle and bridge models adopted for this numerical verification are shown in Fig. 3.4.1. The properties of the numerical simulation are also shown in Table. 3.4.1. Fig. 3.4.2 shows Road unevenness generated by Monte Carlo simulation based on ISO standard [6], [7]. Herein, the proposed method based on indirect mode-shape-based VO-BHM is verified numerically in aspect of uncertain factors in STEP 1, STEP 3 and STEP 4. To verify uncertain factors in the indirect method, two kinds of dynamic simulation are performed. First one demonstrates the coupled vibration between vehicle and bridge with road roughness. The second simulation is a stationary vibration in which bridge modal responses have de-correlation without interaction between vehicle and bridge, but the bridge vibrations are measured by travelling vehicles.

In STEP 1, estimation accuracy of vehicle input may affect the estimation accuracy of mode shape. To verify this step, estimation accuracies of forced displacements which input into the vehicles are evaluated by making a comparison between inverse system estimation (ISE) and frequency response function (FRF) methods.

In STEP 3, there are the problems associated with using interpolation matrix. One of the problems is ill condition problem which occurs in a process of making inverse matrix of the interpolation. This problem is strongly related with the number and interval distance of monitoring vehicles. Other problem also lies in fitting curve of the bridge mode shapes. The bridge mode shapes in intact case can be approximated precisely with Lagrange's and other basis functions. However, because the mode shapes in damage cases have spatially local changes, curve fitting performance may decrease in the damage case.

In STEP 4, the assumption of SVD that the modal responses have de-correlation should affect the estimation accuracy of mode shape.

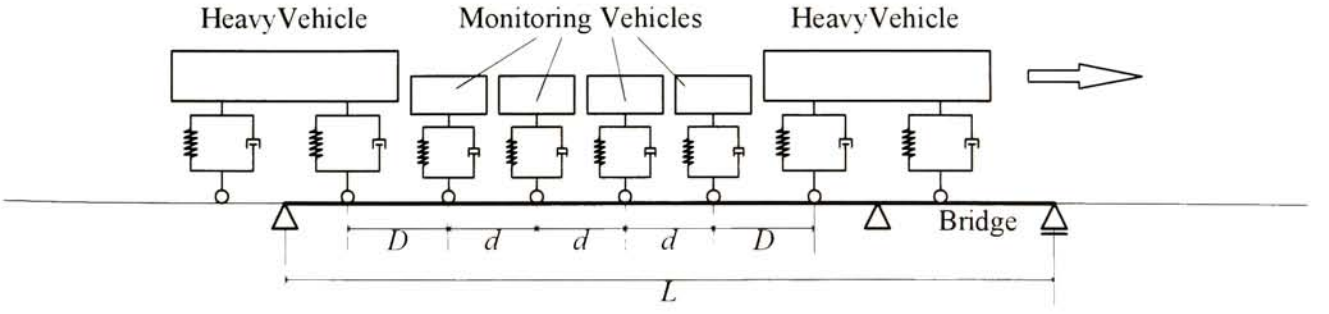

Fig. 3.4.1 Vehicle and bridge model

Table 3.4.1 Properties for numerical simulation of VBI

(a) Vehicle properties

Heavy vehicle	Mass	(kg)	m_s	10000
	Damping	(kg/s)	$c_{s1},\ c_{s2}$	74000
	Spring Stiffness	(kg/s^2)	$k_{s1},\ k_{s2}$	760000
	Inertia		I	90000
	Length	(m)	$L_1,\ L_2$	3.0
Measuring vehicles	Number		$n+1$	4
	Mass	(kg)	m_i	100
	Damping	(kg/s)	c_i	50
	Spring Stiffness	(kg/s^2)	k_i	3950
	Natural Frequency	(Hz)	$f_V = \sqrt{k_i/m_i}/2\pi$	1.00
	Damping Coefficient		$\xi_V = 2c_i\sqrt{m_i k_i}$	0.30
	Interval Distance	(m)	d	0.50
Common	Run Speed	(m/s)	v	10.0
	Distance	(m)	D	2.5

(b) Bridge properties

Physical parameters			Eigen-frequency for the intact case				
Length	Mass per length	Flexural Stiffness	1st	2nd	3rd	4th	5th
(m)	(kg/m)	(Nm)	(Hz)	(Hz)	(Hz)	(Hz)	(Hz)
L	ρA	EI	f_1	f_2	f_3	f_4	f_5
30.0	3000	1.56×10^{10}	3.96	15.75	34.98	61.15	93.64

(c) Road profile

Name	ISO standard	a	b	ξ
Standard	Extra Good	0.001	0.05	2.00
Rough	Good	0.0098	0.08	1.92

(d) Bridge state

Name	Decreasing Ratio of Flexural Stiffness EI	Damage Location	Damage Width
Intact	0 %	$L/10$	$L/150$
Damage -20%	20 %	$L/4$	$L/30$
Damage -40%	40 %	$L/2$	$L/6$
Damage -60%	60 %		
Damage -80%	80 %		

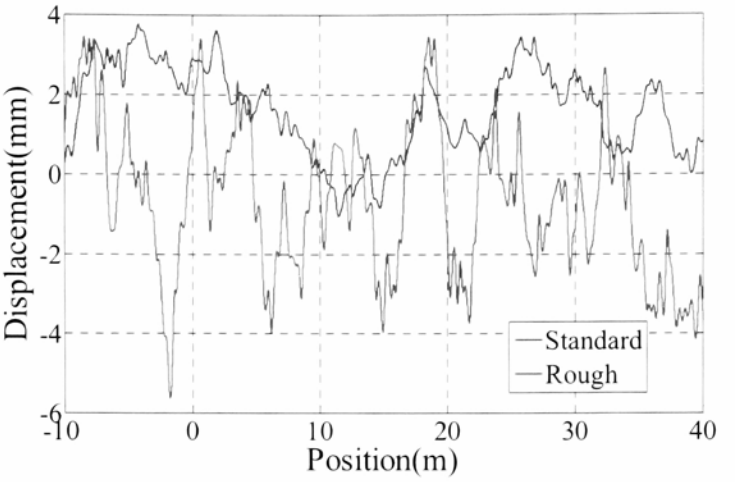

Fig. 3.4.2 Road profile

The estimation accuracy of mode shape based on the proposed VO-BHM method is thought to be affected by these effective factors. Those effects are evaluated by MAC between the correct and estimated mode shapes.

Stochastic verification in which white noise is introduced to the measurements on the vehicle is performed to examine the feasibility of damage identification of this method based on MAC between basis and estimated mode shapes.

3.4.2. Results of Mode Shape Estimation

Fig. 3.4.3 shows examples of estimated and correct bridge mode shapes in STEP 4 of the indirect mode-shape-based VO-BHM. From these figures, the estimation accuracy depends on the vehicle number ($= n + 1$). For n =3, 4 and 5, interval distance of monitoring vehicles is set to 0.5 (m), 2.0 (m) and 2.5(m), respectively. The bridge damage is modeled as local decrease of flexural stiffness by 60% in the position of $L/2$. The width of damage section is 20 (cm) ($= L/150$). Solid and dot lines indicate estimated and correct mode shapes. From Fig. 3.4.3, it is confirmed that the proposed method can estimate bridge mode shape, especially in n =3.

Next, Fig. 3.4.4 shows the estimation accuracy based on MAC between correct and estimated mode shapes. The number of monitoring vehicles is four. Thus, the order of mode shape is three. The ratios of flexural stiffness decreasing are 20%, 40%, 60% and 80%. The horizontal axis in this figure denotes the ratio of the decreased flexural stiffness to intact. Fig. 3.4.4 (a-1) and Fig. 3.4.4 (a-2) show MAC of the cases in which local damage is located in $L/4$ and $L/2$, respectively. Herein, the width of damage is 20 (cm). Adopted road profile is "Standard" shown in Table. 3.4.1 (c). From both them, the estimation accuracies are still very high when the width of local damage is limited, even if the damage severity is very large such as 80%. Fig. 3.4.4 (b-1) and Fig. 3.4.4 (b-2) show MAC of the cases in which relative larger damage is located in $L/4$ and $L/2$, respectively.

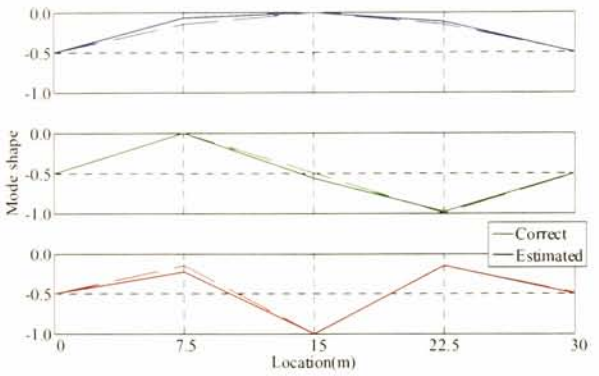

(a-1) Intact, $n = 3$

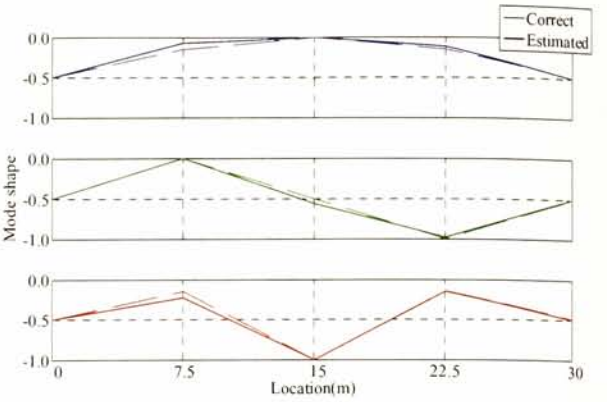

(a-2) Damage, $n = 3$

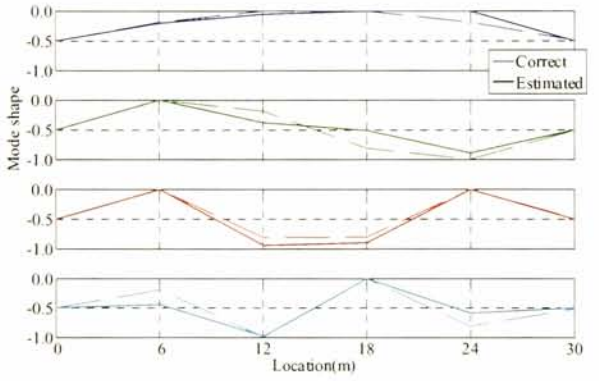

(b-1) Intact, $n = 4$

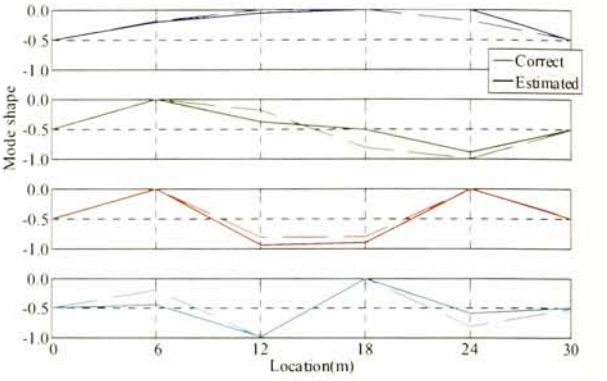

(b-2) Damage, $n = 4$

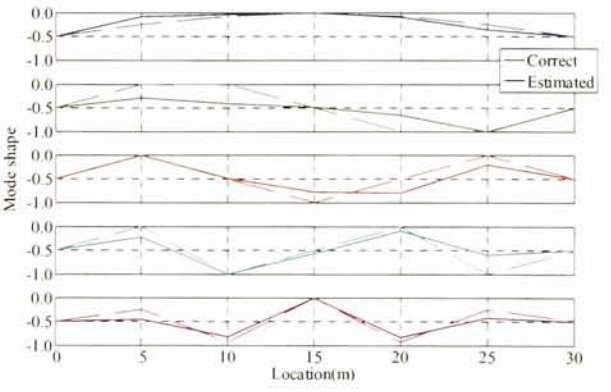

(c-1) Intact, $n = 5$

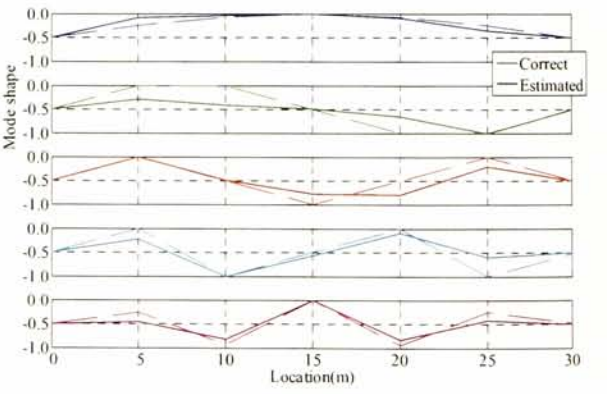

(c-2) Damage, $n = 5$

Fig. 3.4.3 Estimated mode shapes and number of measuring points (= interpolation order n)

Herein, the width of damage is 1 (m). At these cases, on the other hand, the estimation accuracies decrease as the damage increase. It means that the proposed method cannot estimate bridge mode shape under the constant accuracy. Fig. 3.4.4 (c) shows MAC of a local damage case in which road profile is "Rough" shown in Table. 3.4.1 (c), in the same way. From comparison between the results of "Standard" and "Rough" road profile, the estimation accuracy depends on the road profile. Fig. 3.4.4 (d) also shows MAC of global damage case in the same way. Herein, the width of the global

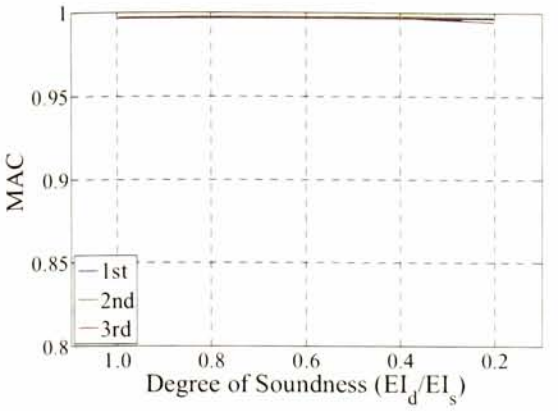

(a-1) Damage: 20 (cm), at $L/10$
Road profile: Standard

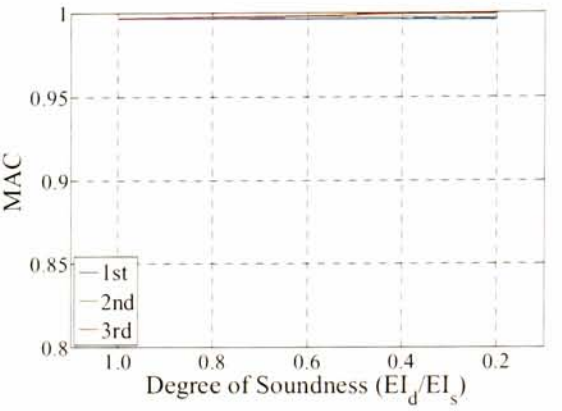

(a-2) Damage: 20 (cm), at $L/2$
Road profile: Standard

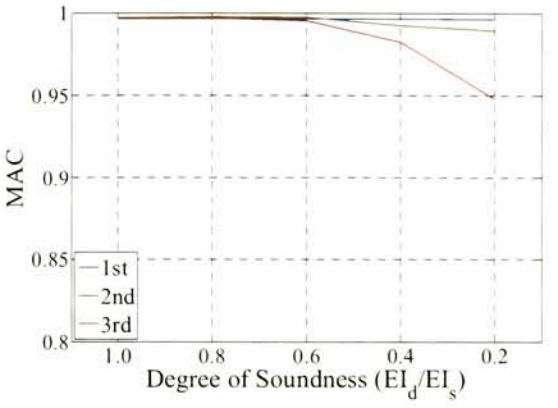

(b-1) Damage: 1 (m), at $L/10$
Road profile: Standard

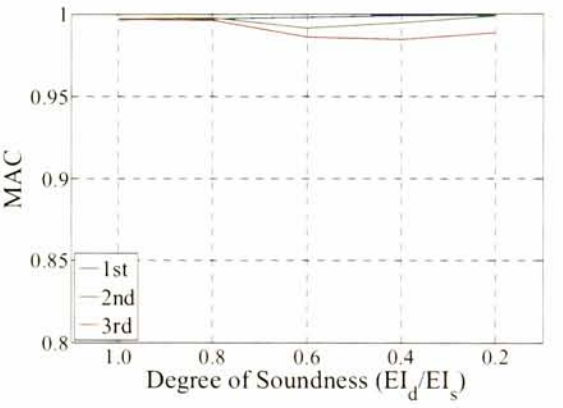

(b-2) Damage: 1 (m), at $L/2$
Road profile: Standard

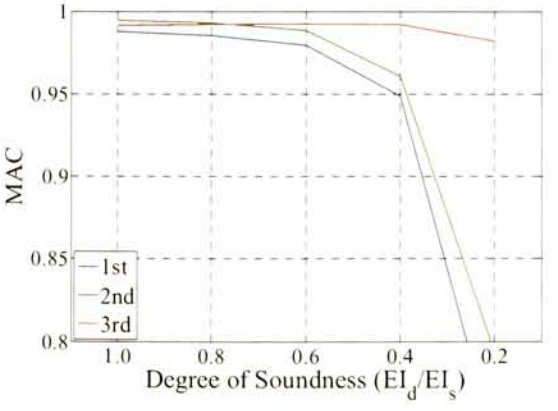

(c) Damage: 1 (m), at $L/10$
Road profile: Rough

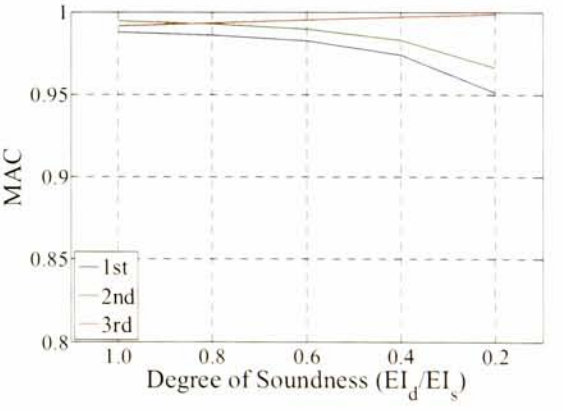

(d) Damage: 5 (m), at $L/2$
Road profile: Rough

Fig. 3.4.4 Estimation accuracy, damage location and severity

damage is 5(m). The estimation accuracy in this case decreases as the global damage increases.

From Fig. 3.4.4, the estimation accuracy depends on the damage width and severity and road profile. This means that larger changes are caused in the estimated mode shapes due to damage

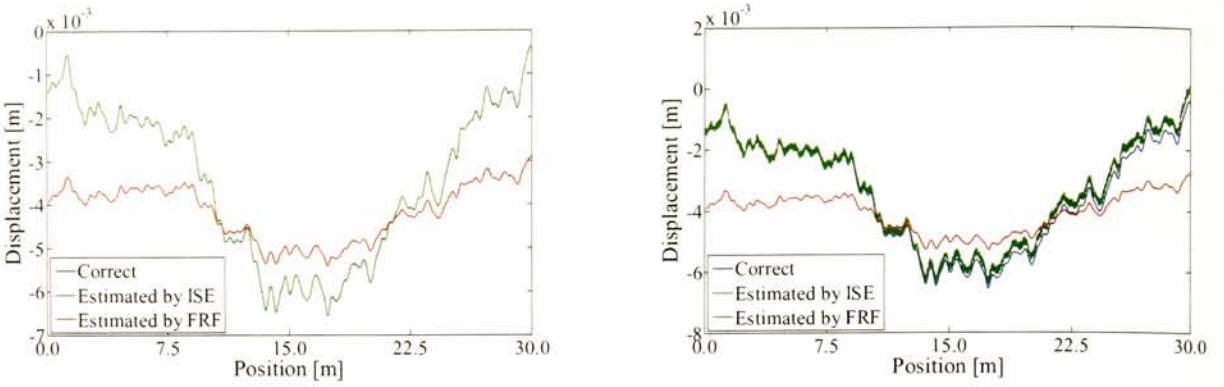

(a) Without noise (b) With 1% white noise

Fig. 3.4.5 Input estimation by ISE and FRF

than changes of the correct mode shapes themselves.

The factors which affect the estimation accuracy are examined in more depth below.

3.4.3. Accuracy of the input estimation

Fig. 3.4.5 shows the input of the vehicle and the estimation by ISE and FRF methods. Blue, green and red lines denote correct input and the estimations by ISE and FRF methods, respectively. Fig. 3.4.5 (a) and Fig. 3.4.5 (b) show the input estimation results without and with white noise, respectively. The blue and green lines are perfect match for each other in Fig. 3.4.5 (a), while there are slight changes between them in Fig. 3.4.5 (b). It means that high precision can be obtained by ISE method. On the other hand, another method using FRF of which estimations are indicated by red lines does not show the same accuracy, especially in low frequency.

From these figures, the errors of estimations by method using ISE increase due to the noise, while the errors for FRF do not change. The reason of the low robustness of ISE method must lie in using two measurements to estimate one input signal at one time. However, using ISE is still superior to using FRF in aspect of accuracy because using ISE can avoid inverse problem of vehicle system identification.

3.4.4. Effect of ill-condition problem in inverse interpolation process

As the number of monitoring vehicles increases and/or the vehicular interval distance decreases, From Eq. (2.41), the (i, j) element of the interpolation matrix $\mathrm{N}_{ij}(t) = N_j(\tilde{x}_i(t))$ approaches the $(i+1, j)$ element for each other. At that case, ill-condition problem occurs in a process of inverse interpolation in STEP 3.

The degree of ill condition can be evaluated using condition number [10]. Herein, a liner function associated with the condition number of inverse interpolation is given by Eq. (2.37) and Eq.

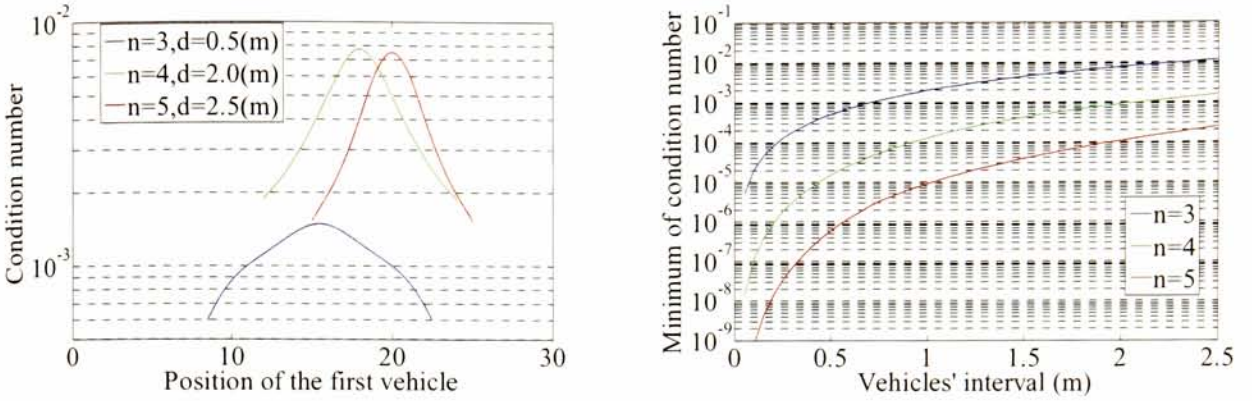

(a) Spatial changing of condition number (b) Condition number and vehicles' interval

Fig. 3.4.6 Ill-condition of Lagrange's interpolation

(2.43) in the form.

$$\tilde{\boldsymbol{y}}(t) = \mathbf{N}(t)\hat{\boldsymbol{y}}(t) \tag{3.33}$$

where $\tilde{\boldsymbol{y}}(t)$ and $\hat{\boldsymbol{y}}(t)$ are estimated bridge vibrations measured at moving and fixed points, respectively. $\tilde{\boldsymbol{y}}(t)$ can be obtained in STEP 2. The condition number is one of the indices for the rate of changes of the solution $\hat{\boldsymbol{y}}(t)$ to the known term $\tilde{\boldsymbol{y}}(t)$. Letting $\boldsymbol{\varepsilon}(t)$ be the error in $\tilde{\boldsymbol{y}}(t)$, the ratio of relative error $\boldsymbol{\kappa}(t)$ in the solution $\hat{\boldsymbol{y}}(t)$ to the error $\boldsymbol{\varepsilon}(t)$ can be expressed by

$$\begin{aligned}\boldsymbol{\kappa}(t) &\equiv \frac{\|\mathbf{N}(t)^{-1}\boldsymbol{\varepsilon}(t)\|/\|\hat{\boldsymbol{y}}(t)\|}{\|\boldsymbol{\varepsilon}(t)\|/\|\tilde{\boldsymbol{y}}(t)\|} \\ &= \frac{\|\mathbf{N}(t)^{-1}\boldsymbol{\varepsilon}(t)\|/\|\mathbf{N}(t)^{-1}\tilde{\boldsymbol{y}}(t)\|}{\|\boldsymbol{\varepsilon}(t)\|/\|\tilde{\boldsymbol{y}}(t)\|} \\ &= \|\mathbf{N}(t)^{-1}\| \cdot \|\mathbf{N}(t)\|\end{aligned} \tag{3.34}$$

where $\|\ \|$ denotes 2-norm. When $\boldsymbol{\kappa}(t)$ is large number, small error in the known term $\tilde{\boldsymbol{y}}(t)$ causes large error in the solution $\hat{\boldsymbol{y}}(t)$. Thus, inverse number of $\boldsymbol{\kappa}(t)$ indicates the accuracy of interpolation.

Fig. 3.4.6 shows the inverse number of condition number of the Lagrange's interpolation. Because the interpolation matrix is a time function, the condition number is also given in the form of a time function. Fig. 3.4.6 (a) shows the inverse number of condition number of $\mathbf{N}(t)$ in three cases which have different matrix size n and interval distance of monitoring vehicles d. The horizontal axis denotes the position of the first monitoring vehicle. Fig. 3.4.6 (b) shows the minimum of the inverse number of condition number during the monitoring trailer system passing through the bridge. From Fig. 3.4.6 (b), it is cleared that the most significant factor is the size of interpolation function matrix. As the number of monitoring vehicles decreases and/or the interval

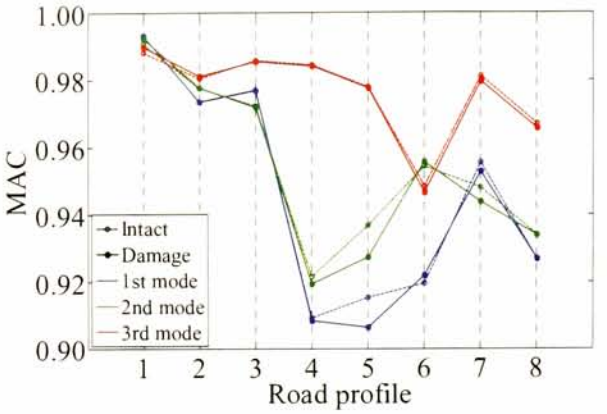

Fig. 3.4.7 Relation between estimation accuracy and road profile

distance increases, the accuracy of converting bridge vibrations measured at moving points into those at fixed points.

3.4.5. Effect of the de-correlation of modal responses

Herein, to confirm the effect of road unevenness on the estimation accuracy, numerical simulations of VBI system are performed by applying eight kinds of road unevenness which have the same spatial frequency characteristics as Standard road profile. Four monitoring vehicles travel over the bridge. Their properties are shown in Table 3.4.1. The bridge damage is modeled as local decrease of flexural stiffness by 60% in the position of $L/10$. The width of damage section is $L/150$.

The estimation accuracy of mode shapes by the proposed method varies even in the same bridge state. Fig. 3.4.7 shows MAC between correct and estimated mode shapes in both intact and damage cases. Solid and dot lines denote MAC in the intact and damage cases, respectively. Blue, green and red lines denote first, second and third mode shapes. After damage is introduced, the estimation accuracy of mode shapes slightly changes.

From Eq. (2.49), The reason of the change in estimation accuracy of mode shape may be the change of de-correlation of the bridge modal response components $\tilde{\boldsymbol{q}}(t)$. SVD assumes orthogonality of not only mode shapes but also modal responses. However, in stationary vibration, modal responses are not always orthogonal. The orthogonality of time function $\tilde{\boldsymbol{q}}(t)$ can be translated to the de-correlation of $\tilde{\boldsymbol{q}}(t)$, and it also means that the matrix $\tilde{\boldsymbol{q}}(t)\tilde{\boldsymbol{q}}(t)^{\mathrm{T}}$ is diagonal. Thus, to evaluate the de-correlation quantitatively, diagonalization degree of covariance matrix of bridge modal response components $\tilde{\boldsymbol{q}}(t)$ can be used.

Diagonalization degree of a matrix $\mathbf{M}$ can be described as

$$F(\mathbf{M}) = \sum_i \log m_{ii} - \log|\det \mathbf{M}| \tag{3.35}$$

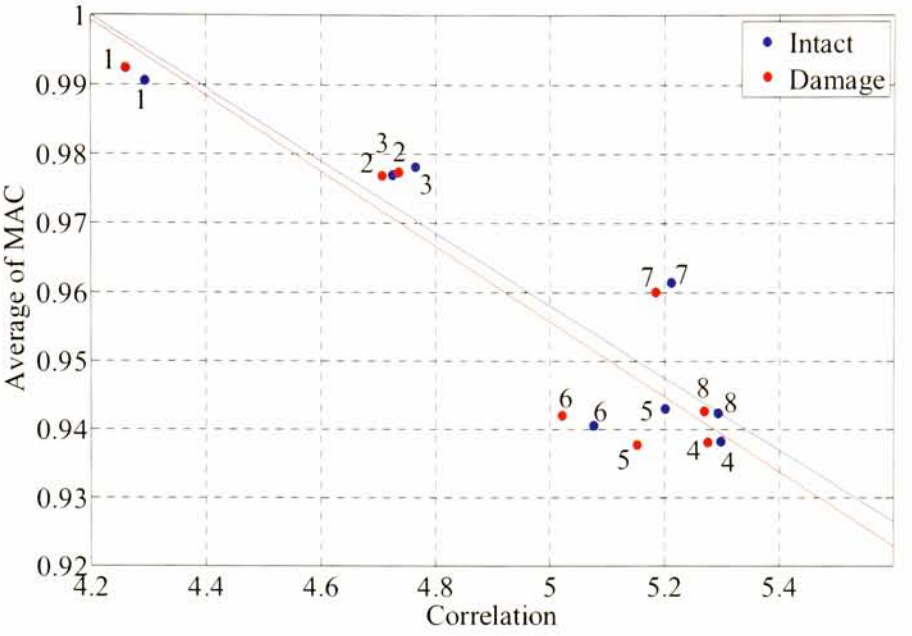

Fig. 3.4.8 Relationship between de-correlation and estimation accuracy

where m_{ij} is (i,j) element of $\mathbf{M}$. $F(\mathbf{M})$ becomes zero when $\mathbf{M}$ is a diagonal matrix. To evaluate the de-correlation of bridge modal response components $\tilde{\boldsymbol{q}}(t)$, $\mathbf{M}$ should be covariance of them described as

$$\mathbf{M} = \mathrm{E}[\tilde{\boldsymbol{q}}(t)\tilde{\boldsymbol{q}}(t)^{\mathrm{T}}] \tag{3.36}$$

where E[ ] indicates an expected value. As $F(\mathbf{M})$ increases, the de-correlation of $\tilde{\boldsymbol{q}}(t)$ decreases.

Fig. 3.4.8 shows relations between de-correlation of $\tilde{\boldsymbol{q}}(t)$ and estimation accuracy of mode shape based on the indirect VO-BHM. The horizontal axis denotes the correlation. The estimation accuracies by the proposed method are evaluated by MAC between correct and estimated mode shape matrix. The vertical axis denotes the average between the MAC values of first and third mode shapes. Blue and red dots indicate the results in intact and damage cases. Numbers ranging from 1 to 8 in Fig. 3.4.8 indicate the road profile number. In the same figure, regression lines are also plotted for intact and damage cases. From Fig. 3.4.8, MAC increases as the correlation decreases. It is also confirmed that MAC values of damage cases tend to be below those of intact cases. However, MAC value of an intact case is not always below that of the damage case for same road profile.

The results about de-correlation mean that the performance of SVD itself strongly depends on the degree of de-correlation of decomposed signals. On the other hand, changes of estimation accuracy between intact and damage cases under the same road profile do not have same tendency. For example, MAC of road profile "1" increases due to damage, while that of road profile "5" decreases.

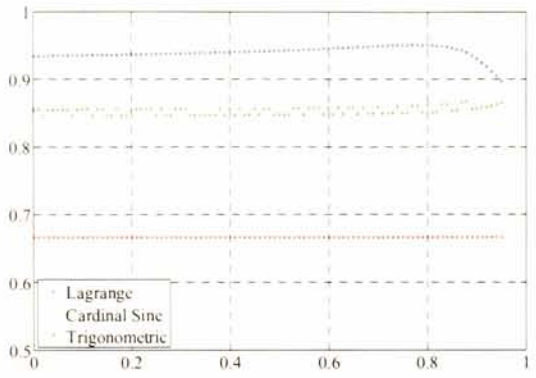

(a) 1 (m) width damage at $L/4$

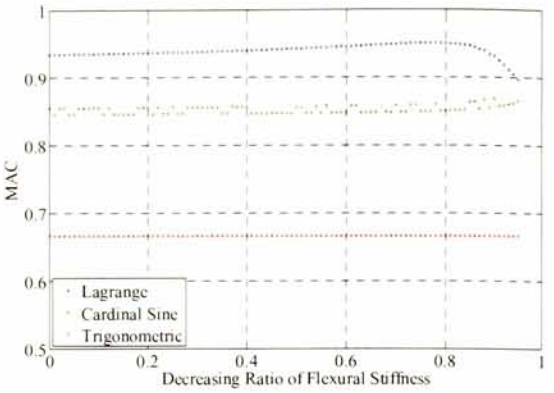

(b) 1 (m) damage at $L/2$

Fig. 3.4.9 Fitting accuracy of interpolation

3.4.6. Effect of the fitting performance of interpolation

Curve fitting in STEP 3 may also affect the accuracy of mode shape estimation. To confirm fitting performances of the interpolation matrices based on Lagrange's, Cardinal sine and trigonometric functions, the stationary vibration simulation is performed. Herein, the monitoring vehicles are the same with those in the former coupled vibration simulation. The number of monitoring vehicles travelling over the bridge is four which means the maximum order of estimated mode shape is three. In this numerical simulation, stationary responses are generated to the bridge regardless of vehicle contact forces. The monitoring vehicles observe only identical bridge response components $\tilde{\boldsymbol{q}}(t)$ which are de-correlative in any case even between intact and damage cases. Thus, damage changes only mode shapes of the bridge. Although discrete mode shape may not change well after damage introduced, fitting error by interpolation for mode shape function has been accumulated during passing of the vehicles.

Fig. 3.4.9 shows the fitting accuracies of Lagrange, Cardinal sine and trigonometric interpolations for the first order mode shapes. In this verification, bridge local damage is modeled as decrease of the flexural stiffness in the position of $L/4$ and $L/2$ shown in Fig. 3.4.9 (a) and Fig. 3.4.9 (b), respectively. Damage width is 1 (m). The horizontal lines indicate decrease ratio of flexural stiffness in the damage section. In these figures, mode shapes are varied by introducing damage of local flexural stiffness decreasing. Blue, green and red lines indicate the estimation accuracy of Lagrange, Cardinal sine and trigonometric interpolations, respectively. From Fig. 3.4.9, the fitting accuracy with Lagrange's basis functions tends to be increased slightly first and decreased precipitously after by the ratio of 80%. Cardinal sine function is very sensitive to small damage. The estimation accuracies both of Cardinal sine and trigonometric functions are always below those of Lagrange's functions.

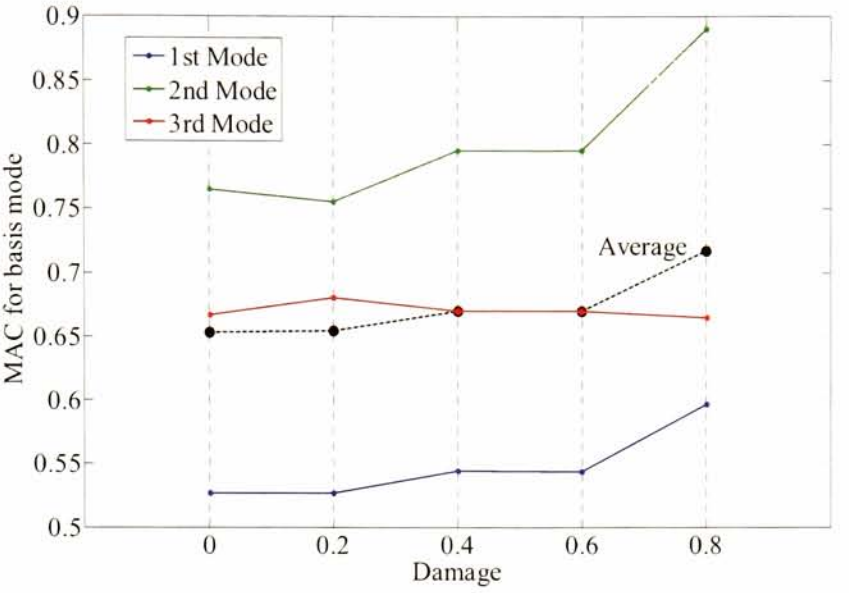

Fig. 3.4.10 Averaged MAC for damage

3.4.7. Damage Identification Accuracy

Finally, the applicability of this method to damage detection is examined by stochastic verification. All measurements include white noise which affects every step. The amplitude of noise is 1% of the maximum amplitude in each measurement. In other words, the white noise is introduced to both of acceleration response and relative displacements measured on the monitoring vehicles passing over the bridge. The assumed number of measuring points n equals three. The damage is modeled as decrease of flexural stiffness in the position of $L/2$. The width of damage is $L/30$. Road profile is "Standard".

Fig. 3.4.10 shows probability distribution of MAC value between estimated and "intact" mode shapes. For actual inspection to detect damage, because the correct damaged mode shape may be unknown, MAC values should be calculated by using basis mode shapes. If the intact mode shape is unknown, you can set any basis mode shape, such as sine curve.

It is expected that MAC of the proposed method tends to be decreased or increased as the damage increased. However, the probability distributions of MAC change very slightly. From this result, it is cleared that the structural changes due to local damage are too small to be detected by the indirect mode-shape-based VO-BHM method. The robustness of this method against white noise is very low. The reason of the low robustness lies in the error accumulation, because the interpolation and SVD themselves in STEP 3 and 4 can demonstrate high performance to convert signals in this method. On the other hand, errors included in measurements are accumulated in each step.

Thus, in this study, the third method, direct mode-shape-based VO-BHM method in which the same interpolation is applied directly to vehicle acceleration, is proposed to overcome this problem about robustness and to identify bridge damage.

3.5. Verification of Direct VO-BHM based on Bridge Mode Shapes

3.5.1. Basic Assumption

The last method verified in this chapter is direct VO-BHM based on bridge mode shape. This method applies interpolation directly to vehicle acceleration responses. Bridge mode shape itself does not change well, but estimation accuracy may be affected significantly by damage. It means that the estimation results of mode shape are also feasible for damage identification. This method can be categorized into two kinds: First one uses inverse interpolation matrix which is same with the indirect method above-mentioned. In the verification of this method, the de-correlation of bridge response components $\boldsymbol{\sigma}(t)$ and the error term $\boldsymbol{\varepsilon}(t)$ in Eq. (2.54) must be confirmed because of the applicability of SVD. The second method uses transpose matrix of interpolation, instead of the inverse matrix. In the same way, in the verification of the second method, the de-correlation of bridge response components $\boldsymbol{\tau}(t)$ and the error term $\boldsymbol{\epsilon}(t)$ in Eq. (2.64) must be examined. To examine the effect of error terms, road profile and mas of the vehicle are varied. Monitoring vehicle is modeled as a half-car shown in Fig. 3.5.1. The properties of numerical simulation models [1] are shown in Table 3.5.1. White noise is added to the vehicle acceleration responses. The amplitude of the noise is 1% of the maximum amplitude of the vehicle acceleration responses.

3.5.2. Verification of $\mathbf{N}^{-1}$-based method

Herein, the mode shapes are estimated in two discrete points by the proposed method. Thus, letting them be x and y, respectively, they can be plotted on 2-D graph. The first mode shape estimated by the direct method using inverse interpolation matrix is shown in Fig. 3.5.2. In this figure, the mode shape is normalized under $x^2 + y^2 = 1$. Left and right figures in Fig. 3.5.2 are overall and close-up views, respectively. There are 10 same colored dots which vary on the unit

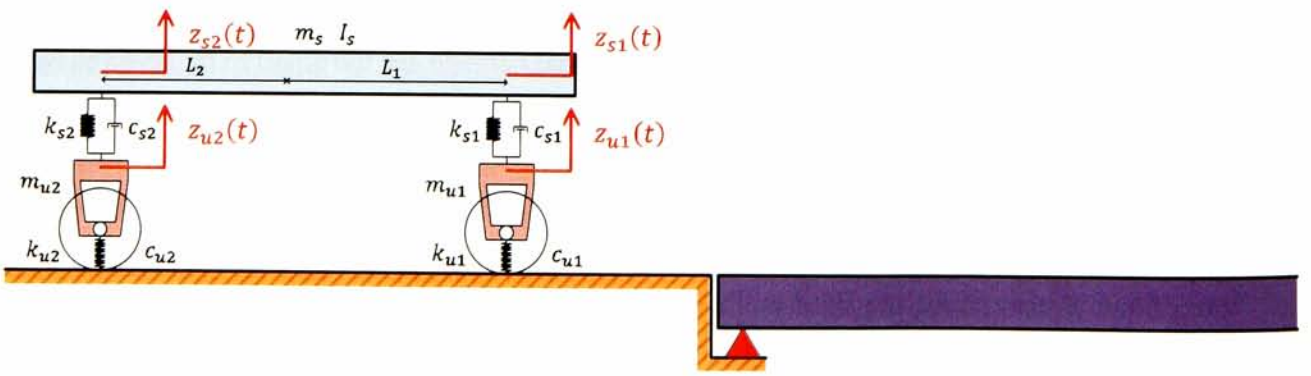

Fig. 3.5.1 Vehicle and bridge model

Table 3.5.1 Model setup of the numerical simulation for curvature estimation verification

(a) Vehicle properties

Sprung-mass	Mass	(kg)	m_s	18000
	Damping	(kg/s)	c_{s1}, c_{s2}	10000
	Spring Stiffness	(kg/s^2)	k_{s1}, k_{s2}	1000000
	Inertia		I	65000
	Length	(m)	L_1, L_2	1.875
Unsprung-mass	Mass	(kg)	m_{u1}, m_{u2}	1100
	Damping	(kg/s)	c_{u1}, c_{u2}	30000
	Spring Stiffness	(kg/s^2)	k_{u1}, k_{u2}	3500000
	Run Speed	(m/s)	v	10.0

(b) Bridge properties

Physical parameters			Eigen-frequency for the intact case				
Length	Mass per length	Flexural Stiffness	1st	2nd	3rd	4th	5th
(m)	(kg/m)	(Nm)	(Hz)	(Hz)	(Hz)	(Hz)	(Hz)
L	ρA	EI	f_1	f_2	f_3	f_4	f_5
30.0	3000	1.56×10^{10}	3.96	15.75	34.98	61.15	93.64

(c) Road profile

Name	ISO standard	a	b	ξ
5-Extra Good	Extra Good	0.001	0.05	2.00
6-Good	Good	0.003	0.02	2.50
7-Standard	Standard	0.0098	0.08	1.92

(d) Bridge state

Name	Decreasing Ratio of Flexural Stiffness EI	Damage Location	Damage Width
Intact	0 %	$L/10$	$L/150$
Damage -20%	20 %	$L/4$	$L/30$
Damage -40%	40 %	$L/2$	$L/6$
Damage -60%	60 %		
Damage -80%	80 %		

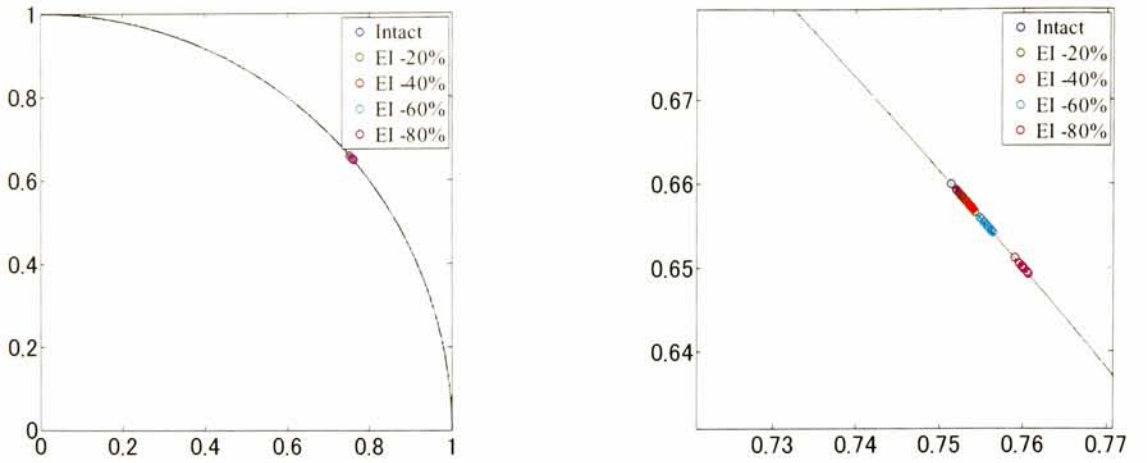

(a) Road profile = Extra Good, Damage location = $L/10$ and Damage width = 1 (m) (= $L/30$)

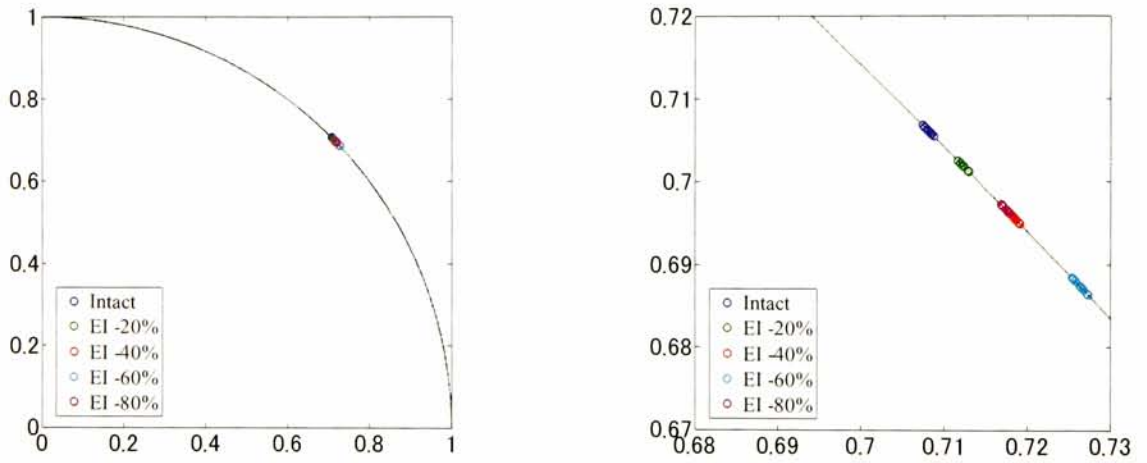

(b) Road profile = Good, Damage location = $L/10$ and Damage width = 1 (m) (= $L/30$)

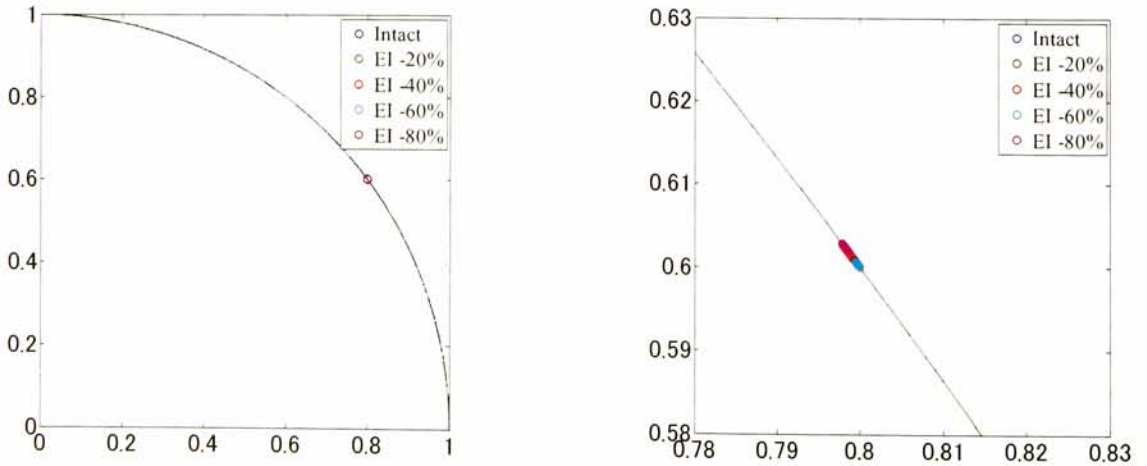

(c) Road profile = Standard, Damage location = $L/10$ and Damage width = 1 (m) (= $L/30$)

Fig. 3.5.2 Estimation results of mode shape when the vehicle speed = 10 (m/s) and mass = 1 (t)

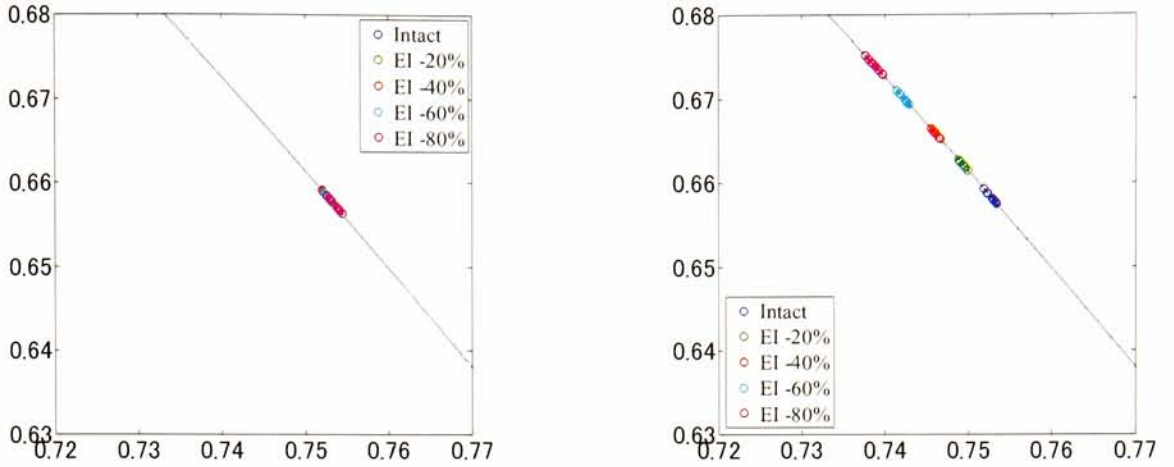

(a) Damage location = $L/10$ (b) Damage location = $L/2$

Fig. 3.5.3 Estimation results of mode shape when the vehicle speed = 10 (m/s) and mass = 1 (t) (Road profile = Extra Good, and Damage width = 20 (cm) (= $L/150$))

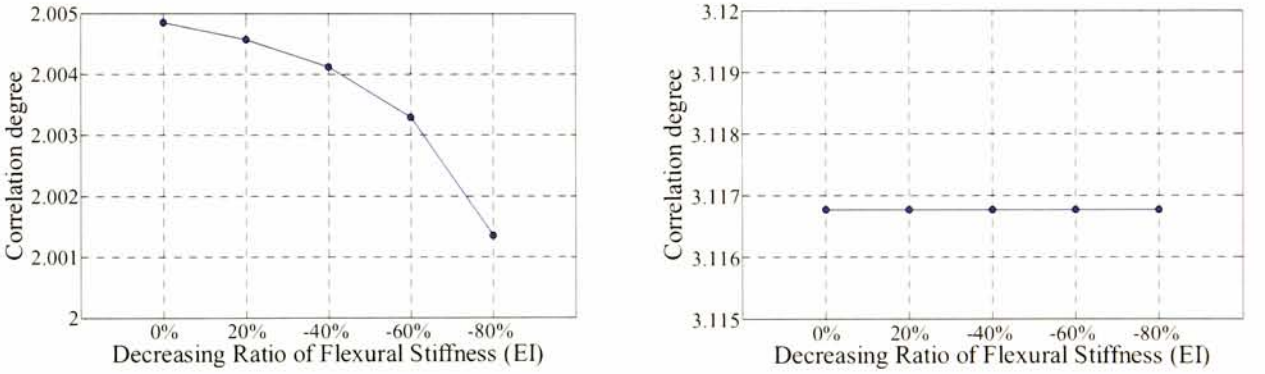

(a) De-correlation of $\boldsymbol{\sigma}(t)$ (b) De-correlation of the error term $\boldsymbol{\varepsilon}(t)$

Fig. 3.5.4 De-correlation and damage

circle due to white noise. Blue and other color dots denote the estimated first mode shapes in intact and damage cases. Fig. 3.5.2 (a), Fig. 3.5.2 (b) and Fig. 3.5.2 (c) shows the estimated mode shapes in the cases using "Extra-Good", "Good" and "Standard" road roughness [6] Damage is located in $L/10$ and the damage width is 1 (m) (= $L/30$). From these figures, change due to damage in estimated mode shape is larger than that due to noise.

This tendency can be confirmed in other damage cases. Fig. 3.5.4 shows comparisons of the estimated first mode shape in different damage locations. Herein, damage width is 20 (cm) (= $L/150$).

The changes of estimated mode shape can be caused by the changes of the de-correlation of bridge response components $\boldsymbol{\sigma}(t)$ and/or errors term $\boldsymbol{\varepsilon}(t)$. Their correlation degrees evaluated by Eq. (3.35) are shown in the Fig. 3.5.4. Herein, damage is located in $L/10$ and the damage width is

1 (m) (= $L/30$). Road unevenness is "Extra Good". Fig. 3.5.4 (a) and Fig. 3.5.4 (b) show correlations of $\boldsymbol{\sigma}(t)$ and $\boldsymbol{\varepsilon}(t)$, respectively. From these figures, change of the de-correlation of the bridge response components $\boldsymbol{\sigma}(t)$ due to local damage affects the SVD process significantly. Thus, the estimated mode shape changes well between before and after damage introduced.

3.5.3. Verification of $\mathbf{N}^{\mathrm{T}}$-based method

Next, the other method which uses transposed interpolation matrix $\mathbf{N}^{\mathrm{T}}$ instead of $\mathbf{N}^{-1}$ is examined in the same way with 3.5.2.

Fig. 3.5.6 shows the first mode shapes estimated by this $\mathbf{N}^{\mathrm{T}}$-based method. Damage is located in $L/10$ and the damage width is 1 (m) (= $L/30$). The vehicle acceleration responses include 1% white noise. From this figure, it can be confirmed that the estimations depend on the road profile, significantly. By comparing between Fig. 3.5.2 and Fig. 3.5.5, changes of the first mode shape estimated by the $\mathbf{N}^{\mathrm{T}}$-based method tend to be larger than those by $\mathbf{N}^{-1}$-based method. Fig. 3.5.6 shows comparisons of the estimated first mode shape in different damage locations. Herein, the damage width is 20 (cm) (= $L/150$). From these figures, by using the $\mathbf{N}^{\mathrm{T}}$-based method, it is confirmed a tendency in which damage change in estimated first mode shape is larger than that by the $\mathbf{N}^{-1}$-based method. Especially, changes due to the local damage of which width is 20 (cm) and located in $L/10$ close to the bridge support can be observed in Fig. 3.5.7 (a).

Fig. 3.5.8 shows the de-correlation of bridge response components $\boldsymbol{\tau}(t)$ and error term $\boldsymbol{\epsilon}(t)$. From this figure, changes of mode shapes estimated by the $\mathbf{N}^{\mathrm{T}}$-based method are caused by changes both of bridge response components $\boldsymbol{\tau}(t)$ and error term $\boldsymbol{\epsilon}(t)$.

3.6. Summary of This Chapter

In this chapter, numerical simulations which use rigid-spring and FEM models as vehicles and bridge are performed to verify three proposed methods: Curvature-based and indirect and direct Mode-Shape-based VO-BHM methods.

First, Curvature-based VO-BHM method can detect damage location based on the wavelet coefficient of measured vehicle acceleration response. The advantages of this method lie in the capability of detecting damage location and usability in which only vehicle acceleration is required.

Second, indirect Mode-Shape-based VO-BHM method does not have feasibility in damage identification due to the low robustness against noise included in measurements. The demerit of this method is to require many data: vehicle acceleration responses, relative displacement between vehicle body and road surface and vehicle position. The noise included measurements affects the estimation more significantly than damage does. On the other hand, in the examinations about

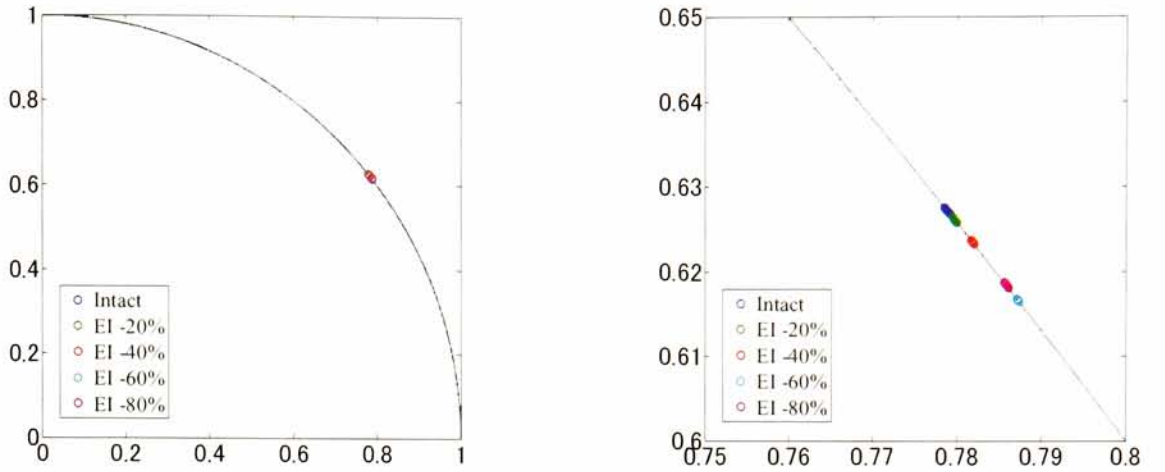

(a) Road profile = Extra Good, Damage location = $L/10$ and Damage width = 1 (m) (= $L/30$)

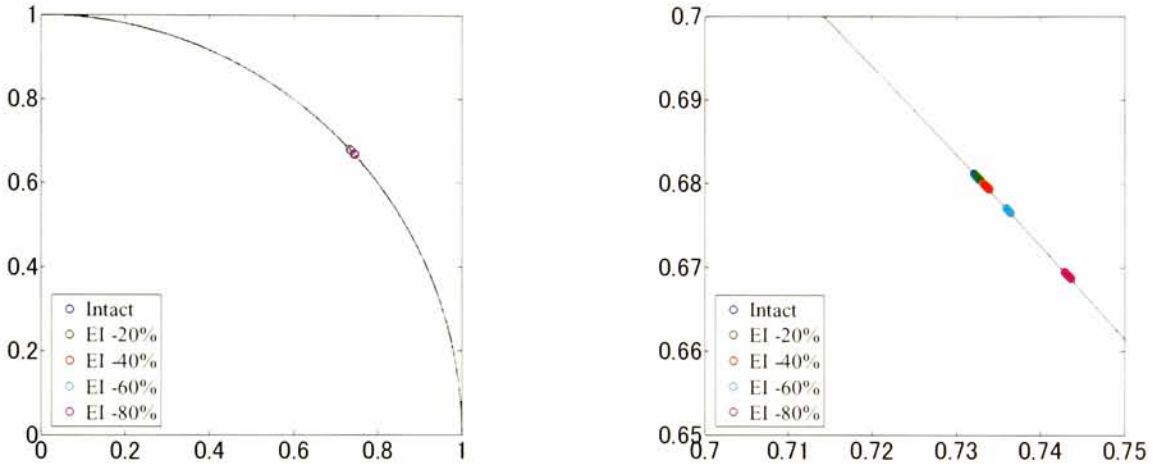

(b) Road profile = Good, Damage location = $L/10$ and Damage width = 1 (m) (= $L/30$)

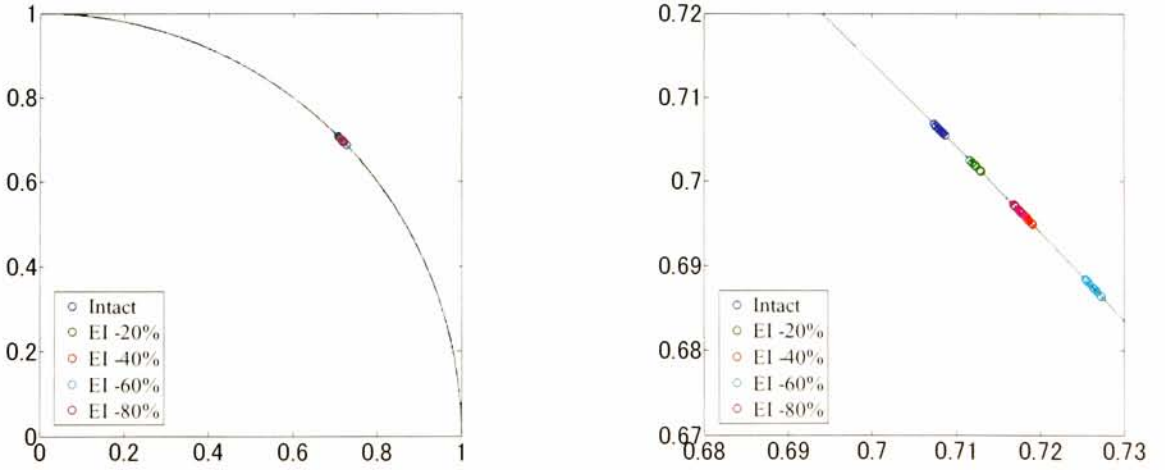

(c) Road profile = Standard, Damage location = $L/10$ and Damage width = 1 (m) (= $L/30$)

Fig. 3.5.6 Estimation results of mode shape when the vehicle speed = 10 (m/s) and mass = 1 (t)

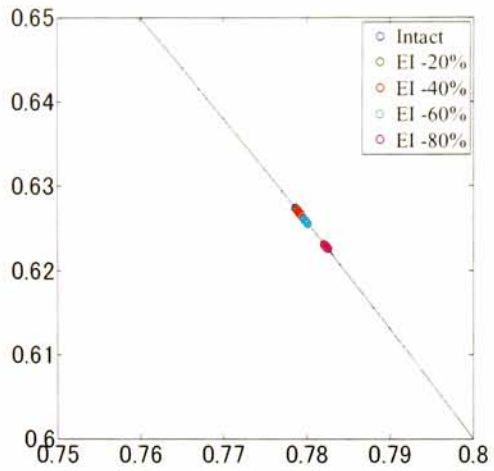

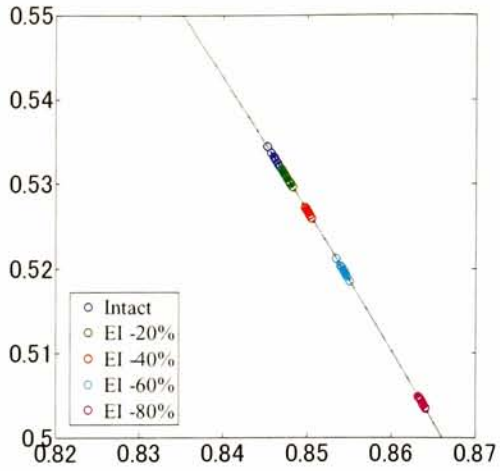

(b) Damage location = $L/10$ (b) Damage location = $L/2$

Fig. 3.5.7 Estimation results of mode shape when the vehicle speed = 10 (m/s) and mass = 1 (t) (Road profile = Extra Good, Damage width = 20 (cm) (= $L/150$))

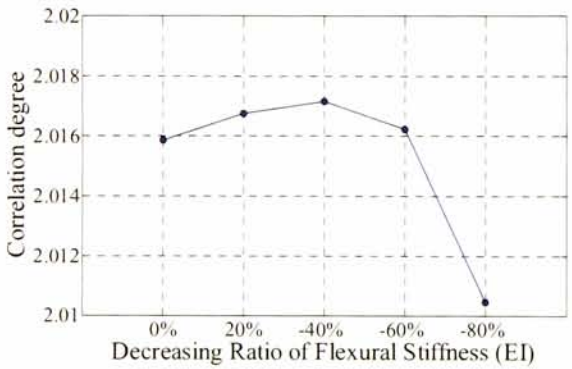

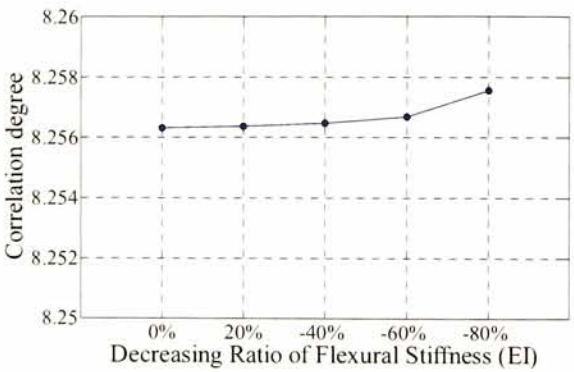

(a) De-correlation of $\boldsymbol{\tau}(t)$ (b) De-correlation of the error term $\boldsymbol{\epsilon}(t)$

Fig. 3.5.8 De-correlation and damage

effective factors, interpolation in STEP 3 of this method can estimate bridge mode shape, accurately.

Third, direct Mode-Shape-based VO-BHM method is verified to show high feasibility of damage identification. This method can be categorized into two kinds: $\mathbf{N}^{-1}$-based and $\mathbf{N}^{\mathrm{T}}$-based methods. They also show high feasibility of damage identification. The effect of 1 % noise is smaller than the effect of local damage on the result.

Below, only Curvature-based and direct Mode-Shape-based VO-BHM methods are applied to experimental data. Note that vehicle position must be measured on the vehicle, but in experiment, the position is measured on the bridge.

Reference

[1] Harris, N.K., Gonzalez, A., Obrien, E.J. and McGetrick, P.: Characteristisation of pavement profile heights using

accelerometer readings and a combinatorial optimisation technique, Journal of Sound and Vibration, Vol.329, pp.497-508, 2010.
[2] Oshima, Y., Yamamoto, K. and Sugiura, K.: Damage identification method of a bridge based on its estimated displacement by the responces of a passing vehicle, Journal of Structural Engineering. A, JSCE, Vol.57A, pp.646-654, 2011.
[3] Yamamoto, K., Oshima, Y., Sugiura. K. and Kawano, H.: Estimation of bridge mode shapes based on vehicle responses,Journal of Japan Society of Civil Engineers, Ser. A1 (Structural Engineering & Earthquake Engineering), Vol.67, No.2, pp.242-257, 2011.
[4] Xiang, Z., Dai, X., Zhang, Y. and Lu, Q.: The Tap-Scan Damage Detection Method for Beam Structures, Advances Interaction & Multiscale Mechanics, pp.541-553, 2010.
[5] Nguyen, K.V. and Tran, H.T.: Multi-cracks detection of a beam-like structure based on the on-vehicle vibration signal and wavelet analysis, Journal of Sound and Vibration, Vol.329, pp.4455-4465, 2010.
[6] Bridge Vibration Monitoring subcommittee, Structural Engineering Committee, JSCE: Guidline for bridge vibration monitoring, pp.110-121, 2000.
[7] Kawatani, M., Kobayashi, Y. and Takamori, K.: Nonstationary random analysis with coupling vibration of bending and torsion of simple girder bridges under moving vehicles, Proc. of JSCE, Vol.570, pp.231-238, 1997.
[8] Roveri, N. and Carcaterra A.: Damage detection in structures under traveling loads by Hilbert-Huang transform, Mechanical Systems and Signal Processing, Vol.28, pp.128-144, 2012.
[9] Zhu, X.Q. and Law, S.S.: Wavelet-based crack identification of bridge beam from operational deflection time history, International Journal of Solids and Structures, 43, pp.2299-2317, 2006.
[10] Lee, S.H.: Effects of condition number on preconditioning for low Mach number flows, Journal of Computation Physics, Vol.231, pp.4001-4014, 2012.

Chapter 4. Experimental Verification in Laboratory

4.1. General Remarks

In this chapter, the proposed methods are examined by laboratory experiment. The main purpose of laboratory experiment is to verify the uncertainties including noise in measurements, bump effect and errors caused by unknown noise which has different characteristics from white noise.

First, the preliminary investigation based on bridge vibration is presented. In the preliminary investigation, the dynamic feature of the bridge system can be confirmed. Then, to verify the proposed methods, wavelet coefficient and mode shape are estimated by the proposed methods.

To detect bridge damage, the proposed methods estimate the spatial characteristics of bridge dynamic behaviors as curvature or mode shape, in this study. By the verification in numerical simulations, it is confirmed that the proposed methods can identify bridge damage under practical conditions. The wavelet coefficient of the vehicle acceleration indicates damage location accurately because it is a non-linear function of the bridge curvature which is a sensitive index to damage. The estimation accuracies of mode shapes based on the proposed methods are often stable to same measuring situations. The mode shape itself does not change even after serious damage introduced. However, the damage, even if it is local and caused at edge location, affects the estimation more significantly than white noise. It means that estimated mode shape can be used for damage index. Thus, in this verification, the Curvature-based and Mode-Shape-based VO-BHM methods are applied to vehicle data. In Mode-Shape-based VO-BHM method, interpolation matrix converts vehicle acceleration directly.

To compare the effect of uncertainty with the index change due to damage, same run scenarios are performed for different damage cases. Used vehicle model is designed to behave in a similar way of a half-car model. To examine accidental factors, bumps are introduced on the vehicle pathway over the bridge.

4.2. Experimental Setup

In this study, a vehicle running laboratory experiment [1]-[3] is performed to evaluate the vehicle-bridge interaction (VBI) system. The experiment setup is summarized in Fig. 4.2.1. The bridge model is H-girder with a height of 66.8 (mm) and damage as shown in Fig. 4.2.1 is introduced by cutting 5 (mm), 10 (mm) and 15 (mm) on the damage section. Fig. 4.2.2 shows Road

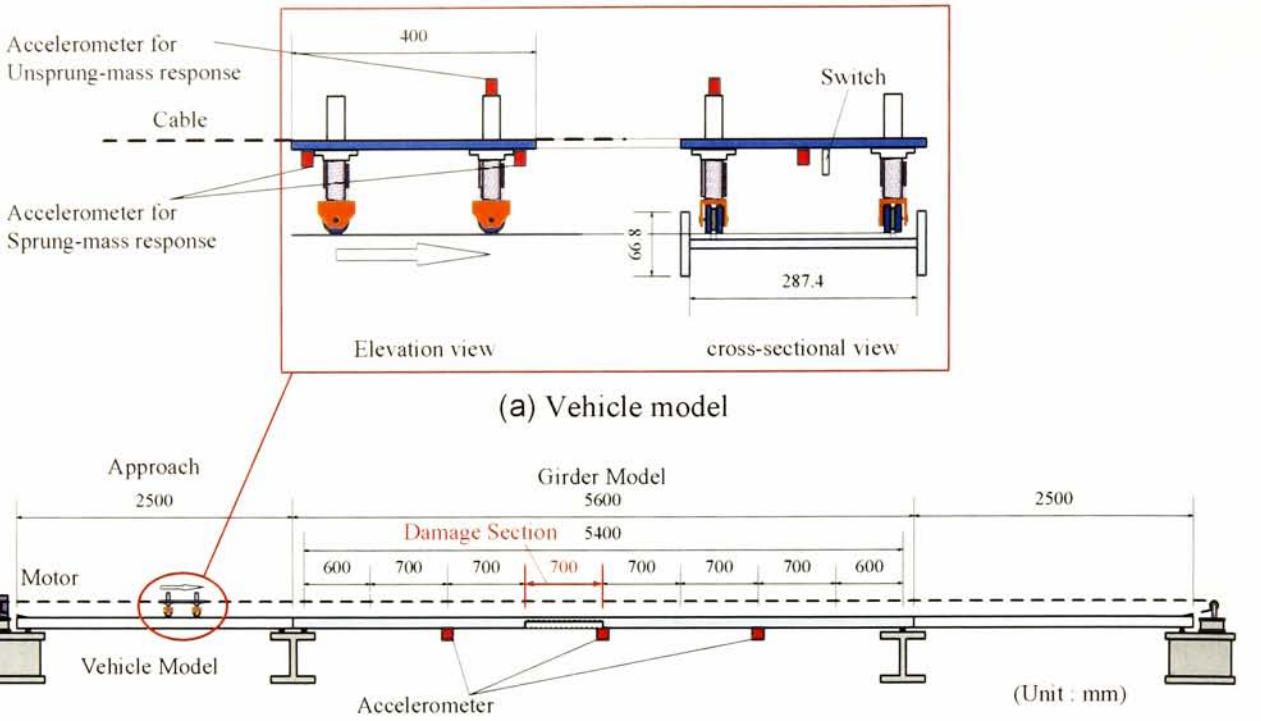

(a) Vehicle model

(b) Bridge model

Fig. 4.2.1 Laboratory experiment setup

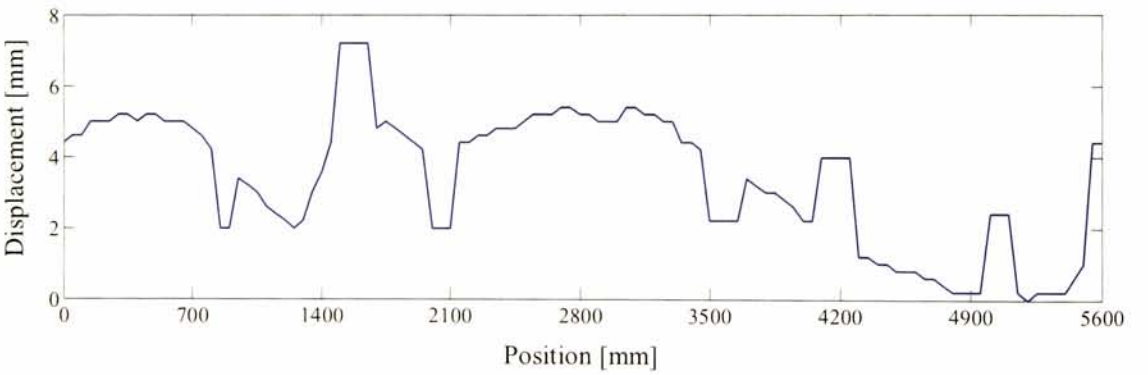

Fig. 4.2.2 Road unevenness with bumps

unevenness is made by referring an actual road roughness data. The bumps are also introduced on the pathway as shown in Fig. 4.2.2. During the experiment, three different vehicle models are considered: V1, V2 and V3, of which the natural frequencies for the bounce motion are changeable using a different set of mass and spring. Each vehicle model runs at three different speed, S1, S2 and S3. These scenarios are summarized in Table 2.3.1. The vehicle model ran 5 times for each scenario. The observation points for acceleration responses of the bridge are located in 1/4, 1/2, 3/4 of the span length. For vehicle model, on the sprung-mass at the front axle, the sprung-mass at the rear axle and the unsprung-mass at the front axle, sensors are installed to measure vertical acceleration responses. In Table 2.3.1 (c), the natural frequency for each case, which is obtained by extracting a peak of Fourier spectrum of the bridge's free vibration, is also shown. By using the free vibration, the

Table 4.2.1 Experiment scenario

(a) Vehicle type

Name	Mass (kg)	Frequency (Hz)
V1	21.4	2.93
V2	21.4	3.71
V3	25.9	2.93

(b) Run scenario

Name	Speed (m/s)
S1	0.93
S2	1.16
S3	1.63

(c) Damage scenario

Name	Cut height (mm)	Natural frequency (Hz)
D0	0	2.66, 10.6, 23.8
D1	5	2.61, 10.5, 23.3
D2	10	2.57, 23.0
D3	15	2.51, 22.6

Table 4.2.2 Experimental bridge model

Span length	5400 (mm)
Young's modulus	2.1×10^{-5} (N/cm^2)
Unit weight	7.8×10^{-2} (N/cm^2)
Area of section	65.43 (cm^2)
Moment of inertia of Area	57.48 (cm^4)

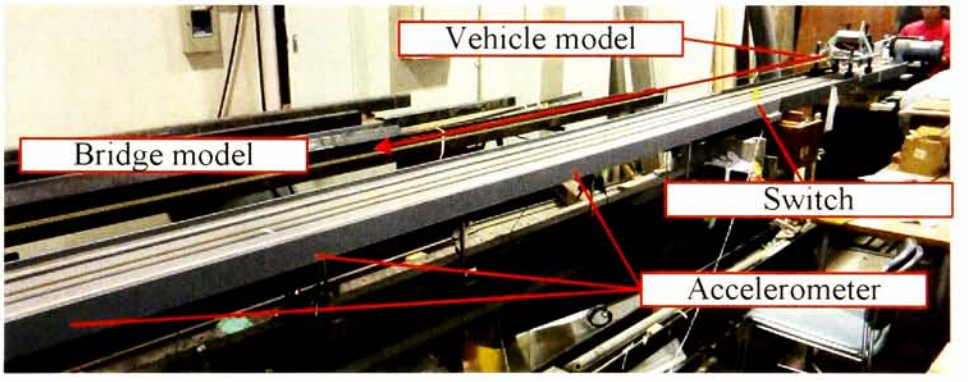

Photo 4.2.1 Experiment model

slightly shifts of eigen-frequencies due to damage can be confirmed.

4.3. Dynamic Behaviors of Bridge and Vehicle

4.3.1. The feature of bridge responses

Fig. 4.3.1 shows the acceleration responses at the span of the bridge model for the case of V1S1D0 in which the vehicle model "V1" runs at speed of "S1" (0.93 m/s) through over the intact bridge model "D0". Measurements in three times of five runs are shown in this figure. Fig. 4.3.1 (a) and Fig. 4.3.1 (b) show the acceleration responses and those power spectra in the case of V1S1D0, respectively. The horizontal axis of Fig. 4.3.1 (a) denotes the position of the vehicle model. From

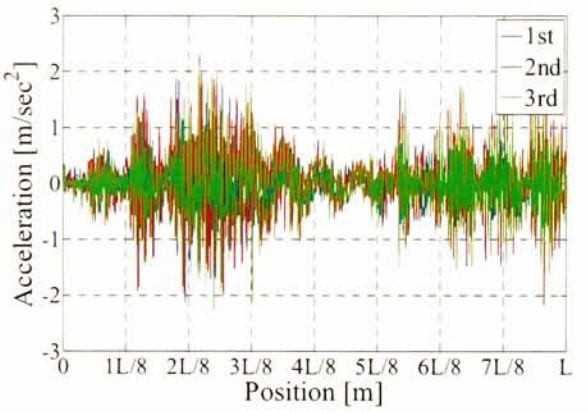

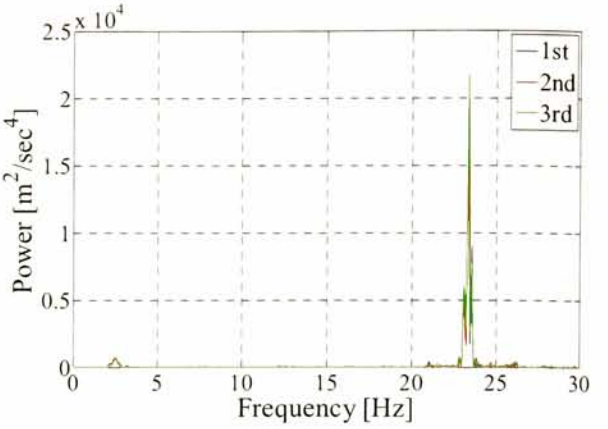

(a) Acceleration responses (b) Power spectra

Fig. 4.3.1 Acceleration responses observed at the middle of the span in the case of V1S1D0

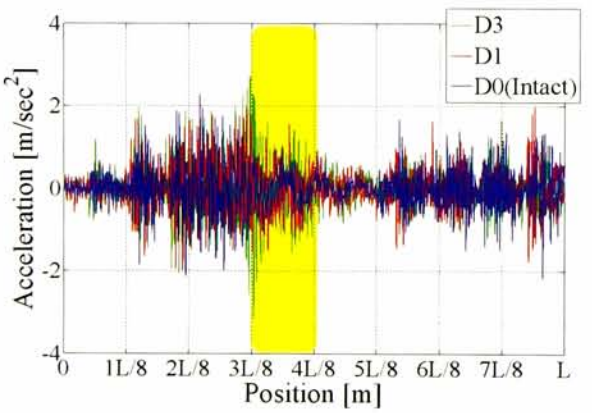

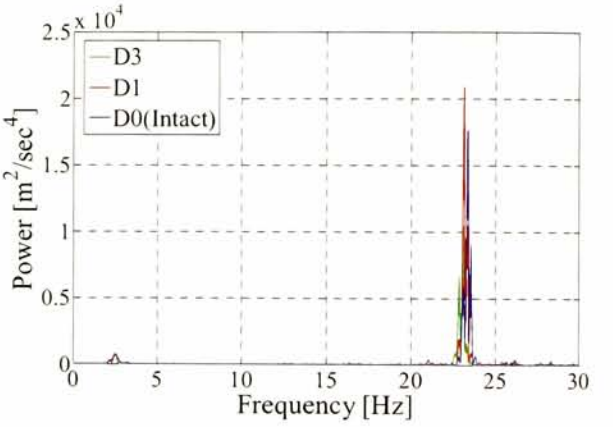

(a) Acceleration responses (b) Power spectrum

Fig. 4.3.2 Comparison of the induced vibrations for V1S1D0 with V1S1D1 and V1S1D3

Fig. 4.3.1 (a), it can be observed that the acceleration responses of the bridge model show high repeatability in spatial domain. Fig. 4.3.1 (b) shows the power spectra of the bridge acceleration responses by Fourier's transform. The power spectra are calculated by the bridge acceleration data only during the vehicle passing on the bridge. It means that peaks in these spectra are just predominant frequencies and may not correspond to bridge eigen-frequencies exactly.

Fig. 4.3.2 shows comparison of bridge responses between the intact ("D0") and damage cases ("D1" and "D3") during the vehicle passing through the bridge section. The bridge acceleration responses are measured at the center of span. Fig. 4.3.2 (a) and Fig. 4.3.2 (b) show the measured bridge acceleration responses and their power spectra, respectively. Blue, green and red lines denote "D0", "D1" and "D3". In Fig. 4.3.2 (a), the horizontal axis indicates the position of the front axle of the vehicle, and yellow box denotes the damaged section. From Fig. 4.3.2 (a), the small changes of the amplitudes between "D0", "D1" and "D3" can be still observed in time domain. From Fig. 4.3.2

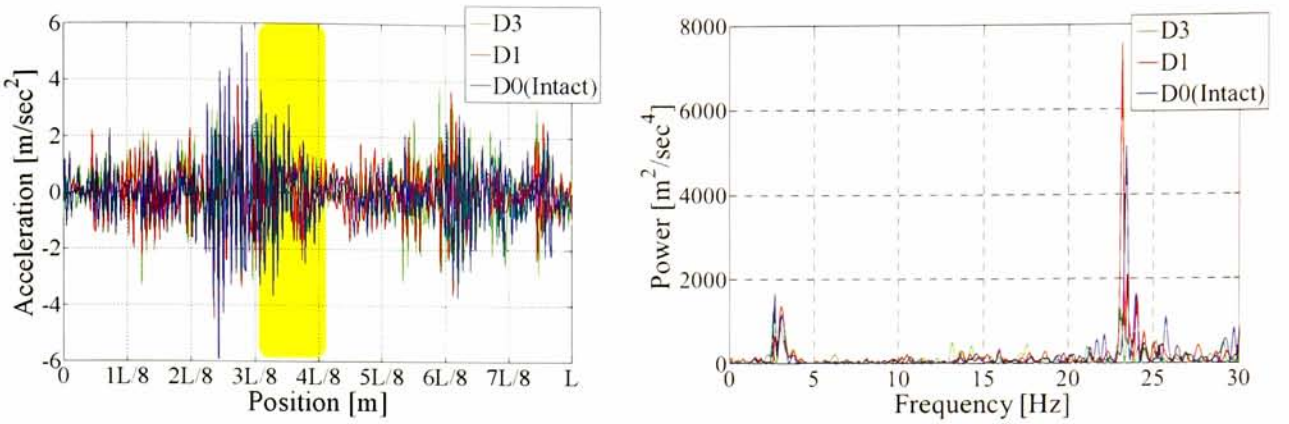

(a) Acceleration responses (b) Power spectrum

Fig. 4.3.3 Comparison of the induced vibrations for V1S3D0 with V1S3D1 and V1S3D3

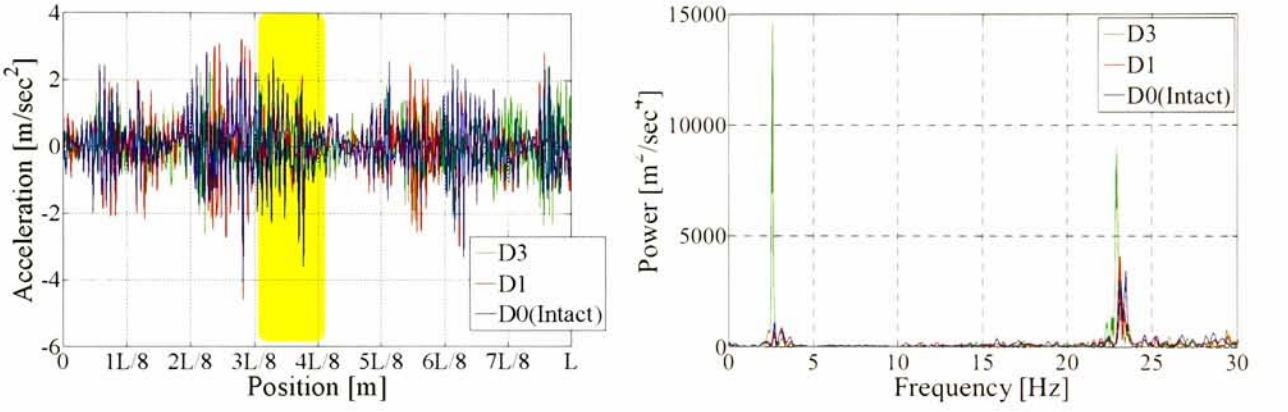

(a) Acceleration responses (b) Power spectrum

Fig. 4.3.4 Comparison of the induced vibrations for V3S3D0 with V3S3D1 and V3S3D3

(b), it can be observed that the second predominant frequency around 20 (Hz) decreases slightly as the damage increases from "D0" to "D3". Fig. 4.3.3 and Fig. 4.3.4 show bridge acceleration responses and their power spectra in the cases of "V1S3" and "V1S4", respectively. From these figures, the bridge responses also show slightly changes of the predominant frequencies due to damage. The amplitudes of second dominant peaks tend to become larger, as the damage increases. But, this tendency is not always confirmed. For example, in Fig. 4.3.3 (b), although the green line denotes the most serious damage case, its amplitude is not larger than others. It means that there is difficulty in using amplitude-based indices for damage detection even in frequency domain.

Nonetheless, from Fig. 4.3.4, both of the amplitude and predominant frequencies change and shift distinctively in a certain rate. It means the probability of the damage detection based on dominant power and predominant frequency.

4.3.2. The vehicle responses

Herein, the feature of vehicle acceleration responses both in spatial and frequency domain is confirmed. Because the bridge vibration changes slightly in frequency domain, the vehicle vibration can be also expected to change as damage increases.

Fig. 4.3.5 shows the acceleration responses in the case of "V1S1D0" both in spatial and frequency domain. The measurements are vehicle accelerations of the sprung-mass at the front axle, the sprung-mass at the rear axle and the unsprung-mass at the front axle. Measurements in three times of five runs are shown in this figure. In this experiment, because the vehicle runs at the constant speed by motor, the time can be converted to the vehicle position. From Fig. 4.3.5 (a-1) and Fig. 4.3.5 (b-1), high repeatability can be also observed in vehicle acceleration responses of the sprung-mass both at the front and rear axles in spatial domain. From Fig. 4.3.5 (a-2) and Fig. 4.3.5 (b-2), the same tendency can be observed in frequency domain. The predominant frequencies and the amplitude of peaks are very similar for each other. On the other hand, from Fig. 4.3.5 (c-1) and Fig. 4.3.5 (c-2), there is not high repeatability in the acceleration responses of the unsprung-mass at the front axle both in spatial and frequency domain.

In Fig. 4.3.5, the sprung-mass responses include the sharp peaks. These peaks are caused by the bumps on the road unevenness. Variation of peaks at the same position tends to be larger than other vibrations. It may be caused by sensor accuracy. This means that noise amplitude included in acceleration measurements may depend on the amplitude, and the accidental factors such as bumps and other impacts may affect the accuracy.

Next, the differences of vehicle acceleration responses between intact (D0) and damage cases (D1 and D3) are confirmed. Fig. 4.3.6 shows time histories and power spectra on the vehicle responses. The measurements in this figure are the acceleration responses of the sprung-mass at the front axle, the sprung-mass at the rear axle and the unsprung-mass at the front axle of the vehicle. Fig. 4.3.6 (a-1), (b-1) and (c-1) shows acceleration responses of them, while Fig. 4.3.6 (a-2), (b-2) and (c-2) shows corresponding power spectra. The shown scenario in this figure is V1S1. Blue, green and red lines denote the case "D0", "D1" and "D3", respectively. By the same way with Fig. 4.3.5, the horizontal axis in Fig. 4.3.6 (a-1), (b-1) and (c-1) is converted from time domain to spatial domain. Yellow boxes in these figures denote the damaged section. The vehicle acceleration responses show the high repeatability even though in comparison between before and after damage in sprung-mass responses. Amplitudes of vehicle acceleration responses in spatial domain increase, as the damage increases from "D0" to "D3". This tendency can be observed especially in the peaks. On the other hand, from Fig. 4.3.6 (a-2) and (b-2), the power of the vehicle responses becomes larger in high frequency domain. Predominant frequencies of the sprung-mass accelerations do not change well, while those of the unsprung-mass accelerations slightly change. In the power spectra of the unsprung-mass responses, it can also observed that the distribution shifts and changes especially in the high frequency domain.

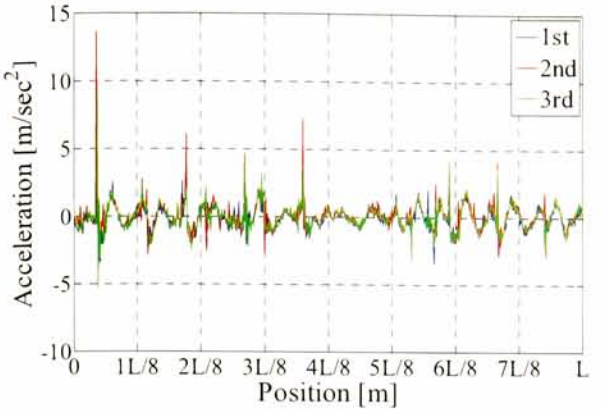

(a-1) Acceleration of sprung-mass at the front axle

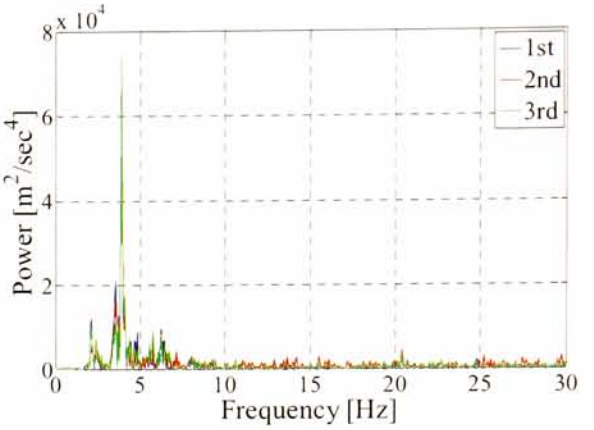

(a-2) Power spectrum of sprung-mass at the front axle

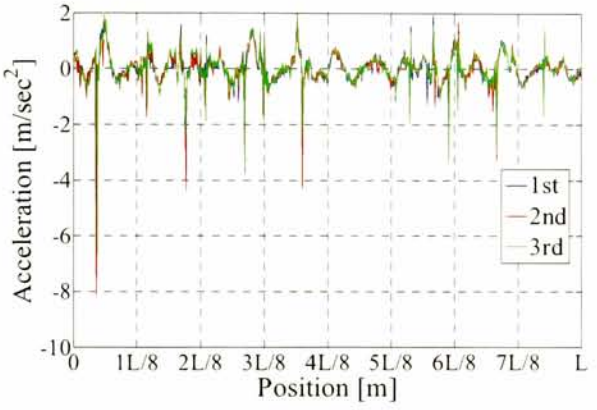

(b-1) Acceleration responses of sprung-mass at the rear axle

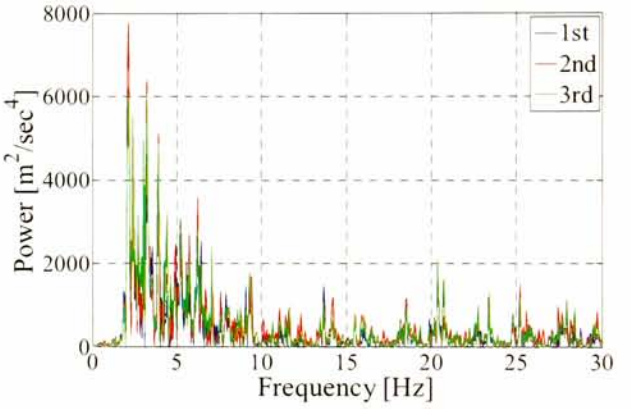

(b-2) Power spectrum of sprung-mass at the rear axle

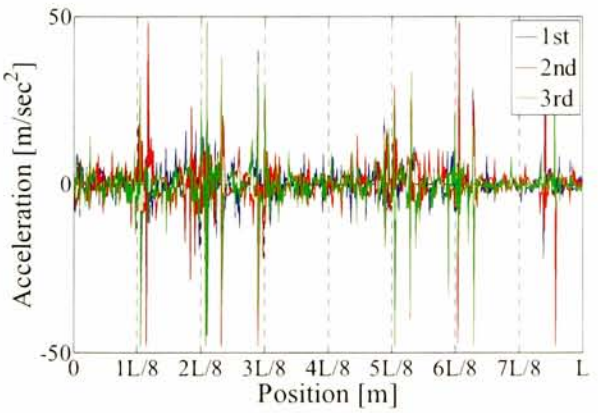

(c-1) Acceleration responses of unsprung-mass at the front axle

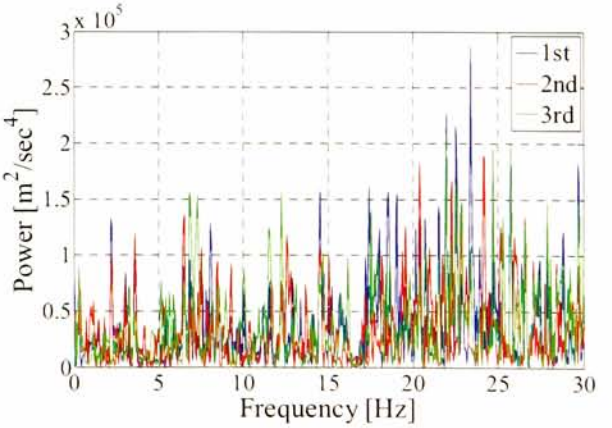

(c-2) Power spectrum of unsprung-mass at the front axle

Fig. 4.3.5 Vehicle dynamic behaviors for V1S1D0

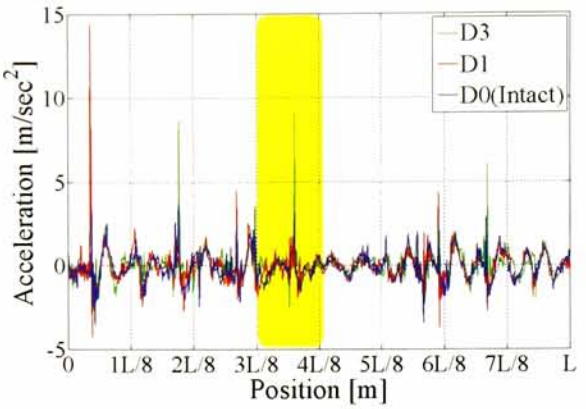

(a-1) Acceleration of sprung-mass at the front axle

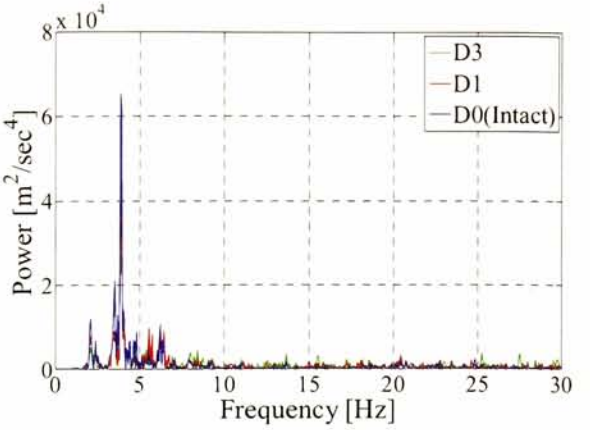

(a-2) Power spectrum of sprung-mass at the front axle

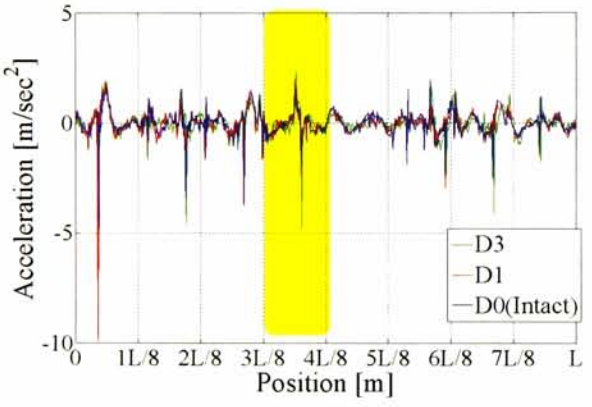

(b-1) Acceleration responses of sprung-mass at the rear axle

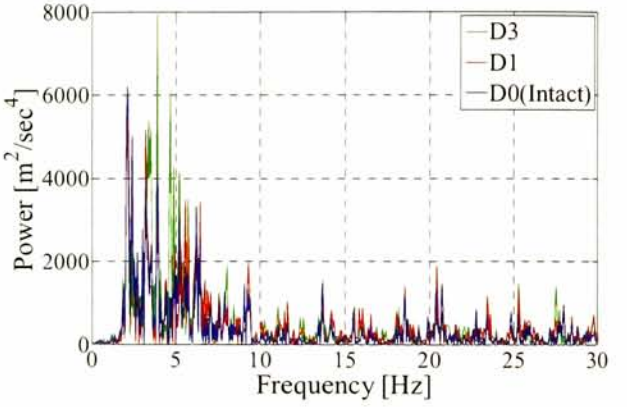

(b-2) Power spectrum of sprung-mass at the rear axle

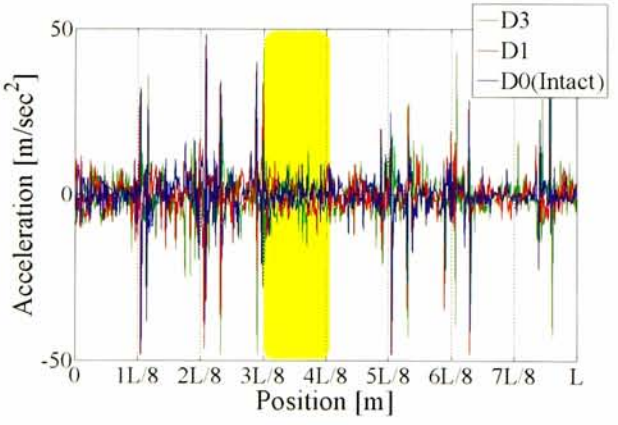

(c-1) Acceleration responses of unsprung-mass at the front axle

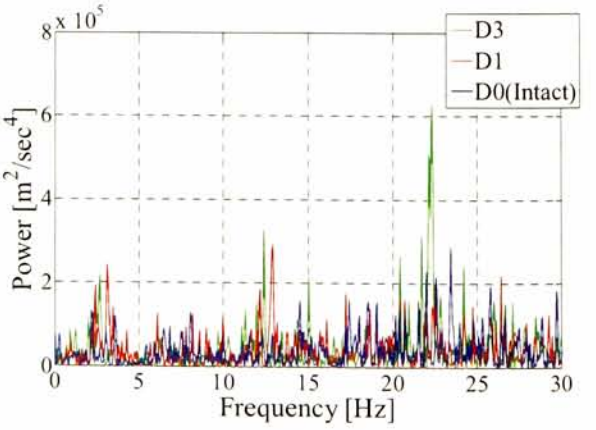

(c-2) Power spectrum of unsprung-mass at the front axle

Fig. 4.3.6 Vehicle dynamic behaviors for V1S1

4.4. Verification for the proposed methods

4.4.1. Curvature-based VO-BHM

Herein, Curvature-based VO-BHM methods are examined. To verify the proposed method, continuous wavelet transform (CWT) is applied to the acceleration responses of the sprung-mass and unsprung-mass of the vehicle model. The power of wavelet coefficient for vehicle acceleration response is a non-liner function of bridge curvature which may change due to damage. In this verification, the mother wavelet is the complex Gaussian wavelet. Because the sampling frequency is 100 (Hz), scale of the mother wavelet is set to 2 and 10, which correspond to 25 (Hz) and 5 (Hz), respectively

Fig. 4.4.1 shows the power of the wavelet coefficient of the vehicle responses for V1S1 run scenarios. The blue, red and green lines denote the intact case "D0" and damage cases "D1" and

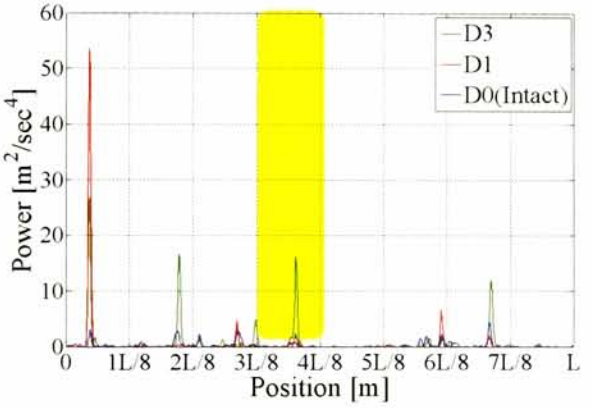

(a-1) Sprung-mass, scale=2

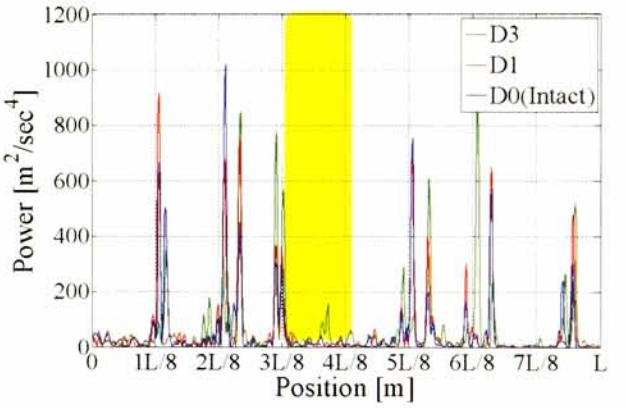

(b-1) Unsprung-mass, scale=2

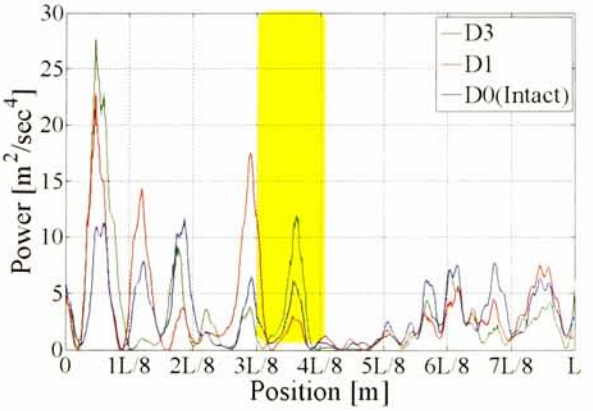

(a-2) Sprung-mass, scale=10

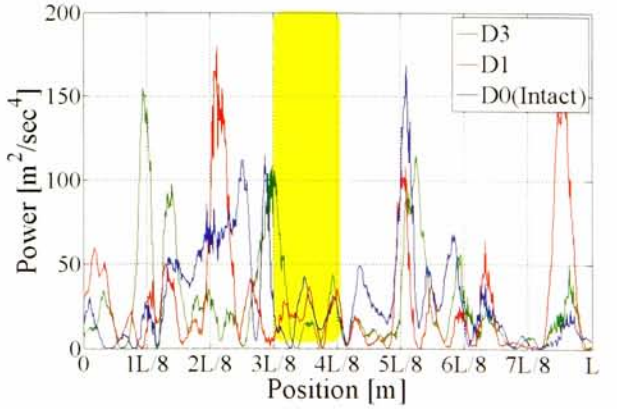

(b-2) Unsprung-mass, scale=10

Fig. 4.4.1 Power of wavelet coefficient of vehicle acceleration response for V1S1

"D3". The horizontal axis indicates the position of the front axle of the vehicle. Fig. 4.4.1 (a-1) and (b-1) show the wavelet coefficients of the front and rear axles, respectively, at the scale of 2. Fig. 4.4.1 (a-2) and (b-2) also show the wavelet coefficients of the front and rear axles, respectively, at the scale of 10. The variation of the power at peaks tends to be larger in this figure, especially in the unsprung-mass. Although the results of the numerical simulations show the high probability of the curvature estimation in low scale CWT, the difference between intact and damage cases in experimental results are not clear. Because there are many peaks, it is difficult to extract only peaks due to damage from others. In this experiment, bumps are introduced to the road unevenness. The wavelet coefficients have many peaks at the bump positions.

Next, wavelet coefficients of acceleration responses measured in the unsprung-mass at the front axle of vehicle are shown in Fig. 4.4.2, for other run scenarios. The horizontal axis denotes the position of the front axle of the vehicle. Yellow boxes indicate the damaged section. From these figures, it is difficult to identify damage location because there are many peaks in other intact

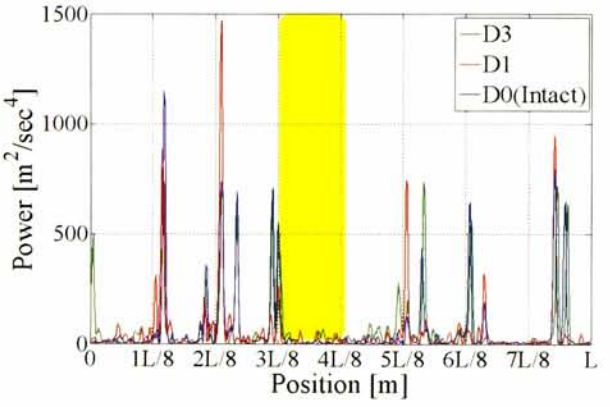

(a) V2S1

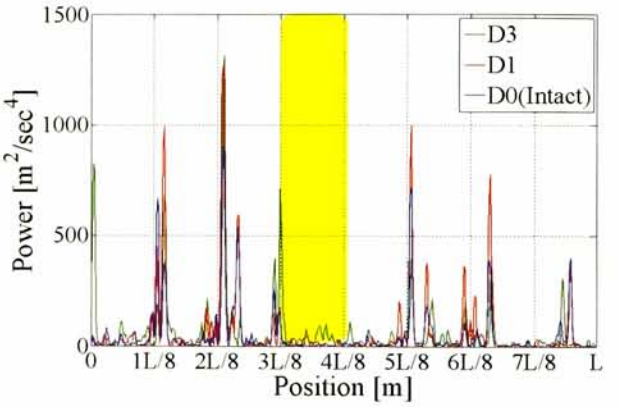

(b) V3S1

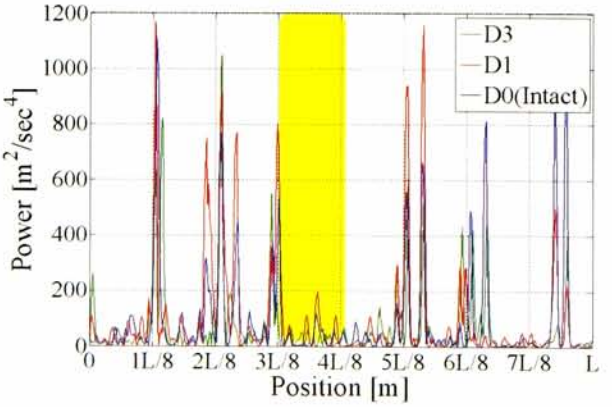

(c) V3S2

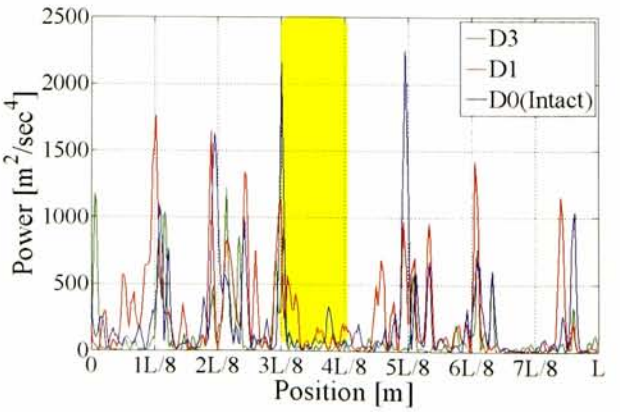

(d) V3S3

Fig. 4.4.2 Power of wavelet coefficients of unsprung-mass acceleration responses at the scale of 2

section. From these figures, the peaks occur at the time when the front and rear axles pass over bumps.

In this experiment, many peaks in the wavelet coefficients are identified, and most of them may be caused by the impact of bump. Then, it is difficult to distinguish the peaks of damage from those of bumps.

4.4.2. Mode-Shape-based VO-BHM

Herein, the direct Mode-Shape-based VO-BHM is also verified by laboratory experiment. The used measurements are sprung-mass vertical accelerations at the front and rear axles of the vehicle model. The objective time range is from when the front axle enters into the bridge span to when the rear axle leaves out. $\mathbf{N}^{-1}$-based method is adopted for VO-BHM.

Fig. 4.4.3 shows estimated mode shapes. In this figure, red lines indicate the estimation based on the proposed VO-BHM method, while blue lines indicate the mode shapes estimated by singular value decomposition (SVD) of bridge accelerations, which is BO-BHM. There are three observation points on the bridge. Fig. 4.4.3 (a-1), (a-2) and (a-3) show the results in the cases of "V1S1" between "D0", "D1" and "D3", while Fig. 4.4.3 (b-1), (b-2) and (b-3) show the same in the cases of "V2S1". By comparison between "V1" and "V2" under same run speed, similar mode shapes are obtained when using bridge acceleration. On the other hand, when using vehicle data, there is difference between "V1" and "V2" even under same run speed. It means that it is important to estimate mode shape under same condition for VO-BHM method. From these figures, estimation errors of VO-BHM obviously vary, as the damage increases. The de-correlation of the decomposed bridge components may change due to damage or accidental factors such as bumps.

The mode shapes estimated by the proposed VO-BHM method can be plotted on 2-D graph, because each of them insists only in two values. Fig. 4.4.4 show the estimated mode shapes for each bridge state in all cases. Amplitudes of mode shapes in this figure are normalized in the same way of numerical verification, in which $x^2 + y^2 = 1$ where x and y denote the values of each mode shape. Black dot circle indicate this unit circle in this figure. Blue, green, red and black dot lines indicate the average angles of the plotted mode shapes for each case, "D0", "D1", "D2" and "D3". The average of estimated mode shape angles changes clearly. However, the variations of them in each case are much larger than their changes between intact and damage cases.

In this experiment, the mode shapes are estimated based on Eq. (2.57). Estimated mode shapes by proposed VO-BHM method are similar to those estimated by SVD of bridge accelerations. The proposed method can estimate bridge mode shapes roughly. But, the variations of the results are larger than the changes due to damage. It may be caused by variation of peaks observed in spatial domain. Amplitudes of peaks observed in spatial domain vary widely due to bumps. This may affect significantly on the estimation results.

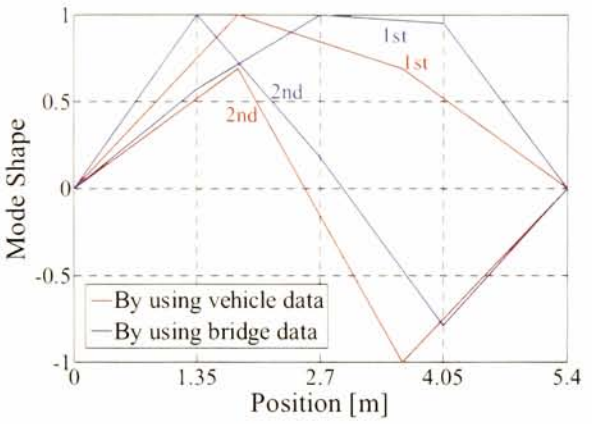

(a-1) V1S1D0

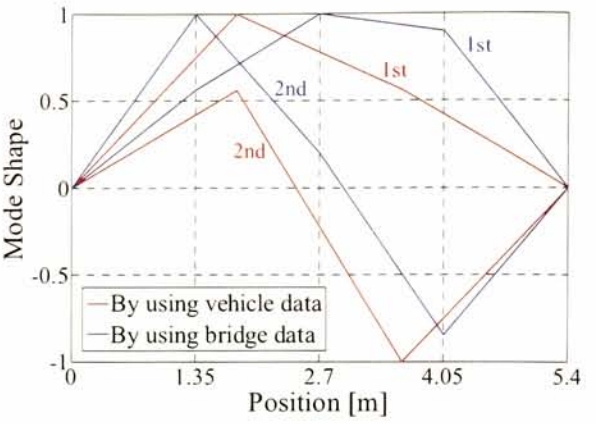

(b-1) V2S1D0

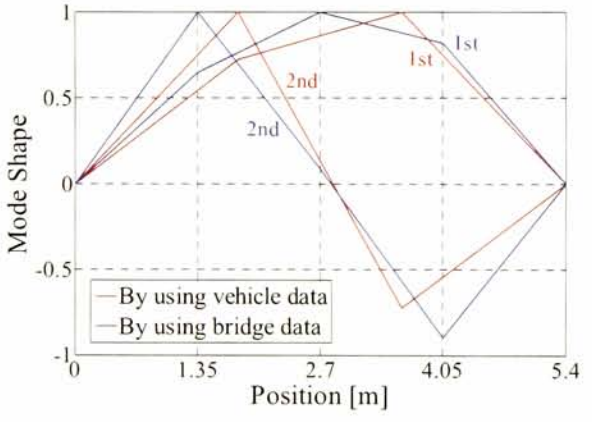

(a-2) V1S1D1

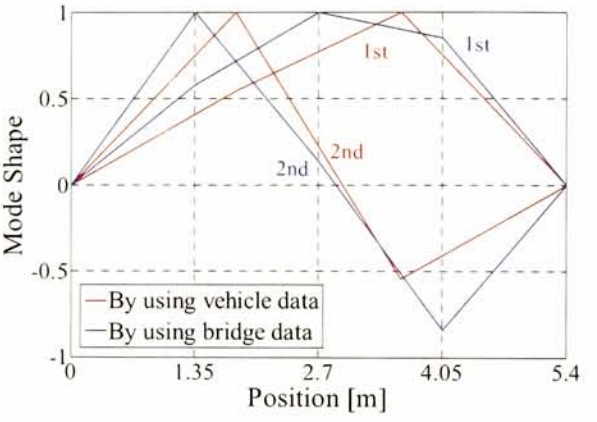

(b-2) V2S1D1

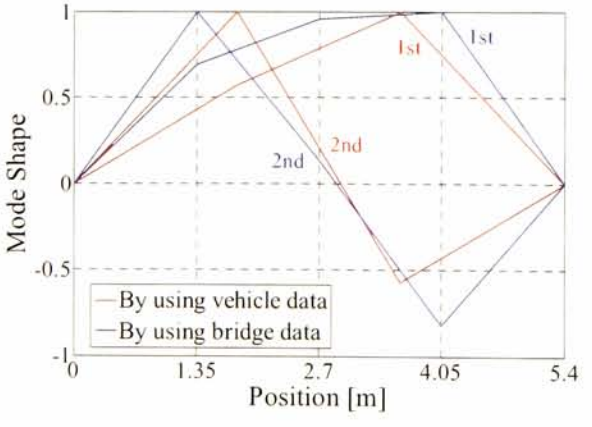

(a-3) V1S1D3

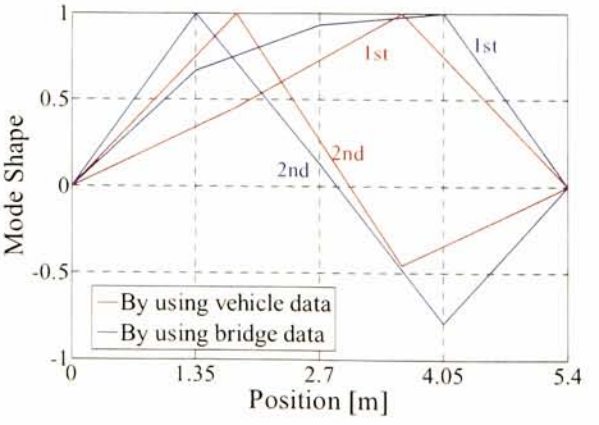

(b-3) V2S1D3

Fig. 4.4.3 Mode shapes estimated by using vehicle responses and bridge responses

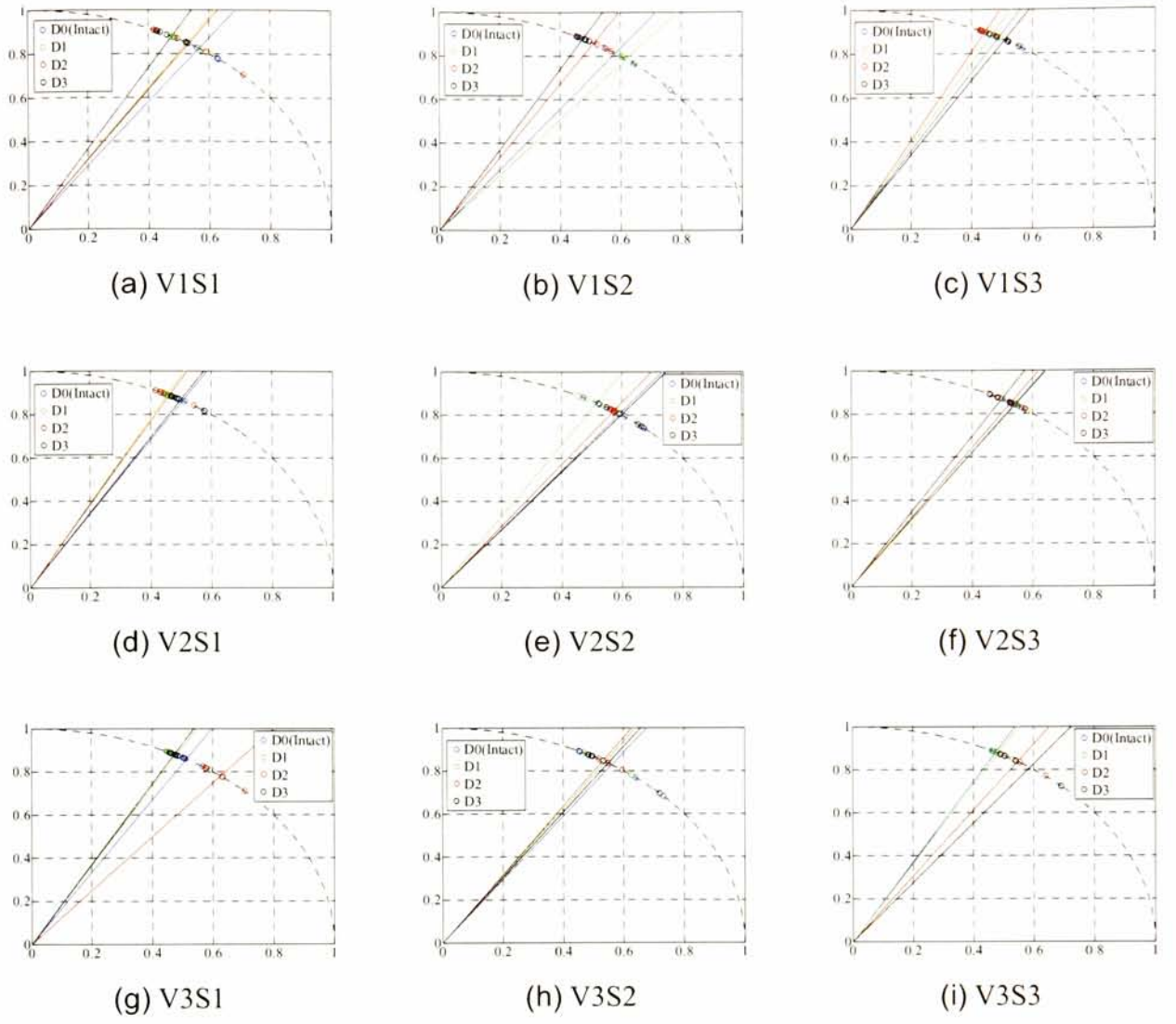

(a) V1S1 (b) V1S2 (c) V1S3

(d) V2S1 (e) V2S2 (f) V2S3

(g) V3S1 (h) V3S2 (i) V3S3

Fig. 4.4.4 Mode shape estimated by using vehicle responses

4.5. Summary of this chapter

In this chapter, the experimental verification is performed by vehicle and bridge model. Three kinds of vehicle run through the bridge model at the three different speeds. Bridge damage is introduced by cutting a part of girder.

In this experiment, difference between intact and damage cases is observed. Acceleration responses and their power spectra both of vehicle and bridge have the high repeatability in each case. But, only for unsprung-mass acceleration of the vehicle, the repeatability is low. It means that there are significant accidental factors which affect differently in each run. In this experiment, the accidental factor is bump introduced on the bridge model. Bumps affect the acceleration significantly

and increase the variation of peaks. However, bumps also excite the vehicle and bridge very well, and it can be confirmed that the predominant frequencies of the bridge shift as the damage increases in this experiment. In power spectra of the unsprung-mass accelerations in high frequency domain, changes of the predominant frequencies can be also observed.

In the verification of Curvature-based VO-BHM method, the variation of the wavelet coefficient of the vehicle responses is much larger than changes due to damage, because the bump affects the high frequency domain.

In the verification of Mode-Shape-based VO-BHM method, it is cleared that this method can estimate the bridge mode shape roughly, but the accuracy of this method may be not enough to identify bridge damage, because the variation of mode shapes is much larger than their changes caused by the damage.

Reference

[1] Toshinami, T., Kawatani, M. and Kim, C.W. : Feasibility investigation for identifying bridges fundamental frequencies from vehicle vibrations, Bridge maintenance, safety, management and life-cycle optimization, IABMAS 2010, pp.317-322, 2010.

[2] Kim, C.W., Isemoto, R., Kawatani, M. and Sugiura, K.: Structural diagnosis of bridge using output-only vibration in moving vehicle laboratory experiment, Journal of JSCE, Ser.A2, Vol.67, No.2 (Applied Mechanics), pp.I-833-842, 2011.

[3] Yamamoto, K., Toshinami, T., Oshima, Y., Kim, C.W., Sugiura, K. and Kawatani, M.: Bridge assessment based on statistical analysis of the response of a vehicle passing over the bridge, Journal of JSCE, Ser.A2, Vol.67, No.2 (Applied Mechanics), pp.I_855-I_864, 2011.

Chapter 5. Field Experiment

5.1. General Remarks

Bridge health monitoring (BHM) based on vibration measurements has been intensively studied to secure bridge safety. Existing studies [1], [2], [3] show the feasibility of detecting bridge damages from changes of dynamic parameters focusing on change of modal frequencies, damping and mode shapes. Most of the studies, however, investigate the feasibility of the vibration-based BHM by means of numerical simulations [4] and laboratory experiments [5], while verifying the validity of the BHM for real bridges is a crucial technical issue. Bridge owners often request data to prove the feasibility for real-world problems when they consider implementation of BHM. Damage experiments on real bridges, however, are generally not allowed by bridge owners from the point of view on public safety, despite of increasing needs of BHM especially for short span bridges. How to vibrate short span bridges effectively is one of important factors in realizing BHM. Traffic-induced vibration experiment on real bridges before and after applying damage, therefore, is very meaningful within the context of BHM to real-world applications. This dissertation presents a damage experiment on a real bridge which is planned to be removed. This section presents a summary of the field damage experiment and verifies the proposed method.

The proposed Curvature-based and direct Mode-Shape-based methods are applied to vehicle acceleration responses. Although the position of the vehicle must be measured in the inspection, it is measured by photoelectric sensors installed on the bridge. In future, it is expected to be measured accurately by GPS system.

5.2. Experimental Setup

The field experiment [6] is conducted on a steel cantilever truss bridge which is planned to be removed. The bridge comprises 9 spans as shown in Fig. 1, and the 5th span is the monitored span of which length is about 65m. Fig. 5.2.1 shows an overview of the field experiment: Sensors deploying map is shown in Fig. 5.2.2; Fig. 5.2.3 shows the cross sectional view of the bridge with vehicle

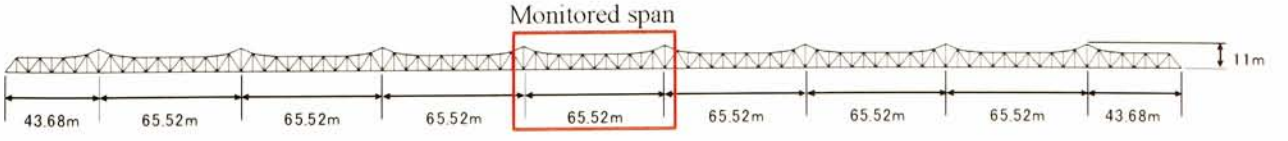

Fig. 5.2.1 Elevation view of bridge

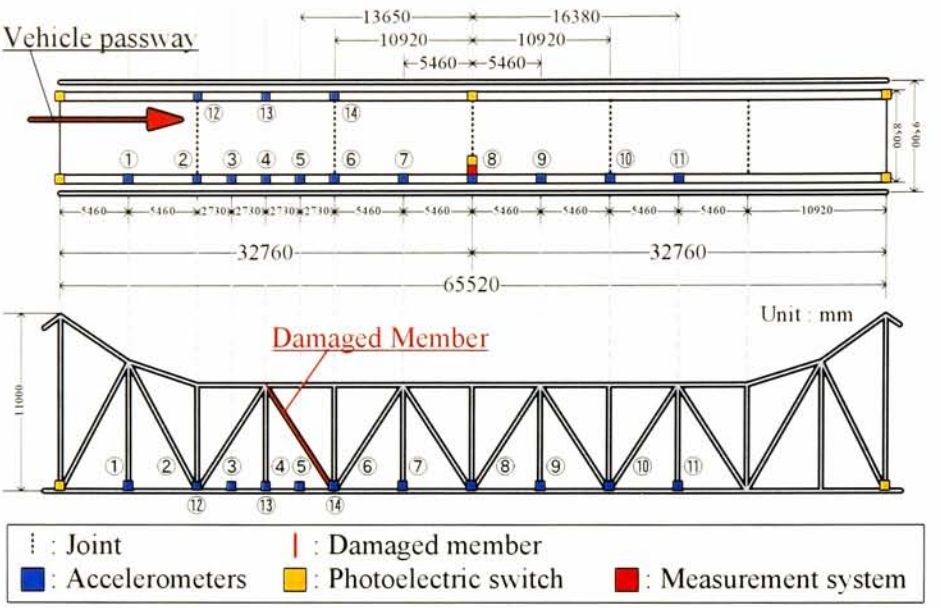

Fig. 5.2.2 Sensor deployment, plan and elevation view

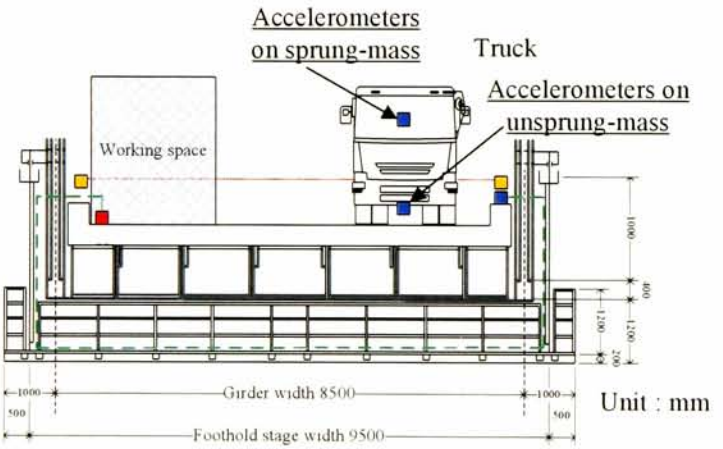

Fig. 5.2.3 Cross sectional view and vehicle loading

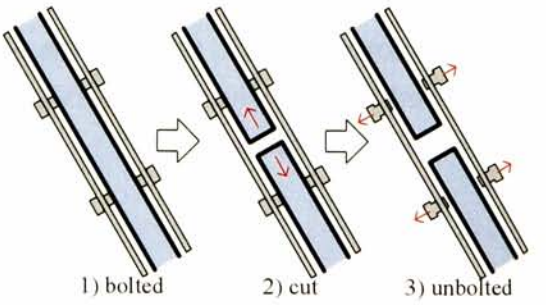

Fig. 5.2.4 Damage installation steps

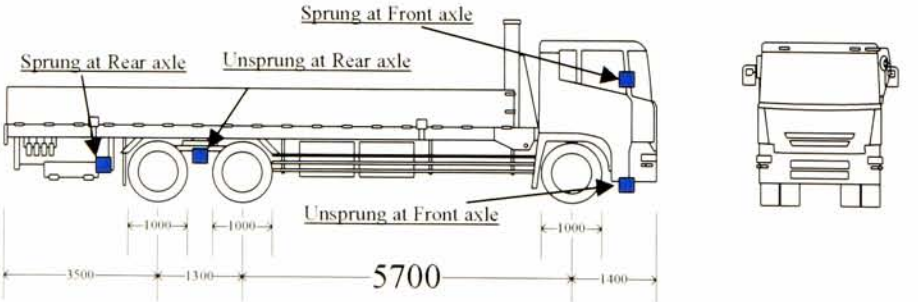

Fig. 5.2.5 Truck model

path; and Fig. 5.2.4 shows how to apply damage. Bridge sensors are arranged closely around the damage member. The diagonal tension member located in L/3 is cut as an artificial damage as shown in Fig. 5.2.4 in which the red colored truss member indicates the damaged member.

Fig. 5.2.5 shows the vehicle outline and sensor deploying map of the vehicle. Axle loads of the passing vehicle are summarized in Table 5.2.1. Experimental scenarios are shown in Table 5.2.2. The identical vehicle is used in the two days experiment, but the vehicle weights are slightly different because location of the load block on the vehicle is slightly changed. Four sensors are mounted on the vehicle to measure vibrations of bounce and axle hop motions at the front and rear axles. To synchronize two independent data loggers on the vehicle and bridge, pulse signals are transmitted to both data loggers at the same time. Photoelectric switches mounted on the entrance, span center and end of the span are used to estimate location and average speed of the passing vehicle. Table 5.2.1 shows planned and measured vehicle speed. Photo 5.2.1 shows photographs of the field experiment.

Table 5.2.1 Vehicle weight

	First day				Second day			
	Front	Rear 1	Rear 2		Front	Rear 1	Rear 2	
Left	41.7	47.8	35.8		41.9	47.7	37.0	
Right	45.7	48.1	34.1	Total	45.9	49.7	36.2	total
Total	87.4	95.9	69.9	253	87.8	97.4	73.2	258

(Unit: kN)

Table 5.2.2 Experiment scenarios

Bridge state	Run speed (km/h)			Vehicle weight (kN)			
	10	20	40	Front	Rear 1	Rear 2	Total
Intact	1st	1st	1st	87.4	95.9	69.9	253
		2nd	2nd, 3rd	87.8	97.4	73.2	258
Damage	1st, 2nd, 3rd	1st, 2nd, 3rd	1st, 2nd, 3rd	87.8	97.4	73.2	258

Table 5.2.3 Planned and measured vehicle speed

Run Case	Run speed (km/h)	
	Planned	Measured
Intact 1st	40.0	37.6
Intact 2nd	40.0	36.5
Intact 3rd	40.0	36.6
Damage 1st	40.0	35.7
Damage 2nd	40.0	36.2
Damage 3rd	40.0	36.7

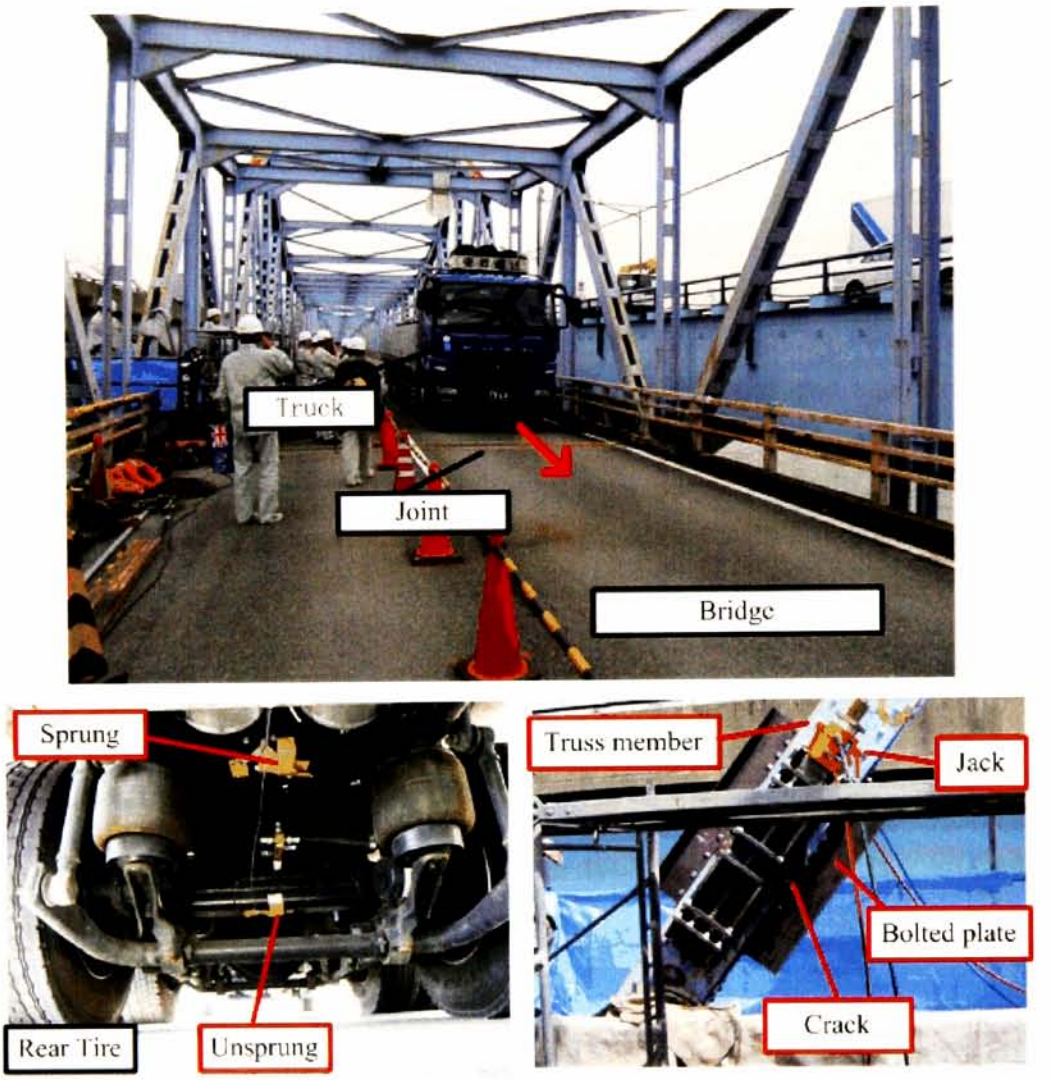

Photo 5.2.1 Photographs of the field experiment

5.3. Dynamic Behaviors of Bridge and Vehicle

5.3.1. The bridge responses

The bridge acceleration response at the point 4 ($3L/12$) and point 8 ($L/2$) are shown in Fig. 5.3.1. The objective run cases are 40 (km/h) runs for intact and damage. The horizontal axis denotes the vehicle position which is measured by three photoelectric switches. A sign 'V' in this figure indicates the location of a joint. In time domain, the bridge acceleration responses show the high repeatability, which agrees the laboratory experimental data. From Fig. 5.3.1, the variation of the vehicle run speed as shown in Table 5.2.3 does not affect the bridge responses in spatial domain. This may be because of the road profile which affects the VBI system significantly in spatial domain.

Fig. 5.3.2 shows Fourier's power spectra for the same cases as shown in Fig. 5.3.1. The peaks in this figure denote the dominant frequencies, which does not always correspond to

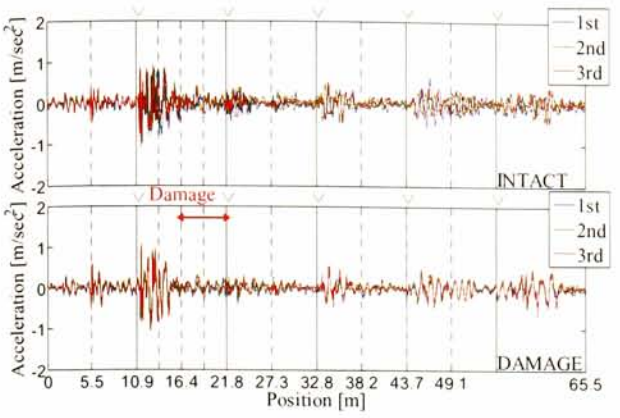

(a) At the measuring point 4 (16.4 (m))

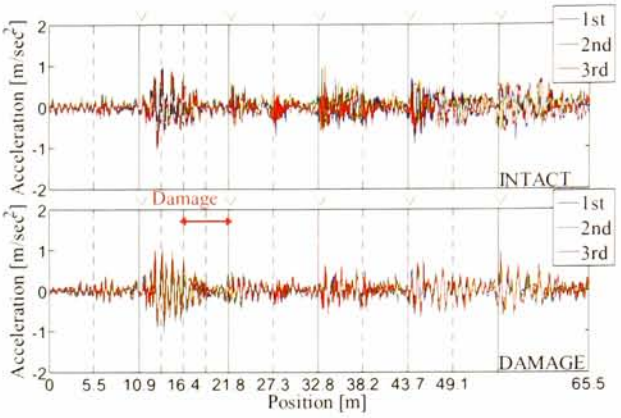

(b) At the measuring point 8 (32.8 (m))

Fig. 5.3.1 Bridge response (Upper: Intact, Lower: Damaged)

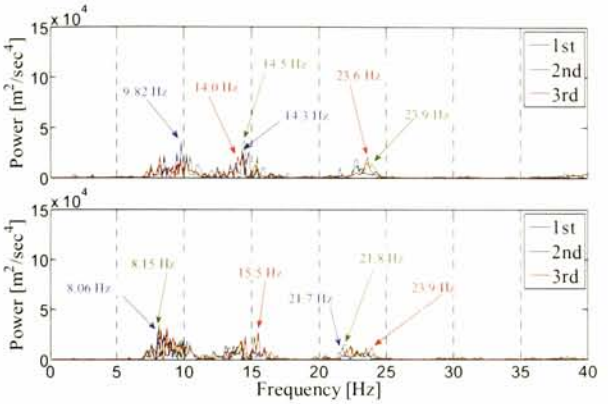

(a) At the measuring point 4 (16.4 (m))

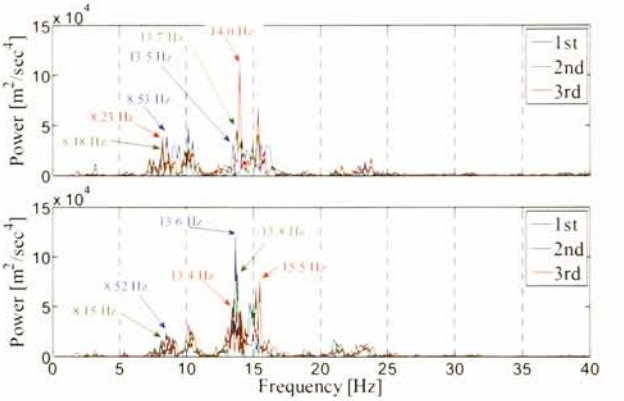

(b) At the measuring point 8 (32.8 (m))

Fig. 5.3.2 Bridge response in frequency domain (Upper: Intact, Lower: Damaged)

eigen-frequencies of the bridge. The objective time range is from the moment when the front axle enters into the bridge to the moment when the last axle leaves out. The measurements are only forced vibrations and do not include free and stationary vibrations. The dominant frequencies varies in all cases. On the basis of experimental results in the laboratory, the dominant frequencies are expected to change due to damage. However it is difficult to confirm the changes in frequency domain even after the damage is introduced.

The bridge vibration in VBI system is mostly affected by the motion of moving vehicles which is generated by road unevenness and thus the frequencies of input signals are proportional to the vehicle speed. The relation between the spatial frequency Ω_r and the frequencies f is definable as

$$\Omega_r v_V = f \tag{5.1}$$

where v_V is the speed of the vehicle. Eq. (5.1) is also rewritable as Eq. (5.2) for different vehicle s

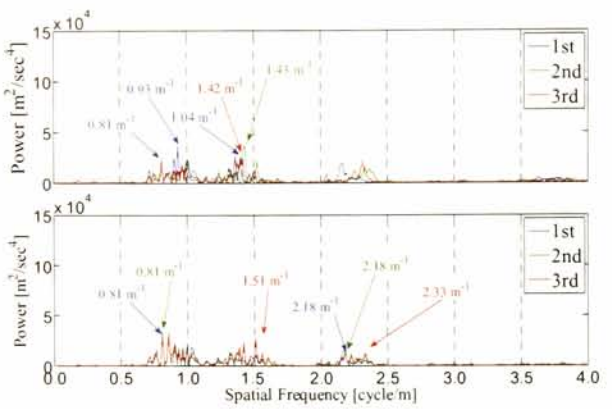

(a) At the measuring point 4 (16.4 (m))

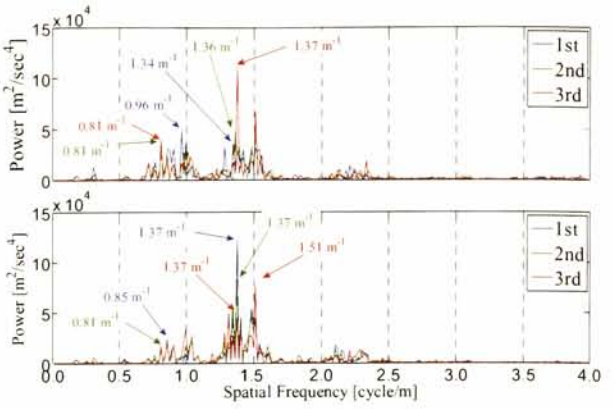

(b) At the measuring point 8 (32.8 (m))

Fig. 5.3.3 Bridge response in spatial frequency domain (Upper: Intact, Lower: Damaged)

peeds v_{V_1} and v_{V_2}:

$$\Omega_r = \frac{f_1}{v_{V_1}} = \frac{f_2}{v_{V_2}}. \tag{5.2}$$

Fig. 5.3.3 shows the Fourier's power spectra in spatial frequency domain. The each peak matches for each other under identical state of bridge in spatial-frequency domain, while they are located in different frequency.

Bridge mode shape is the most common vibration index defined in spatial domain. Here, the mode shapes are estimated by FDD applied to the bridge acceleration responses.

Fig. 5.3.4 shows singular spectra before and after damage in the case where the vehicle runs at speed of 10 (km/h). Fig. 5.3.5 also shows the mode shapes corresponding to the peaks in singular spectra. Blue and red lines indicate the mode shape for each side. The blue line denotes the mode shape in the side in which there is the damage-introduced member. The red one denotes the opposite side where the vehicle runs. Yellow boxes in this figure denote the damage section. Although there is a serious damage which is almost penetrated crack on the tension member, many bridge mode shapes of the damage case do not change in comparison with them of the intact case. Only in higher mode, for example, seventh predominant mode in Fig. 5.3.5 changes before and after the damage.

Fig. 5.3.6 also shows singular spectra before and after damage in the case where the vehicle runs at speed of 20 (km/h). In this figure, as opposed to Fig. 5.3.3, the singular spectrum of the bridge acceleration responses change well under 5 (Hz) and in the range from 10 (Hz) to 15 (Hz). Predominant peaks can be observed at frequencies of 2.73 (Hz), 7.42 (Hz) and 10.16 (Hz) in the intact case, while there are peaks at 1.95 (Hz), 7.42 (Hz) and 11.72 (Hz) in the damage case. Then, Fig. 5.3.7 shows the mode shapes corresponding to the peaks in singular spectra in the cases in which the run speed is 20 (km/h). From this figure, the amplitudes of mode shapes in the pathway

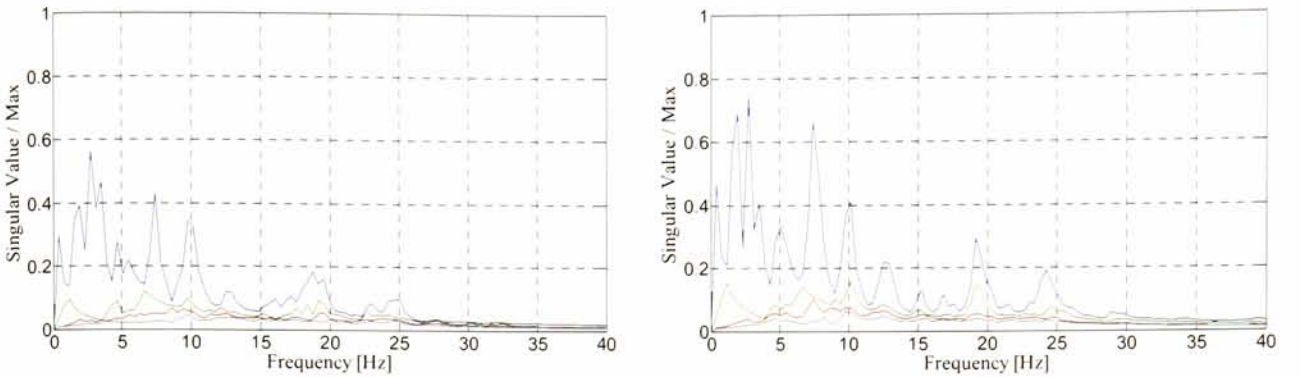

(a) Intact (1^{st}) (b) Damaged (2^{nd})

Fig. 5.3.4 Singular spectra before and after damage in the case where the vehicle runs at the speed of 10 (km/h)

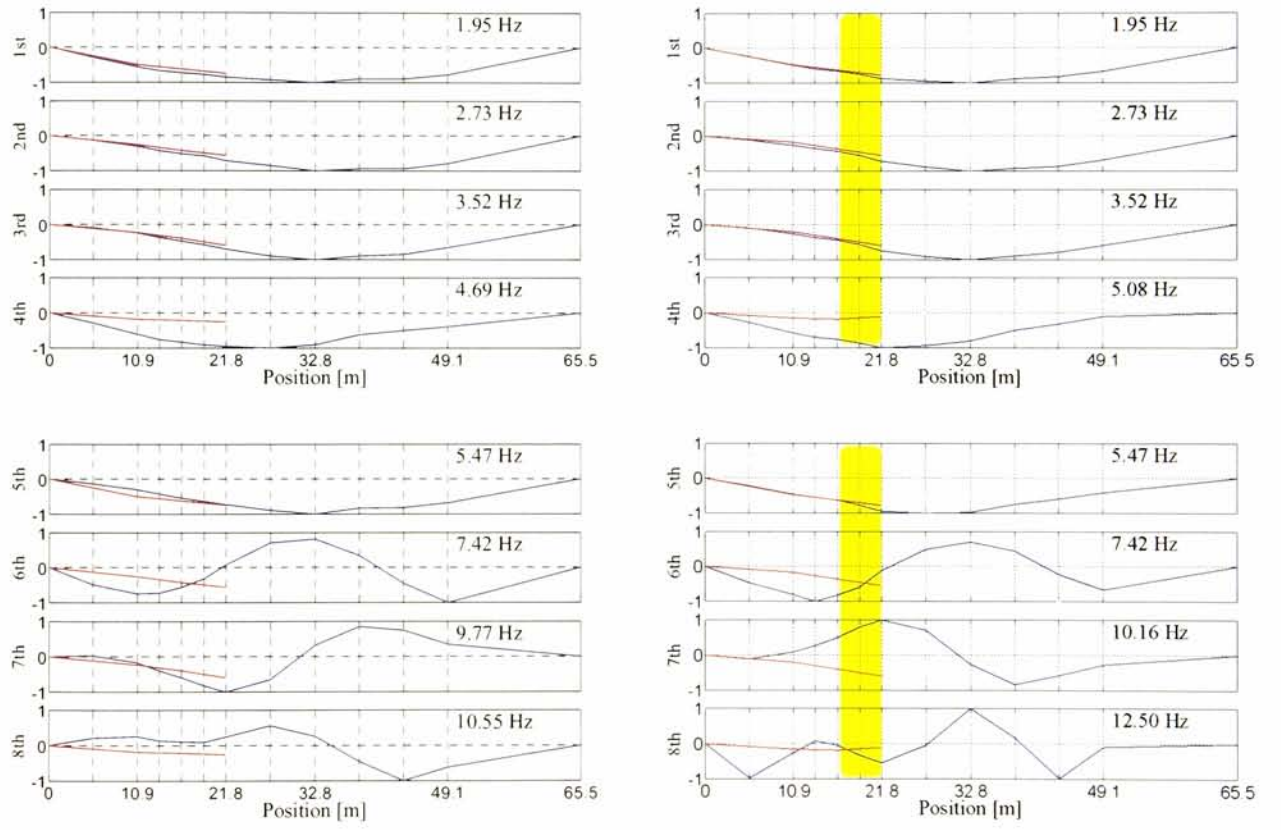

(a) Intact (1^{st}) (b) Damaged (2^{nd})

Fig. 5.3.5 Estimated mode shapes before and after damage in the case where the vehicle runs at the speed of 10 (km/h)

side tend to be decreased after damage. It means that the amplitude of the damaged side is increased due to damage, which agree with the results of an existing studies[1].

Fig. 5.3.8 shows the singular spectra of the cases in which the run speed is 40 (km/h) in the

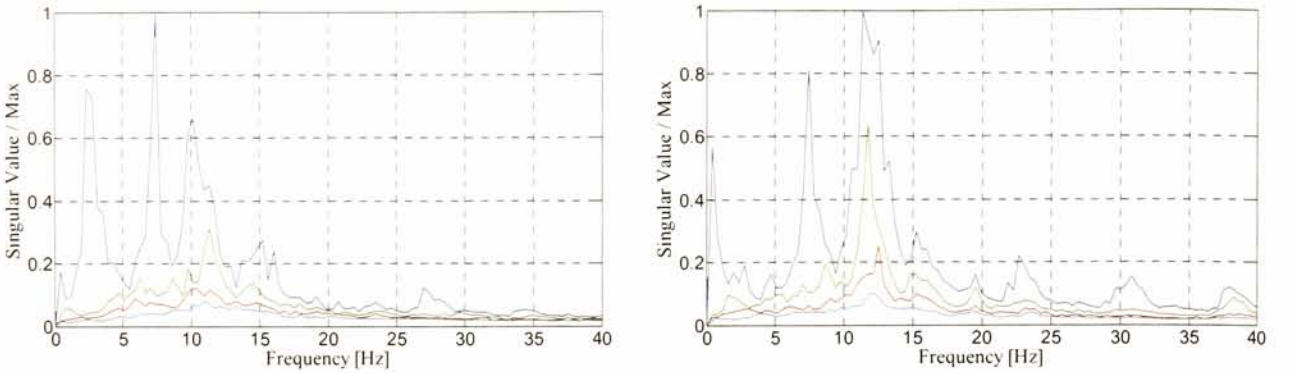

(a) Intact (2^{nd}) (b) Damaged (2^{nd})

Fig. 5.3.6 Singular spectra before and after damage in the case where the vehicle runs at the speed of 20 (km/h)

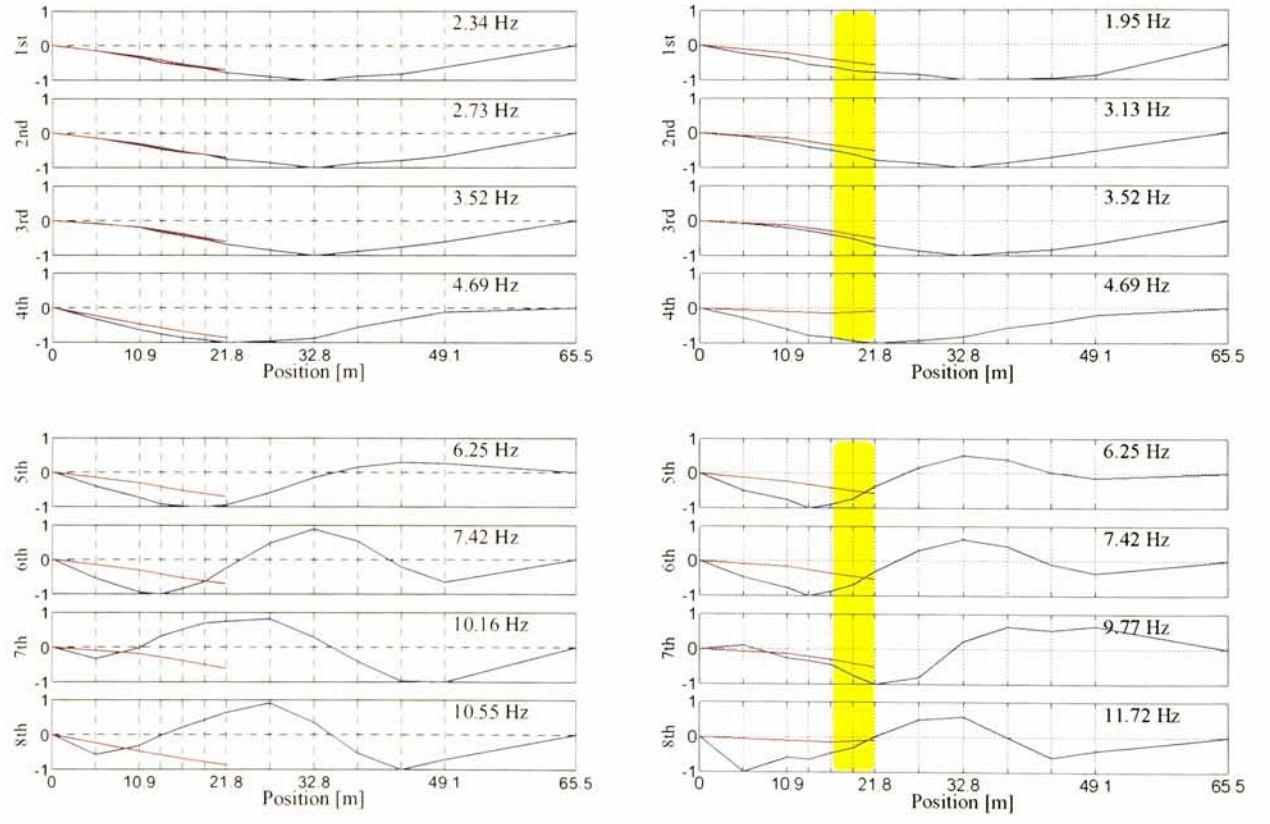

(a) Intact (2^{nd}) (b) Damaged (2^{nd})

Fig. 5.3.7 Estimated mode shapes before and after damage in the case where the vehicle runs at the speed of 20 km/h

same way. The singular spectrum of every case is very similar to each other even before and after damage. Fig. 5.3.9 also shows the mode shapes in same way. Yellow boxes indicate the damage section. It can be observed that the amplitude of mode shape in damaged side tends to increase due to damage. Only in damage section, there is no significant difference between intact and damages cases.

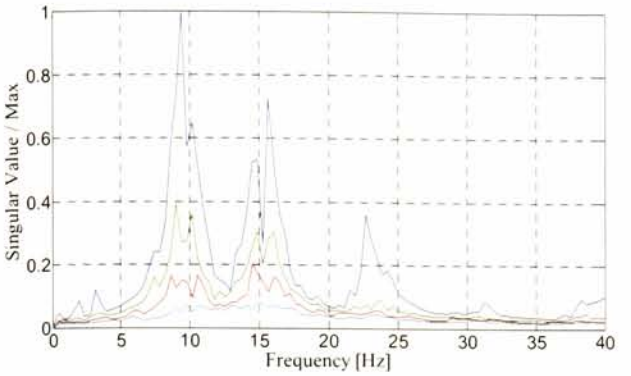

(a-1) Intact (1st)

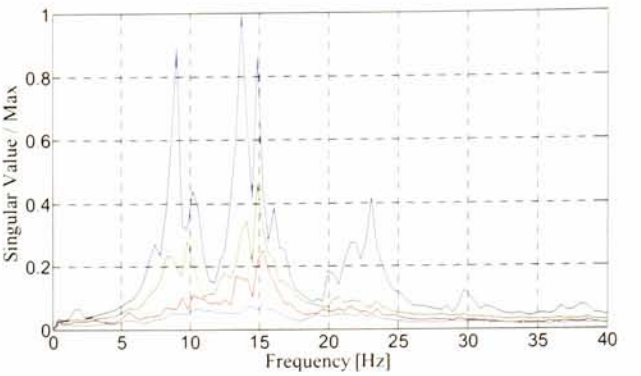

(b-1) Damaged (1st)

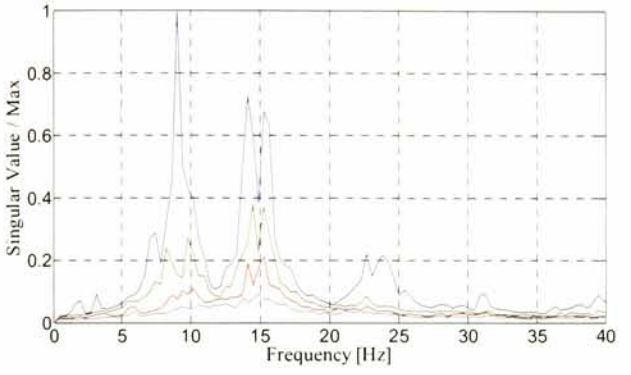

(a-2) Intact (2nd)

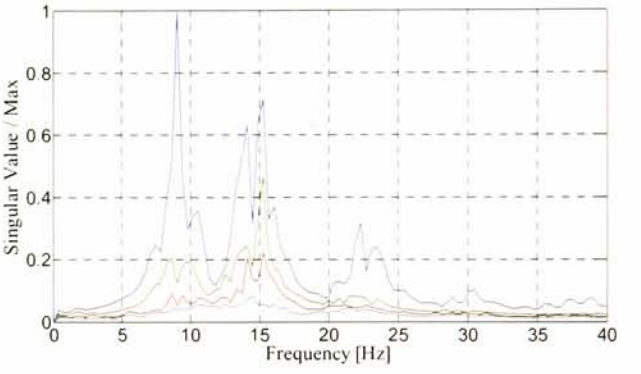

(b-2) Damaged (2nd)

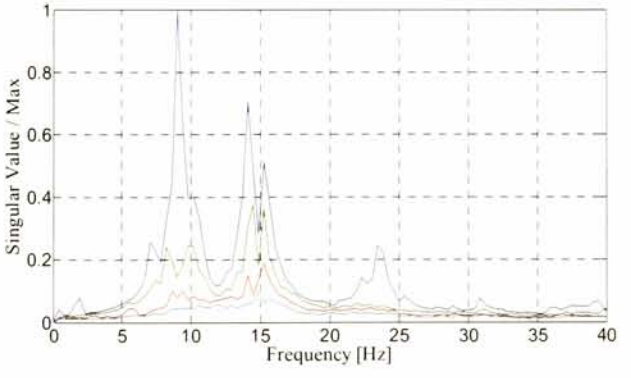

(a-3) Intact (3rd)

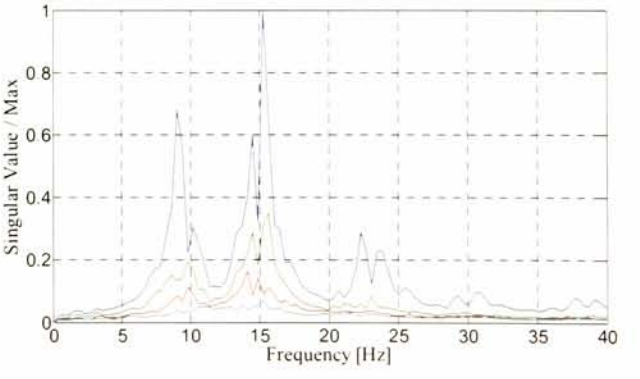

(b-3) Damaged (3rd)

Fig. 5.3.8 Singular spectra before and after damage in the case where the vehicle runs at the speed of 40 (km/h)

From the results of the analyses, it is cleared that the bridge vibration depends on the road profile significantly. In practical variation of vehicle run speed as shown in Table 5.2.3, the bridge responses in spatial domain show the high repeatability. The single power spectra in frequency domain as shown in Fig. 5.3.2 vary, while the singular spectra, which are one kind of cross power

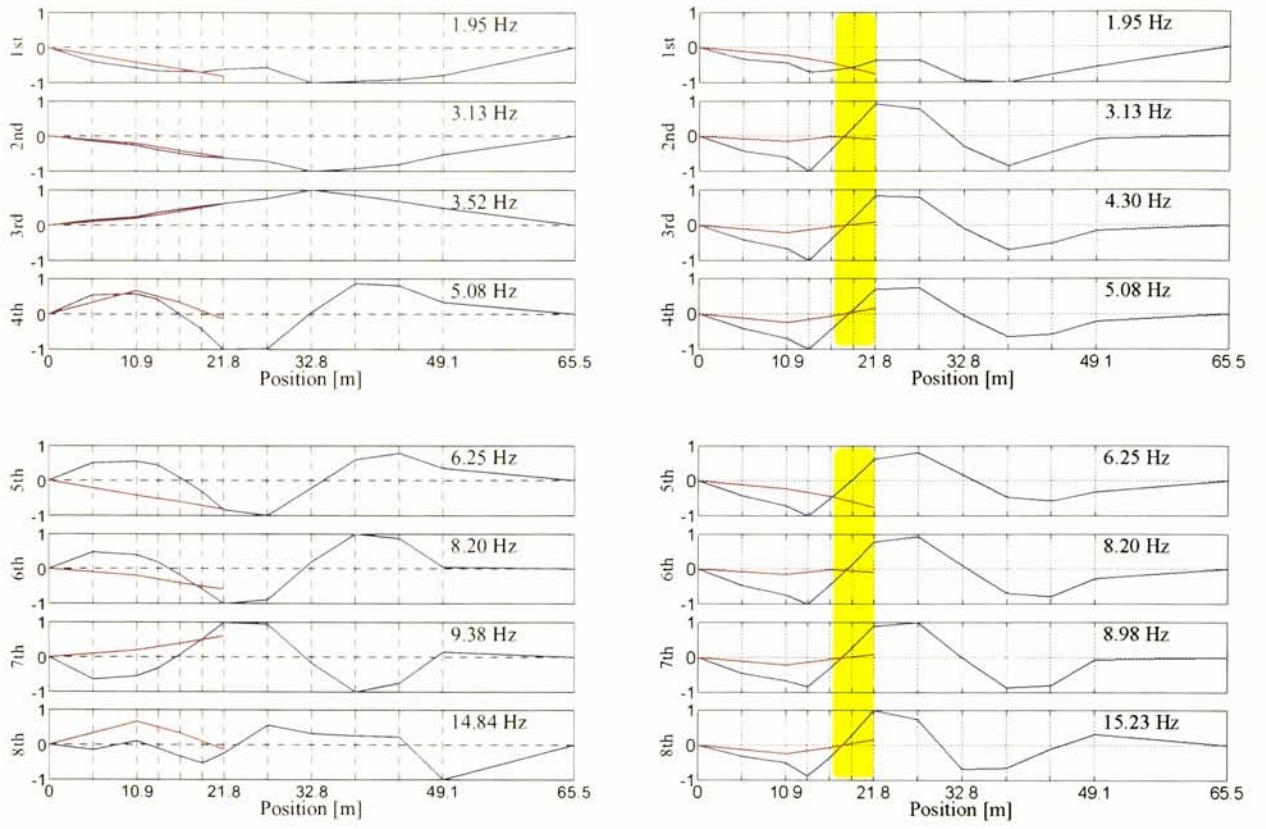

(a) Intact (1^{st}) (b) Damaged (2^{nd})

Fig. 5.3.9 Estimated mode shapes before and after damage in the case where the vehicle runs at the speed of 40 (km/h)

spectra, do not vary. The mode shapes estimated by FDD method are different in cases where the vehicle runs at the different speed even in identical bridge state. It means that FDD method estimate just operational mode shapes. Although the mode shape excited by the vehicle travelling at the speed of 10 (km/h) does not change after damage, the damaged side amplitude of mode shape excited by the vehicle travelling at the speed of 40 (km/h) increases. It means that the changes due to damage in mode shape depends on the excitation characteristics.

5.3.2. The vehicle responses

In this section, the vehicle vibration characteristics measured in the field experiment are presented. The average speeds of the vehicle are varied slightly, so, the vehicle responses are synchronized in spatial domain here. Power spectra are also calculated in spatial frequency domain because of deduction of the effect of the vehicle speed.

Fig. 5.3.10 and Fig. 5.3.11 show the acceleration responses in spatial and spatial-frequency domain, respectively. Fig. 5.3.10 (a), (b), (c) and (d) show acceleration responses of the sprung-mass at the front axle, sprung-mass at the rear axle, unsprung-mass at the front axle and

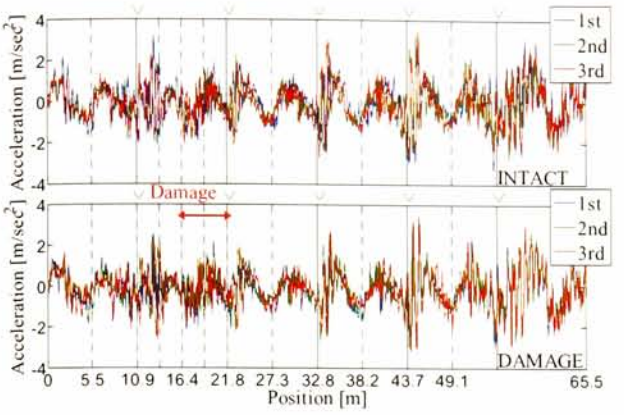

(a) Sprung-mass at the front axle

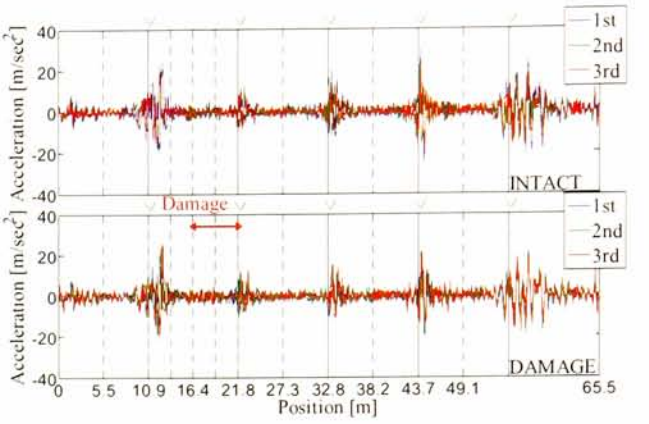

(b) Sprung-mass at the rear axle

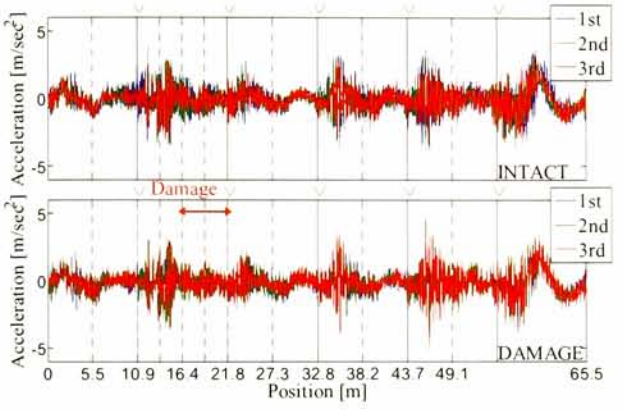

(c) Unsprung-mass at the front axle

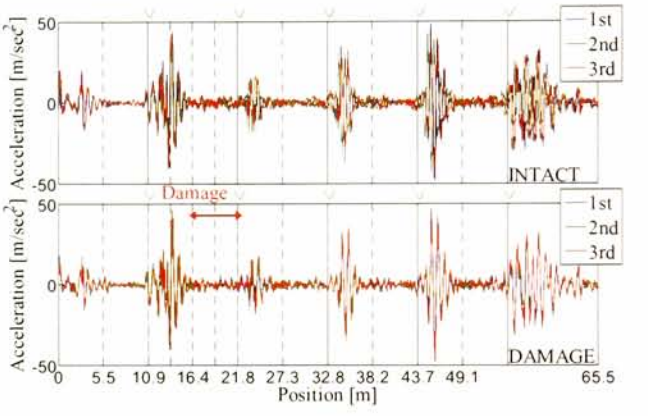

(d) Unsprung-mass at the rear axle

Fig. 5.3.10 Vehicle acceleration response (Upper: Intact, Lower: Damaged) in the case where the vehicle runs at the speed of 40 (km/h)

unsprung-mass at the rear axle of the vehicle at the speed of 40 (km/h), respectively. The horizontal axis denotes the position of the front axle of the passing vehicle. From these figures, the high repeatability can be obtained in all measurements. From Fig. 5.3.11, the power spectra in spatial-frequency domain also show the high repeatability even before and after damage. The predominant spatial-frequencies exactly match for each other.

Generally, because a vehicle has strong damping for driver's comfortable feeling while riding, a intrinsic vibration response of the vehicle system is suppressed and road unevenness affect the vehicle response significantly in spatial domain. Joints also affect the acceleration responses in spatial domain, obviously. This tendencies agree with the experimental measurements of laboratory. On the other hand, from Fig. 5.3.11, the power spectra of the vehicle in spatial-frequency domain distribute in limited range. This is caused by difference of the frequency response functions between the measuring points. The measured data includes the information of the vehicle vibration system. This may affect the estimation accuracy of the proposed method, but the low effect can be expected because the frequency ranges of the unsprung-mass at the front and rear axles are very similar.

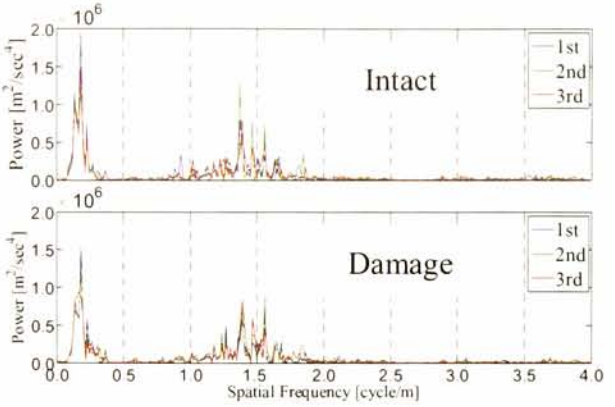

(a) Sprung-mass at the front axle

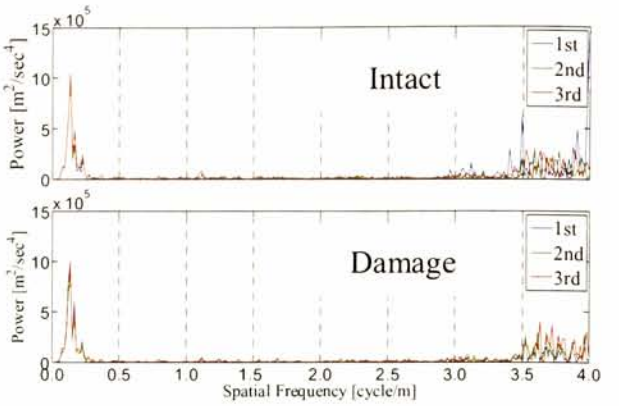

(b) Sprung-mass at the rear axle

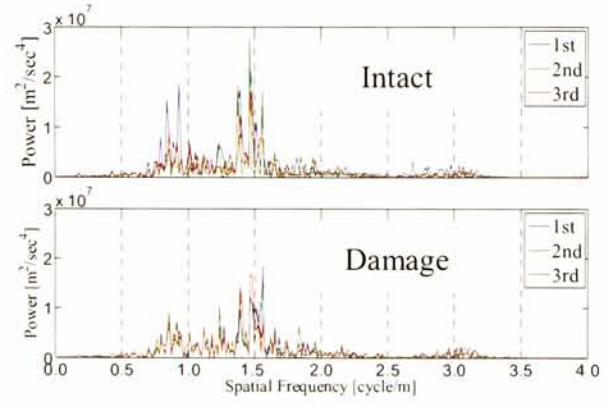

(c) Unsprung-mass at the front axle

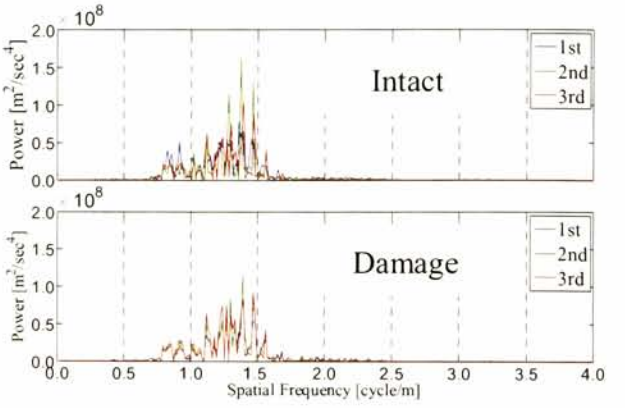

(d) Unsprung-mass at the rear axle

Fig. 5.3.11 Vehicle acceleration response (Upper: Intact, Lower: Damaged) in the case where the vehicle runs at the speed of 40 (km/h)

5.4. Verification of the proposed methods

5.4.1. Curvature-based VO-BHM

Now, the proposed methods are applied to the vehicle vibration acceleration responses of this field experiment. Herein, verified methods are Curvature-based and direct Mode-Shape-based VO-BHM methods. The used measurements are the unsprung-mass acceleration responses at the front and rear axles of the vehicle.

The powers of wavelet coefficients for the vehicle acceleration responses measured in three times for each bridge state are shown in Fig. 5.4.1. Because the sampling rate is 200 (Hz), the scale is set to 10, which corresponds to 25 (Hz). The horizontal coordinate denotes the position of the vehicular front axle. The lines denote the average of wavelet coefficients in three times in which the vehicle runs at the speed of 40 (km/h). The blue and red lines indicate for the intact and damage cases, respectively. From this figure, the red line becomes slightly larger around the damage section than the blue line. It agree with well with the results of the numerical verification. Yellow boxes

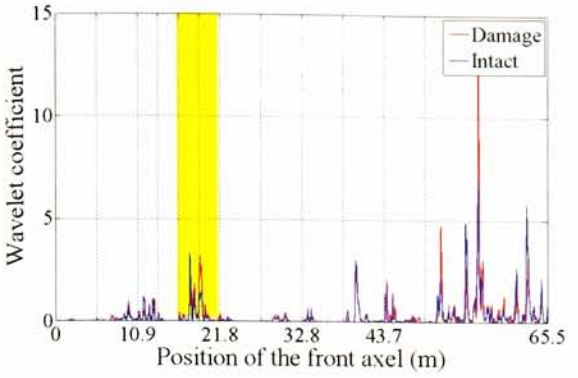

(a) Sprung-mass at the front axle

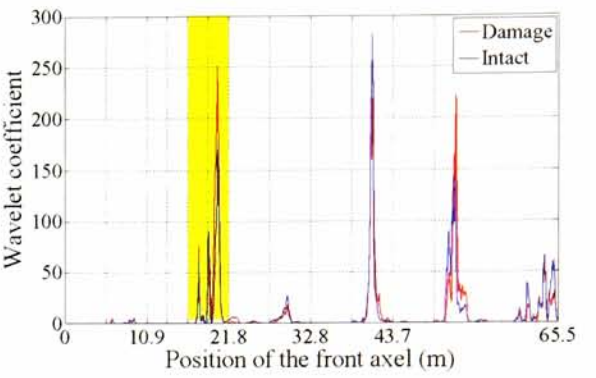

(b) Sprung-mass at the rear axle

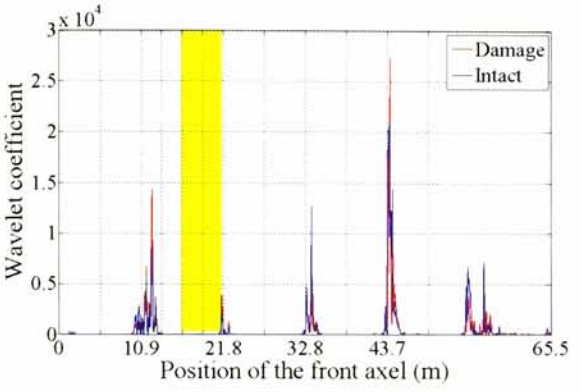

(c) Unsprung-mass at the front axle

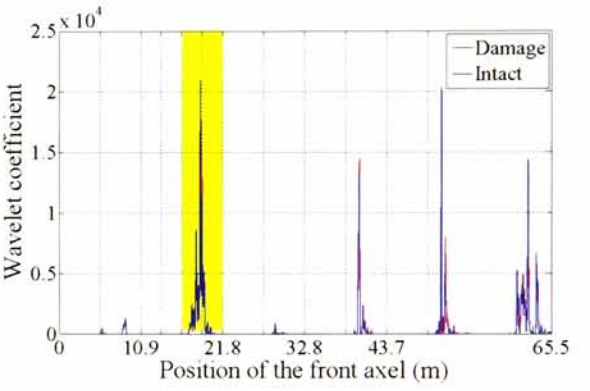

(d) Unsprung-mass at the rear axle

Fig. 5.4.1 CWT power of wavelet coefficient of vehicle acceleration (Run speed: 40 (km/h))

indicate the damage section. However, it is difficult to detect damage changes around damage section between blue and red lines. It may be because the proposed curvature-based method is too sensitive to road unevenness which corresponds to the term of D_3 in Eq.(2.20). In this experiment, the road unevenness may be relatively rough to affect the results significantly.

5.4.2. Mode-Shape-based VO-BHM

Finally, the verification for proposed method of VO-BHM based on bridge mode shape is carried out. Fig. 5.4.2 shows the estimated bridge mode shape by using the unsprung-mass acceleration responses of the vehicle. This estimation is performed by SVD of $\mathbf{N}^{-1}(t)\begin{Bmatrix}\ddot{z}_{u1}(t)\\ \ddot{z}_{u2}(t)\end{Bmatrix}$. Herein, the vehicle runs at the speed of 40 (km/h) and the bridge is intact.

The mode shapes estimated by the proposed VO-BHM method can be plotted on 2-D graph, because each of them insists only in two values. Fig. 5.4.3 shows the estimated first mode shape for cases in which the vehicle runs at the speed of 10, 20 and 40 (km/h). Amplitudes of mode shapes in this figure are normalized under $x^2 + y^2 = 1$ where x and y denote the values of each mode

shape. Black dot circle indicate this unit circle in this figure. Blue and red dots indicate the intact and damage cases, respectively. The estimation depends on changes of planed run speed significantly. But, under same planned run speed, the variation of estimation is smaller than their changes due to damage. It means the high feasibility of this method for damage identification.

Fig. 5.4.4 also shows the estimation mode shapes by the $\mathbf{N}^{\mathrm{T}}$-based method. It means that the estimation is performed by SVD of $\mathbf{N}^{\mathrm{T}}(t)\begin{Bmatrix}\ddot{z}_{u1}(t)\\ \ddot{z}_{u2}(t)\end{Bmatrix}$. Blue and red dots indicate the intact and damage cases, respectively. From this figure, it is cleared that the damage changes of estimation by the $\mathbf{N}^{\mathrm{T}}$-based method is more clear than those by the $\mathbf{N}^{-1}$-based method. The high feasibility of damage identification of the $\mathbf{N}^{\mathrm{T}}$-based method is also confirmed from this figure.

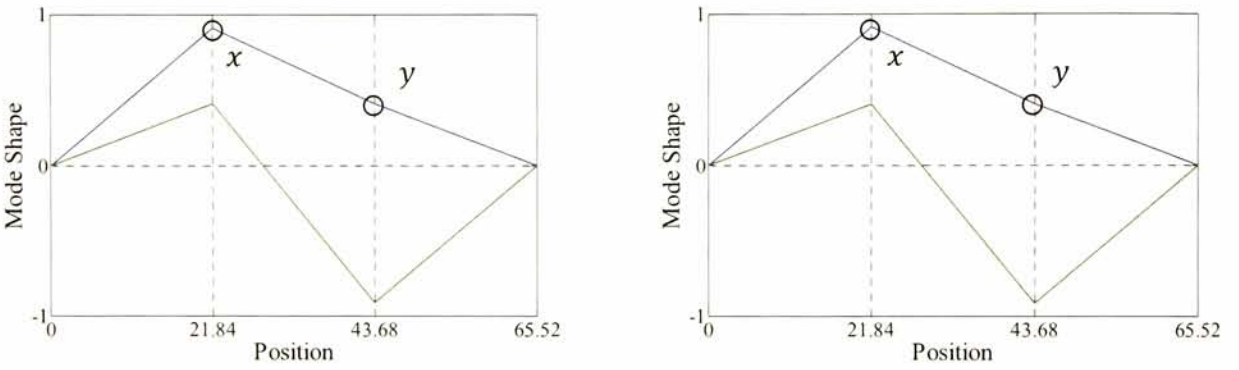

(a) Intact (b) Damage

Fig. 5.4.2 example of estimated mode shape

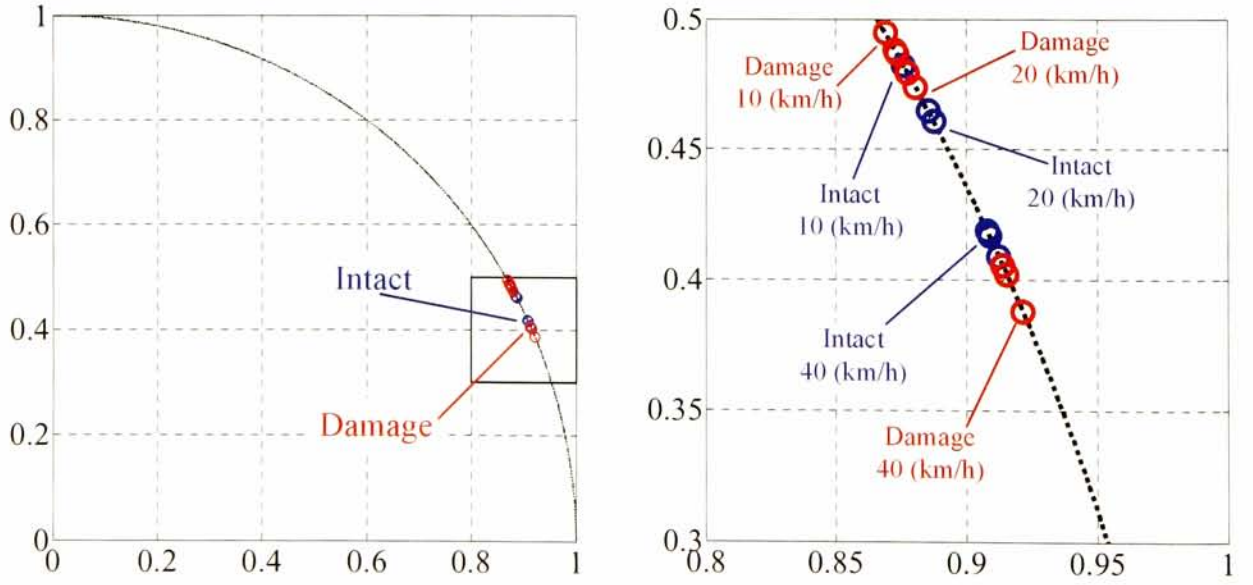

(a) Overall view (b) Close-up

Fig. 5.4.3 Estimated first mode shapes for all cases

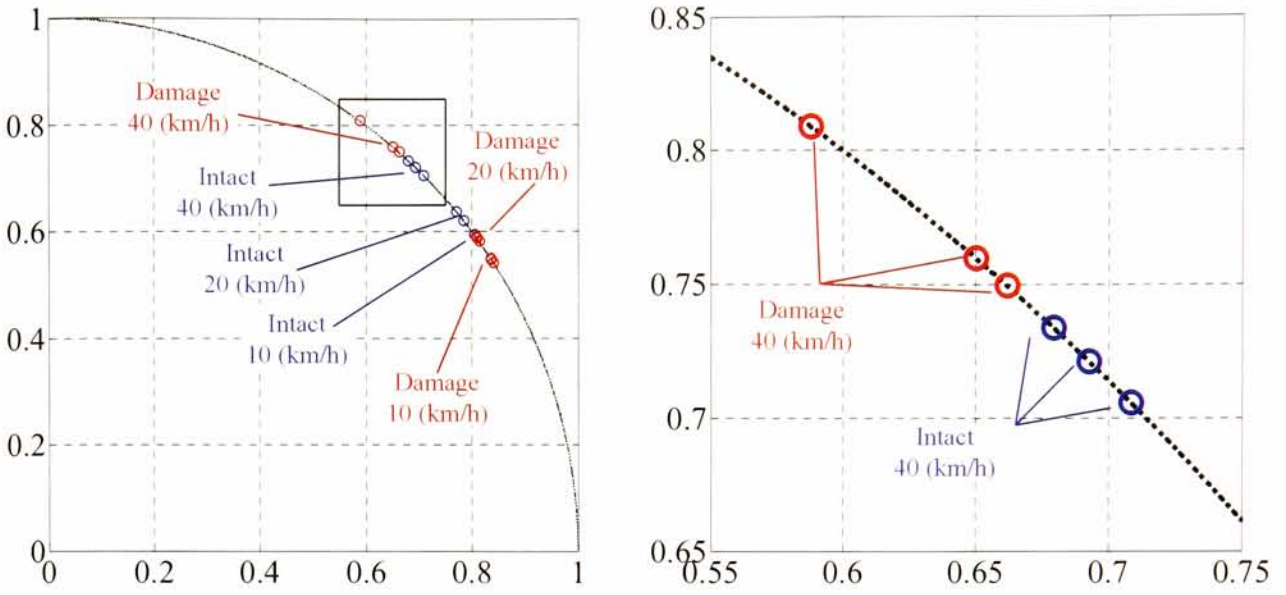

(a) Overall view (b) Close-up only for 40(km/h) run cases

Fig. 5.4.4 Estimated first mode shapes for all cases

5.5. Summary of this chapter

In this chapter, the results of field experiments are presented. The purpose of this experiment is verification of the proposed methods. First, by the preliminary examination, predominant frequency is not appropriate index because of the low accuracy to eigen-frequency and because of the larger shift by the effect of run speed than damage. Thus, spatial frequencies which can consider the effect of the vehicular run speed are confirmed. In the preliminary verification, bridge mode shapes estimated by bridge acceleration responses are calculated by FDD. Mode shapes in damage side increases.

First, the Curvature-based VO-BHM is verified by using the experimental data. However, the significant damage changes cannot be detected from the power of wavelet coefficient of vehicle responses. From existing studies, the bridge curvature is very sensitive damage index, because it is associated significantly with local changes of flexural stiffness. The estimation of the curvature is expected to be feasible for damage detection. However, errors due to road unevenness are significant in the results.

Next, the direct Mode-Shape-based VO-BHM method is verified. In this verification, it is confirmed that the distinct changes can be observed between intact and damage cases. The direct Mode-Shape-based VO-BHM method can be categorized into two method mainly: the $\mathbf{N}^{-1}$-based and $\mathbf{N}^{T}$-based methods. The difference of them is the equation which they are based on. The $\mathbf{N}^{-1}$-based method estimates the bridge mode shape based on the equation of motion of the vehicle, while the $\mathbf{N}^{T}$-based method estimates it by that of bridge mode. In the results of verification, the $\mathbf{N}^{T}$-based method shows significant changes due to damage under the identical measuring condition.

Reference

[1] Nishimura A., Fujii, M., Miyamoto, A. and Kagayama, T.: Sensitivity of mechanical behavior of bridges for their damage assessment, Doboku Gakkai Ronbunsyu, JSCE, Vol.1987, No.380, pp.355-364, 1987.

[2] Furukawa, A., Otsuka, H. and Umebayashi, F.: Damage identification of steel truss bridge by vibration testing using micro shaker, Journal of Applied Mechanics, JSCE, Vol.9, pp.1103-1110, 2006.

[3] Kim, C.W., Isemoto, R., Kawatani, M. and Sugiura, K.: Structural diagnosis of bridge using output-only vibration in moving vehicle laboratory experiment, Journal of JSCE, Ser.A2, Vol.67, No.2 (Applied Mechanics), pp.I-833-842, 2011.

[4] Sugiura, K., Kitagaki, K., Yamaguchi, T., Kitada, T. and Hashimoto, K.: Laboratory experiment for estimation of bridge eigen-frequency based on moving vehicle's responses, Proceedings of the 64th Annual conference of the Japan Society of Civil Engineers, I-291, pp.581-582, 2009.

[5] Zhu, X.Q. and Law, S.S.: Wavelet-based crack identification of bridge beam from operational deflection time history, International Journal of Solids and Structures, 43, pp.2299-2317, 2006.

[6] Yamamoto, K., Isemoto, R., Oshima, Y., Kim, C.W. and Sugiura, K.: Evaluation of acceleration responses in a steel truss bridge and passing vehicle before and after member's breakage, Journal of Structural Engineering, JSCE, Vol.58A, pp.180-193, 2012.

Chapter 6. Conclusion

In this study, three only-Vehicle-data-Oriented Bridge Health Monitoring (VO-BHM) methods for bridge damage identification are proposed. These method use spatial indices as damage detection indices, which are bridge curvature and mode shape. The purpose of this study is to verify the proposed method analytically, numerically and experimentally.

Curvature-based method applies continuous wavelet transform (CWT) to the vehicle acceleration responses. in this study, it is shown that wavelet coefficient which can be obtained by CWT of vehicle response can be described as a non-linear function of bridge curvature, analytically. This method shows the high feasibility in numerical simulation. The wavelet coefficient of vehicle acceleration response has distinctive peaks at the location where the local damage occurs. However, in the laboratory and field experiment, the changes of wavelet coefficient due to damage cannot be observed because its variation due to uncertain factors are usually larger than the damage change.

Second, indirect Mode-Shape-based method is proposed. To estimate bridge mode shape, this method estimate bridge vibration components and apply interpolation matrix to the estimated bridge vibration components indirectly. The estimated bridge vibration components are transformed from the measurements at the moving observers to those at the observers fixed on the bridge by the interpolation matrix. The advantage of this method is analytical consistency to the mode theory. If there is no noise, the estimated mode shape changes as the damage increases. However, in this method, because there are many steps in mode shape estimation, the obtained mode shape is affected significantly by many uncertain factors included in each step. The estimation results of the mode shape becomes very low, and it is cleared that damage identification is difficult by numerical verification when noise is considered.

Direct Mode-Shape-based method is the method applying the interpolation matrix to vehicle acceleration response directly to estimate the bridge mode shape as the damage index. This method can be categorized into two methods mainly: $\mathbf{N}^{-1}$-based and $\mathbf{N}^{T}$-based methods. They do not have high analytical consistency to mode theory, because their basic equations include the error terms which is function of sprung-mass responses of the vehicle and road unevenness. However, these error terms can be managed under identical condition. Thus, the estimated mode shape can be used as efficient damage indices. Numerical simulation shows the high feasibility of this method, but laboratory experiment does not. In the field experiment, the estimation of mode shape changes larger only due to damage. This is because the direct Mode-Shape-based method consists of only two steps. Applying interpolation and mode decomposition by singular value decomposition (SVD). This also means that variation of the uncertainties are smaller than the changes due to damage.

In Chapter 1, social demand for bridge screening technology can be applied to the number of bridge is shown, and the previous studies about the BHM are summarized, first. Then, the

technical issues such as the problem of non-linearity caused by observers moving and of non-stationary signals in challenges for VO-BHM technology are explained.

In Chapter 2, three VO-BHM method for damage identification are proposed and shown their efficiencies analytically.

In Chapter 3, three proposed methods are verified in numerical simulations. In this chapter, first, the vehicle-bridge interaction (VBI) system is explained. Then, the simple mass spring and rigid-spring models are assumed as the passing vehicle, while the bridge is modeled as one-dimensional finite element model. In the verification of the proposed method, errors of the estimations are examined. For indirect Mode-Shape-based method, ill condition, curve fitting performance of the interpolation and de-correlation of the decomposed signals are significant factors.

In Chapter 4, three proposed methods are verified in laboratory experiment. In this experiment, simple vehicle and bridge models are used. Road unevenness and bumps are introduced on the vehicle pathway. The aim of this verification is to examine the effect of uncertainties. As a result, it is cleared that low feasibility of the proposed method because the uncertainties affect the estimation results significantly.

In Chapter 5, three proposed methods are verified in field experiment in which 250 (kN) truck passes over the actual steel truss bridge before and after artificial damage introduced. Although the laboratory experiment show the low feasibility of the proposed methods, this verification resulted the high feasibility for direct Mode-Shape-based VO-BHM method for damage identification.

In this study, the high feasibility of the direct Mode-Shape-based VO-BHM method for damage identification is shown by numerical and experimental verification. Although the bridge mode shape itself does not change well due to local damage, mode shape estimated by SVD changes and can be used for damage detection index. Damage changes not only mode shape but also modal responses. SVD in the process of the direct Mode-Shape-based method cannot consider the change of modal responses due the assumption of SVD. Thus, the changes of modal responses due to damage is estimated as the changes of mode shapes. This mechanism can be explained by the de-correlation of the decomposed signals.

Despite of the advantages of this method, there are still challenges to utilization. In this method, the vehicle position is necessary to make interpolation matrix. Thus, the position should be measured on the vehicle. But, in these verifications, the vehicle position is measured by sensors installed on the bridge. Next, using GPS sensors for identification of vehicle position will be examined. And if it needs, the method for handling of position estimation error should be developed. Vehicle run speed, mass changes, environmental factors and changes of road unevenness should be

examined as the uncertain factors in the respect of damage identification.

Direct Mode-Shape-based VO-BHM method cannot identify the damage location. Thus, the accuracy of Curvature-based VO-BHM method will be improved for damage identification.

More detailed statistical verifications should be performed to improve the accuracy of damage severity identification.

Field experiments of other bridges will be performed. It will give strong evidence to the proposed methods.

APPENDIX

A. Modal Parameter Sensitivity

A.1 Basic Assumptions

Herein, the changes of the modal parameters due to damage are confirmed numerically. The modal parameters which are focused on in this section are bridge eigen-frequency and mode shape. The numerical simulation is demonstrated by modal analysis which is on a basis of Eq. (3.7). In this simulation, by mass and flexural stiffness matrices of one-dimensional finite element beam, modal parameters are calculated in varying damage width, location and severity. The bridge properties shown in Table A.1.1.

A.2 Results and Discussion

A.2.1 Eigen-frequency sensitivity

The results are shown in Fig. A.2.1. The x-, y- and z-axes of the figure indicate damage location, degree of soundness and characteristic value, respectively. The introduced damage width is ranges between 1 (m) and 3 (m). The location of the damage corresponds to the center of the damage section. Now, the ratio of the flexural stiffness EI of the damage section is used as the degree of soundness of bridge. Only flexural stiffness varies ranging from 1% to 99%. The characteristic value is the ratio of the eigen-frequencies of the intact and damaged cases in Fig. A.2.1. As the flexural stiffness decreased, eigen-frequency usually decreases. From these figures, eigen-frequency changes much when the damage occurs around the location where the corresponding mode shape is large. As the damage width increases, the changes of bridge frequencies also increases. Bridge eigen-frequencies tend to decrease as damage becomes larger. However, the sensitivities of the eigen-frequencies to local damage are too small. If the damage occurs around the supports, the sensitivity is much lower. The low sensitivity to edge damage is the prior technical issues of BHM technology. The eigen-frequency may be a good damage index for global damage such as damage which is relatively wide. Moreover, if the high order mode eigen-frequencies are available despite of difficulties of estimation, they should show high sensitivity to the edge damage.

Table A.1.1 Bridge properties

Physical parameters			Eigen-frequency for the intact case				
Length	Mass per length	Flexural Stiffness	1st	2nd	3rd	4th	5th
(m)	(kg/m)	(Nm)	(Hz)	(Hz)	(Hz)	(Hz)	(Hz)
L	ρA	EI	f_1	f_2	f_3	f_4	f_5
30.0	3000	1.56×10^{10}	3.96	15.75	34.98	61.15	93.64

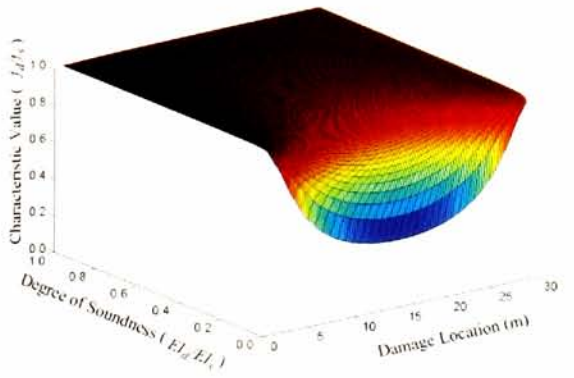

(a) First eigen-frequency: damage width = 1.0 m

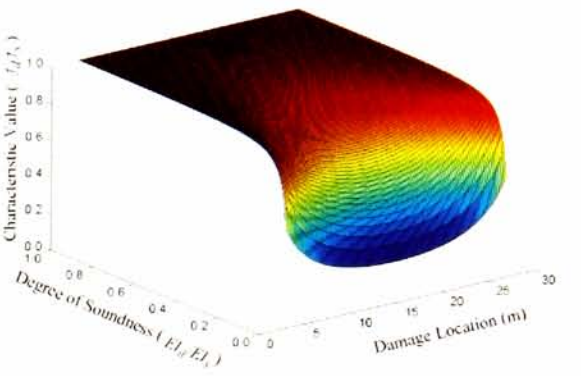

(b) First eigen-frequency: damage width = 3.0 m

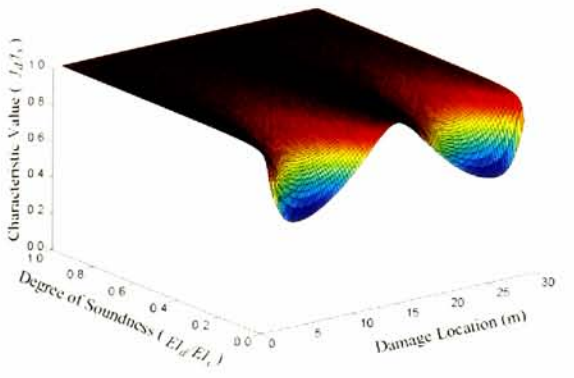

(c) Second eigen-frequency: damage width = 1.0 m

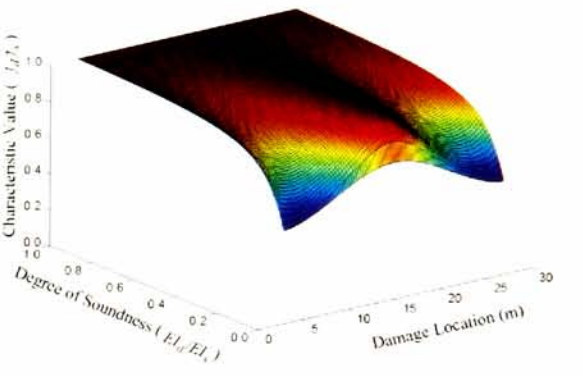

(d) Second eigen-frequency: damage width=3.0 m

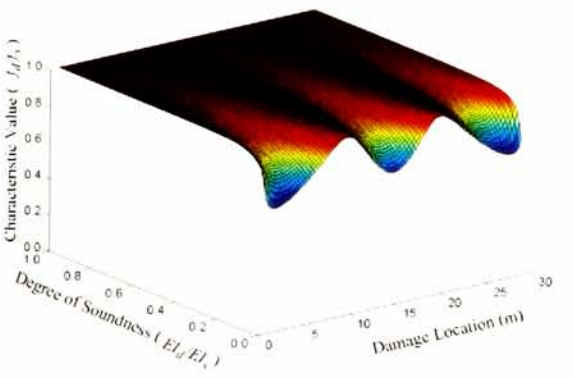

(e) Third eigen-frequency: damage width = 1.0 m

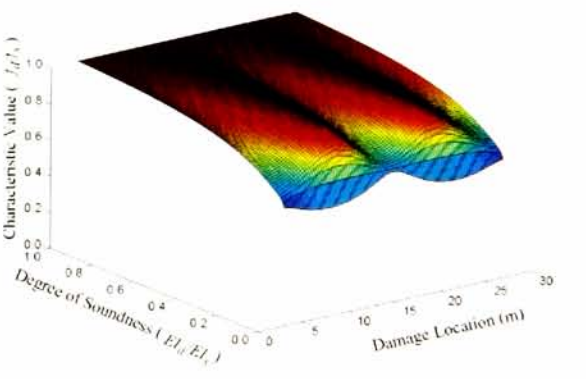

(f) Third eigen-frequency: damage width = 3.0 m

Fig. A.2.1 Sensitivity of the bridge eigen-frequency to damage

A.2.2 Mode shape sensitivity

To detect local damage, it is important to detect changes of the local impedance of the bridge. In frequency domain, the characteristic value is averaged spatially, while the flexural stiffness decreasing should be occurred in local. Mode shape is one of the spatial indices of vibration. This index keeps the information about the local impedance.

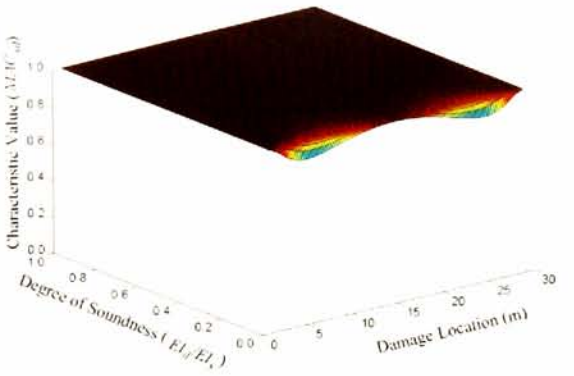

(a) First mode shape : damage width = 1.0 m

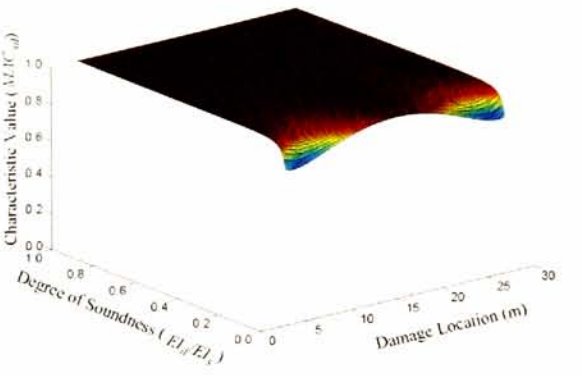

(b) First mode shape : damage width = 3.0 m

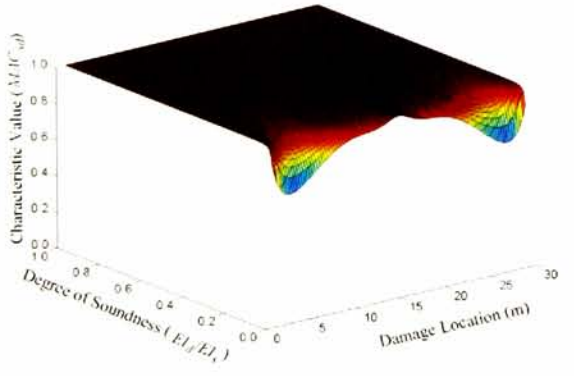

(c) Second mode shape : damage width = 1.0 m

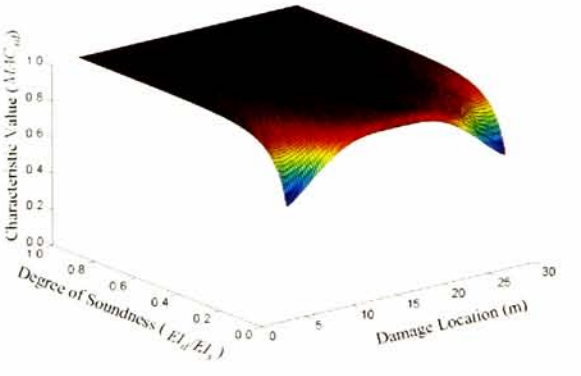

(d) Second mode shape : damage width = 3.0 m

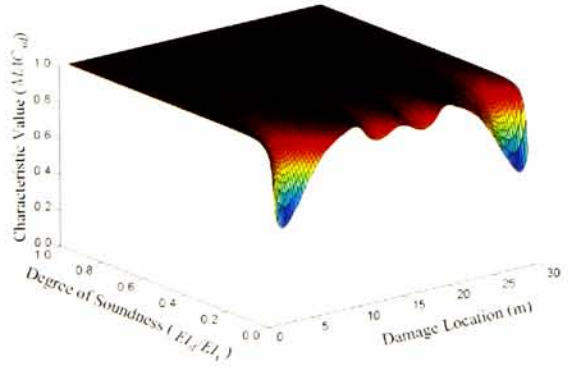

(e) Third mode shape : damage width = 1.0 m

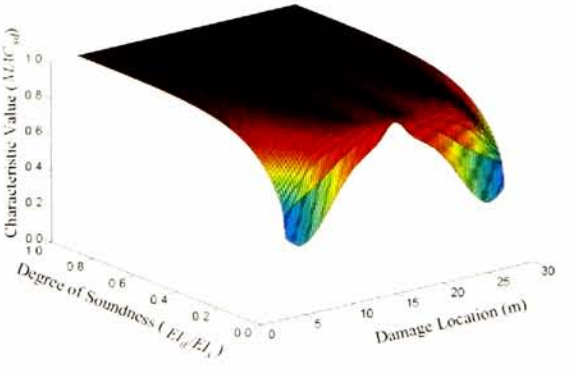

(f) Third mode shape : damage width = 3.0 m

Fig. A.2.2 Sensitivity of the bridge mode shape to damage

For the same cases of Fig. A.2.1, calculated mode shapes are shown in Fig. A.2.2. In this figure, characteristic value is MAC. Note that the mode shape of damage case is more similar to that of intact case as the MAC value is close to 1. Fig. A.2.2 shows the diagonal components of MAC matrix. From this figure, the changes of MAC for the case in which damage occurs around the supports are larger than that in the cases in which damage occurs in the center of the span. This tendency is more significant in higher mode shapes.

B. Frequency domain decomposition (FDD) method

B.1.1 Estimation Flow of Mode Shape

Brinker et al [1] proposes a new frequency domain decomposition (FDD) technique for modal identification of output-only systems. This technique is capable to be applied to estimate the structural modal parameters without any information about the inputs exciting the system. It is going to be applied to many analyses of actual structures. Nagae et al [2] showed the high applicability of FDD by numerical and experimental verification.

The relationship between the unknown inputs $\boldsymbol{F}(\omega)$ and the measured outputs $\boldsymbol{Y}(\omega)$ are described as

$$\boldsymbol{Y}(\omega) = \mathbf{H}(\omega)\boldsymbol{F}(\omega) \tag{B.1}$$

where $\boldsymbol{F}(\omega) \in \mathrm{C}^n$ and $\boldsymbol{Y}(\omega) \in \mathrm{C}^n$ are vibration data in frequency domain at n points on the structure. $\mathbf{H}(\omega) \in \mathrm{C}^{n\times n}$ is the frequency response function (FRF) matrix. The $(i,\ j)$ element of the FRF matrix $\mathbf{H}(\omega)$ is the response at the i-th point induced by the force working at the j-th point. Both $\boldsymbol{F}(\omega)$ and $\boldsymbol{Y}(\omega)$ are calculated from time-series data $\boldsymbol{F}(t)$ and $\boldsymbol{Y}(t)$ by Fourier's transform. The cross power spectrum of outputs $\mathbf{G}_{yy}(\omega) \in \mathrm{C}^{n\times n}$ can be described as

$$\mathbf{G}_{yy}(\omega) = \boldsymbol{Y}(\omega)\boldsymbol{Y}(\omega)^{\mathrm{H}} \tag{B.2}$$

where $(\ \ )^{\mathrm{H}}$ denotes the Helmite operator (the complex conjugate and transpose). By using the cross power spectrum of inputs $\mathbf{G}_{ff}(\omega) \in \mathrm{C}^{n\times n}$ and that of outputs $\mathbf{G}_{yy}(\omega)$, Eq. (B.1) can be rewritten as

$$\begin{aligned}\mathbf{G}_{yy}(\omega) &= \boldsymbol{Y}(\omega)\boldsymbol{Y}(\omega)^{\mathrm{H}} \\ &= \mathbf{H}(\omega)\boldsymbol{F}(\omega)\boldsymbol{F}(\omega)^{\mathrm{H}}\mathbf{H}^{\mathrm{H}}(\omega) \\ &= \mathbf{H}(\omega)\mathbf{G}_{ff}(\omega)\mathbf{H}^{\mathrm{H}}(\omega)\end{aligned} \tag{B.3}$$

On the other hand, the FRF can be written in partial fraction form as

$$\mathbf{H}(\omega) = \sum_{r=1}^{n}\left(\frac{\mathbf{R}_r}{j\omega - \lambda_r} + \frac{\mathbf{R}_r^*}{j\omega - \lambda_r^*}\right) \tag{B.4}$$

where j, λ_r and $\mathbf{R}_r$ is imaginary unit, r-th modal pole and residue matrix, respectively. ( )* denotes the conjugate. The modal pole λ_r is

$$\lambda_r = -h_r\omega_r + j\sqrt{1-h_r^2}\omega_r \tag{B.5}$$

where ω_r and h_r are r-th modal eigen radian frequency and damping ratio. The residue matrix can be described as

$$\mathbf{R}_r = \boldsymbol{X}_r\boldsymbol{X}_r^{\mathrm{T}} \tag{B.6}$$

where $\boldsymbol{\psi}_r$ is r-th mode shape vector. Eq. (2.34) becomes

$$\mathbf{H}(\omega) = \sum_{r=1}^{n}\left(\frac{\boldsymbol{X}_r\boldsymbol{X}_r^{\mathrm{T}}}{j\omega-\lambda_r} + \frac{\boldsymbol{X}_r^{\mathrm{H}}\boldsymbol{X}_r^{*}}{j\omega-\lambda_r^{*}}\right) \tag{B.7}$$

Suppose the input at the each point is white noise which has same amplitude for each others, the cross power spectrum matrix $\mathbf{G}_{ff}(\omega)$ is described as

$$\mathbf{G}_{ff}(\omega) = \begin{bmatrix} f^2 & & \\ & \ddots & \\ & & f^2 \end{bmatrix} = f^2\mathbf{I} \tag{B.8}$$

Then, a new mode shape vector which proportionate mode shape $\boldsymbol{X}_r$ is defined as Eq. (B.9).

$$\boldsymbol{\phi}_r = \sqrt{\frac{\boldsymbol{X}_r^{\mathrm{T}}\boldsymbol{X}_r^{*}}{2h_r\omega_r}}\boldsymbol{X}_r \tag{B.9}$$

By substitution of Eq. (B.6), Eq. (B.8) and Eq. (B.9) to Eq. (B.3), Eq.(B.3) becomes

$$\begin{aligned}\mathbf{G}_{yy}(\omega) &= \sum_{r=1}^{n}\sum_{s=1}^{n}\left(\frac{\mathbf{R}_r}{j\omega-\lambda_r} + \frac{\mathbf{R}_r^{*}}{j\omega-\lambda_r^{*}}\right)f^2\mathbf{I}\left(\frac{\mathbf{R}_s}{j\omega-\lambda_s} + \frac{\mathbf{R}_s^{*}}{j\omega-\lambda_s^{*}}\right)^{\mathrm{H}} \\ &= f^2\sum_{s=1}^{n}\left(\frac{\boldsymbol{\phi}_r\boldsymbol{\phi}_r^{\mathrm{H}}}{j\omega-\lambda_r} + \frac{\boldsymbol{\phi}_r^{*}\boldsymbol{\phi}_r^{\mathrm{T}}}{j\omega-\lambda_r^{*}} + \frac{\boldsymbol{\phi}_r\boldsymbol{\phi}_r^{\mathrm{H}}}{-j\omega-\lambda_r} + \frac{\boldsymbol{\phi}_r^{*}\boldsymbol{\phi}_r^{\mathrm{T}}}{-j\omega-\lambda_r^{*}}\right)\end{aligned} \tag{B.10}$$

where the first and second terms indicates the positive delay and the third and forth terms indicates the negative delay of the cross correlation function of the $\mathbf{g}_{yy}(t)$ which is defined by

$$\mathbf{g}_{yy}(t) = \boldsymbol{y}(t) \otimes \boldsymbol{y}(t)^{\mathrm{T}} \tag{B.11}$$

where $(\ )\otimes(\ )$ denotes the convolution and $\boldsymbol{y}(t)$ is the output vector in time domain which can be calculated by inverse Fourier transform of the $\boldsymbol{Y}(\omega)$. Then, by extracting only the positive delay components from Eq. (B.11) in time domain and applying Fourier transform again, the positive delay components $\mathbf{G}_{yy}^{+}(\omega)$ can be obtained.

$$\mathbf{G}_{yy}^{+}(\omega) = f^2 \sum_{s=1}^{n} \left(\frac{\boldsymbol{\phi}_r \boldsymbol{\phi}_r^{\mathrm{H}}}{j\omega - \lambda_r} + \frac{\boldsymbol{\phi}_r^{*} \boldsymbol{\phi}_r^{\mathrm{T}}}{j\omega - \lambda_r^{*}} \right) \tag{B.12}$$

Eq. (B.10) denotes the pseudo-FRF which has all information about modal parameters as well as FRF of Eq. (B.7). To satisfy the assumption of Eq. (B.8), it should be performed to calculate the average of several $\mathbf{G}_{yy}^{+}(\omega)$ calculated by using the limited range data extracted from the original data.

Brinker et al showed that FDD method is capable to estimate mode shapes accurately for large scale structures subjected to forced vibration. Their proposed method is to apply singular value decomposition (SVD) to the cross power spectrum matrix of measurements $\mathbf{G}_{yy}^{+}(\omega)$ at the predominant frequencies of the singular spectrum, which can be described as

$$\mathbf{G}_{\boldsymbol{YY}}^{+}(\omega) = \mathbf{U}(\omega)\mathbf{S}^{+}(\omega)\mathbf{U}(\omega)^{\mathrm{H}} \tag{B.13}$$

where $\mathbf{S}^{+}(\omega) \in \mathrm{R}^{n \times n}$ is a diagonal matrix of which elements are singular values arranged in descending order, and $\mathbf{U}(\omega) \in \mathrm{C}^{n \times n}$ is a unitary matrix of which columns indicate the estimation of mode shape vectors $\boldsymbol{\phi}_k$. Around peaks of spectra $\mathbf{S}^{+}(\omega)$ corresponding to k-th mode, the first column $\boldsymbol{u}_1(\omega)$ of the $\mathbf{U}(\omega)$ is the estimated mode shape of k-th mode $\widehat{\boldsymbol{\phi}}_k$.

$$\boldsymbol{u}_1(\omega_k) = \widehat{\boldsymbol{\phi}}_k \tag{B.14}$$

where ω_k is the radian frequency which is corresponding or may close to the eigen radian frequency of k-th mode. Brinker et al noted that the first singular vector $\boldsymbol{u}_1$ always indicates the strongest mode shape accurately in the case where two modes are dominated , while the first two singular vectors $\boldsymbol{u}_1$ and $\boldsymbol{u}_2$ are unbiased estimated mode shapes in the case where the two modes are orthogonal.

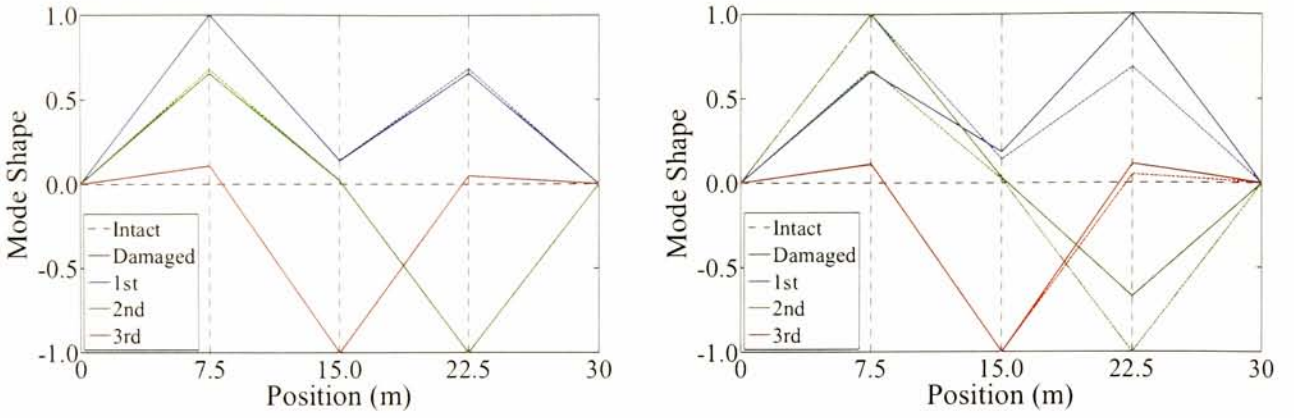

(a) Road Profile = Standard (b) Road Profile = Rough

Fig. B.1.1 Estimated mode shapes by VRA using FDD

B.1.2 Application of FDD method to indirect VO-BHM

Herein, FDD method is applied to STEP 4 of indirect Mode-Shape-based VO-BHM method, instead of SVD. This new method insists in ISE input estimation, deduction of road unevenness, canceling moving effect by Lagrange's interpolation [3] and mode shape estimation by FDD. This method is applied to the same numerical data as the section of 3.4. The detailed properties are shown in Fig. 3.4.1, Fig. 3.4.2 and Table 3.4.1.. The mode shapes estimated by this method is shown in Fig. B.1.1. Solid and dot lines indicate intact and damage cases. Blue green and red lines indicate first, second and third estimated mode shapes, respectively. The decreasing ratio of the flexural stiffness in the figure is 60%. Fig. B.1.1 (a) and (b) show the estimation results in the cases in which the road profile is "Standard" and "Rough", respectively. The accuracies of the estimations are obviously lower than those of the method using SVD. This is caused by the assumption of FDD that the external force is white noise. However, because the estimated mode shapes based on FDD method change after the damage introduced, especially in "Rough "road profile, those mode shapes estimated by FDD can be used as damage identification index, instead of those by SVD.

C. Application of Statistics

C.1 Numerical Verification

C.1.1 Basic Assumptions

The required accuracy for eigen-frequency and mode shape to detect local damage is quite high because they have low sensitivity to the local damage. However, the statistical characteristics of bridge responses may change due to the local damage when vehicles pass over the bridge, because the responses are one of the probability process and change due to the local damage.

Now, dynamic numerical simulation is performed to investigate statistical characteristics of the bridge responses by using models shown in Fig. C.1.1. The properties of the models are shown in Table C.1.1. trailer system consists of two rigid-spring models have two axle and four simple mass spring models have one axle between them runs over the bridge. The bridge span is 30 (m) and the first eigen-frequency is 3.96 (Hz). Four road profiles are generated by Monte Carlo simulation based on the ISO standard [4] shown in Table C.1.1. The spatial frequency function of the road unevenness is

$$S = \frac{a}{\Omega^{\xi} + b^{\xi}} \tag{C.1}$$

First road profile called Standard has the spatial frequency profile of "Extra Good" of ISO standard. Double and Three Times are just double and three times height of Standard. Rough has different spatial frequency profile from Standard. Its profile is "Good" of ISO standard. Standard and Rough are shown in Fig. C.1.2. The objective data time range is from the time at the first axle entering to the time at the last axle leaving. Assumed damage width is 0.20 (m) and 1.00 (m).

To investigate bridge response characteristics, the variance and kurtosis are focused on. As stiffness decreases, the amplitudes of the bridge acceleration responses may be increase. But, this idea is valid when it is global damage, while the bridge damage affects only on local impedance.

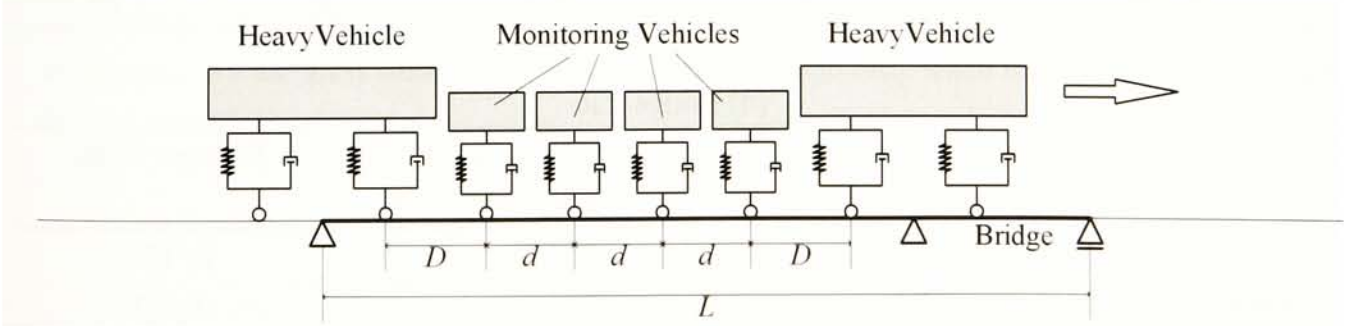

Fig. C.1.1 Vehicle and bridge model

Table C.1.1 Properties for numerical simulation of VBI

(a) Vehicle properties

Heavy vehicle	Mass	(kg)	m_s	10000
	Damping	(kg/s)	$c_{s1},\ c_{s2}$	74000
	Spring Stiffness	(kg/s^2)	$k_{s1},\ k_{s2}$	760000
	Inertia		I	90000
	Length	(m)	$L_1,\ L_2$	3.0
Measuring vehicles	Number		$n+1$	4
	Mass	(kg)	m_i	100
	Damping	(kg/s)	c_i	50
	Spring Stiffness	(kg/s^2)	k_i	3950
	Natural Frequency	(Hz)	$f_V = \sqrt{k_i/m_i}/2\pi$	1.00
	Damping Coefficient		$\xi_V = 2c_i\sqrt{m_i k_i}$	0.30
	Interval Distance	(m)	d	0.50
Common	Run Speed	(m/s)	v	10.0
	Distance	(m)	D	2.5

(b) Bridge properties

Physical parameters			Eigen-frequency for the intact case				
Length	Mass per length	Flexural Stiffness	1st	2nd	3rd	4th	5th
(m)	(kg/m)	(Nm)	(Hz)	(Hz)	(Hz)	(Hz)	(Hz)
L	ρA	EI	f_1	f_2	f_3	f_4	f_5
30.0	3000	1.56×10^{10}	3.96	15.75	34.98	61.15	93.64

(c) Road profile

Name	ISO standard	a	b	ξ
Standard	Extra Good	0.001	0.05	2.00
Double	(2×Standard)	(0.002)	(0.05)	(2.00)
Three Times	(3×Standard)	(0.003)	(0.05)	(2.00)
Rough	Good	0.0098	0.08	1.92

(d) Bridge state

Name	Decreasing Ratio of Flexural Stiffness EI	Damage Location	Damage Width
Damage -20%	20 %	$L/2$	$L/150$
Damage -40%	40 %		$L/30$
Damage -60%	60 %		
Damage -80%	80 %		

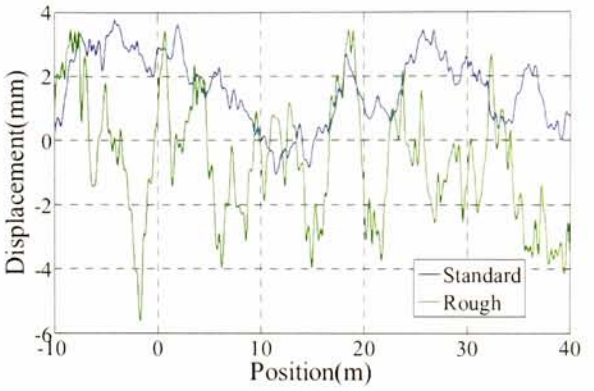

Fig. C.1.2 Road profile

this may lead to local change in the responses. Kurtosis is one of the forth order statistics and is known to be sensitive to peaks of signal. Then, the kurtosis of the signal $\boldsymbol{y}(t)$ is

$$kurt(\boldsymbol{y}(t)) = \frac{\mathrm{E}\{(\boldsymbol{y}(t) - \mathrm{E}\{\boldsymbol{y}(t)\})^4\}}{(\mathrm{V}\{\boldsymbol{y}(t)\})^2} - 3 \tag{C.2}$$

C.1.2 Results and Discussions

Variance and kurtosis of the bridge acceleration responses at the center of the span when the vehicles passes over the bridge are shown in Fig. C.1.3. In this figure, black dot lines denote the values for the intact case without road unevenness. From these figures, variance is much affected by road unevenness and changes of the variance as road unevenness height is larger than the changes as the flexural stiffness EI decreasing. On the other hand, kurtosis is not so sensitive to road unevenness while it is sensitive to local EI decreasing.

These results mean that the variance of bridge response is not appropriate index to detect local damage because of its low robustness to noise such as road unevenness, while the kurtosis of bridge response is appropriate index to local damage. However, it is noted that the kurtosis does not change linearly as damage increases. Moreover, by comparing with "Standard" and "Rough" road in Fig. C.1.3, the kurtosis in "Rough" road case is different from that in "Standard" road case significantly, which means that the kurtosis robustness depends on spatial frequency profile of road unevenness. As for local damage, the responses may change only when the vehicle passes on the damage section.

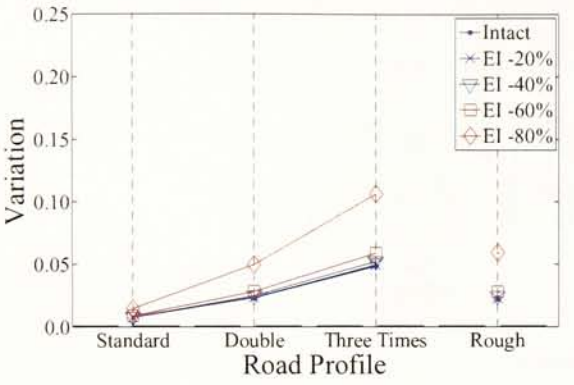

(a) Variance for the damage of 20 (cm) width

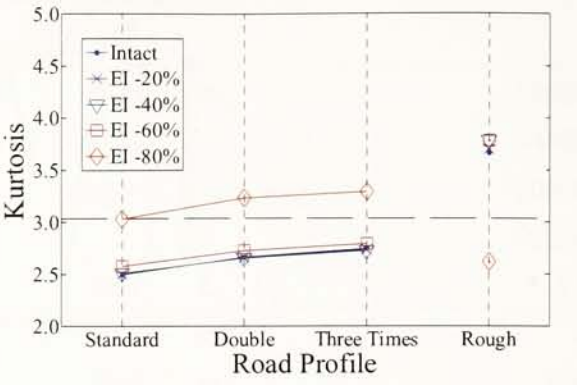

(b) Kurtosis for the damage of 20 (cm) width

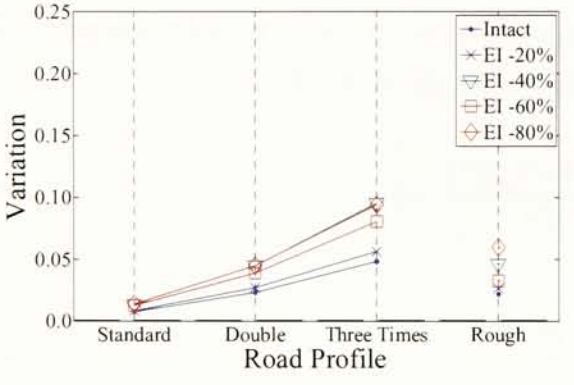

(c) Variance for the damage of 1 (m) width

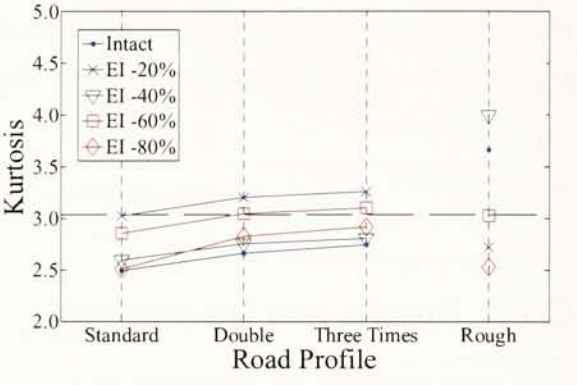

(d) Kurtosis for the damage of 1 (m) width

Fig. C.1.3 Statistics of the bridge acceleration response at the center of the span during the vehicles passing over the bridge

C.2 Experimental Verification

C.2.1 Independent Component Analysis

If local damage affects bridge responses locally, damage signal occurs in limited range of bridge responses. Herein, damage signal is the changes in time histories due to damage. It means that the damage signal has larger amplitude only around damage section. When traffic-induced vibration is focused on, the damage signal becomes larger when travelling loads are passing over the damage section. Thus, the damage signal is expected to be a signal which has peaks locally. This kind of signals has a probability distribution of which skirt is wide. Because kurtosis is very sensitive to height of the skirt of a probability distribution, damage signal can be evaluated by kurtosis.

On the other hand, in Fast-ICA [5], which is one of the most popular independent component analysis (ICA) methods, independent components are evaluated by kurtosis. Because of that, there is probability that damage signals can be extracted by Fast-ICA method.

In this verification, Fast-ICA method is applied to bridge acceleration responses measured at the same location to extract damage signal at the location. The bridge acceleration responses measured on the actual bridge are used. The detail of measurements are shown in Chapter 5.

C.2.2 Results and Discussions

Fig. C.2.1 shows the independent component of bridge responses. ICA is applied to bridge responses measured three times at same location. The horizontal coordinate denotes the position of the vehicle front axle. Dot lines indicate the measuring points. All independent components are normalized by making their norm 1.0. Fig. C.2.1 (a) shows the independent components of bridge acceleration responses measured three times at the center of the span. The kurtoses of transformed signals do not vary well. Fig. C.2.1 (b) also shows ICA results for the measuring point 4, which is closer to the damage member. At this case, the kurtosis of one independent component becomes 25.8 which is distinctively larger after damage than before. The effect of damage could appear spatially.

Then, Fig. C.2.2 shows the kurtoses of independent components for each location. The values tend to be larger nearby the damage section. These results mean that the damage signal occurs in spatially limited locations.

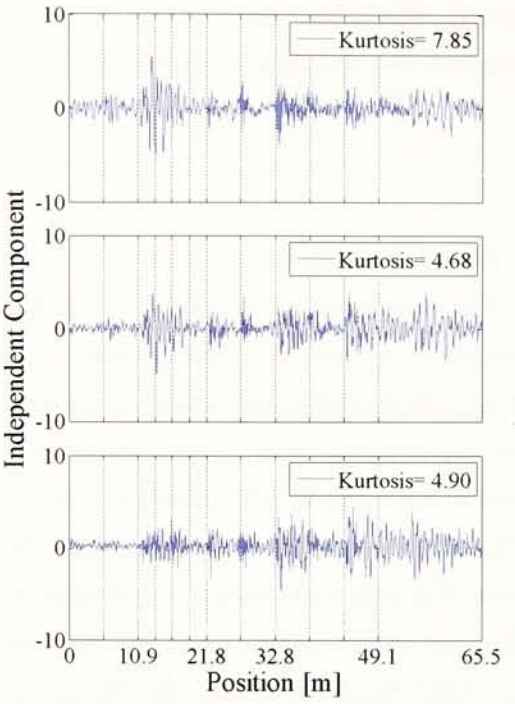

(a-1) Intact case

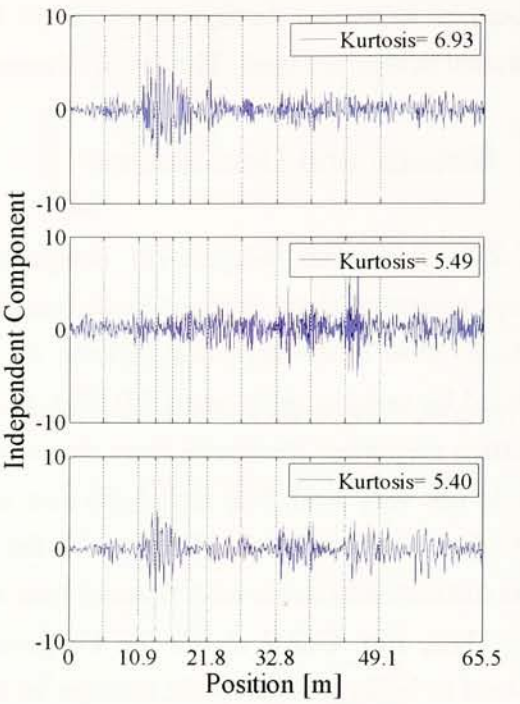

(a-2) Damage case

(a) At the No.8 point (the center of the span)

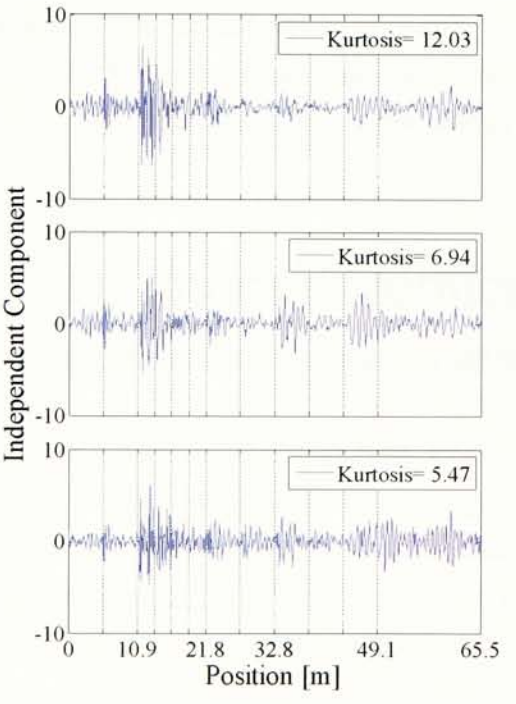

(b-1) Intact case

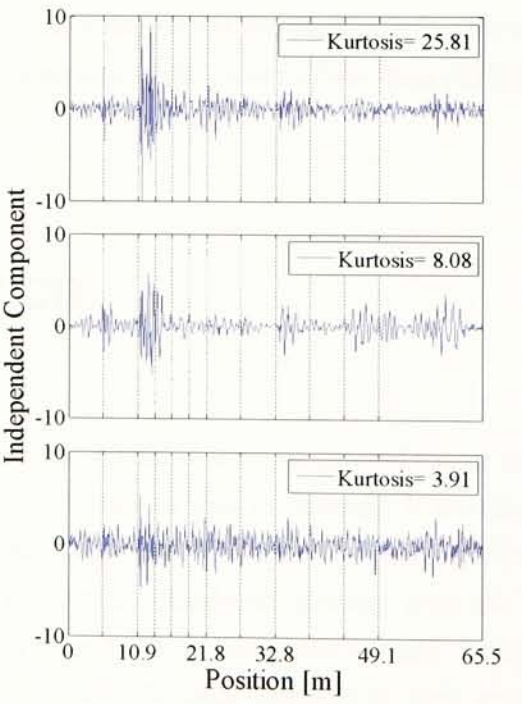

(b-2) Damage case

(b) At the No.4 point (close to damage member)

Fig. C.2.1 Kurtosis of independent components of the bridge responses which are spatially synchronized by the vehicle position

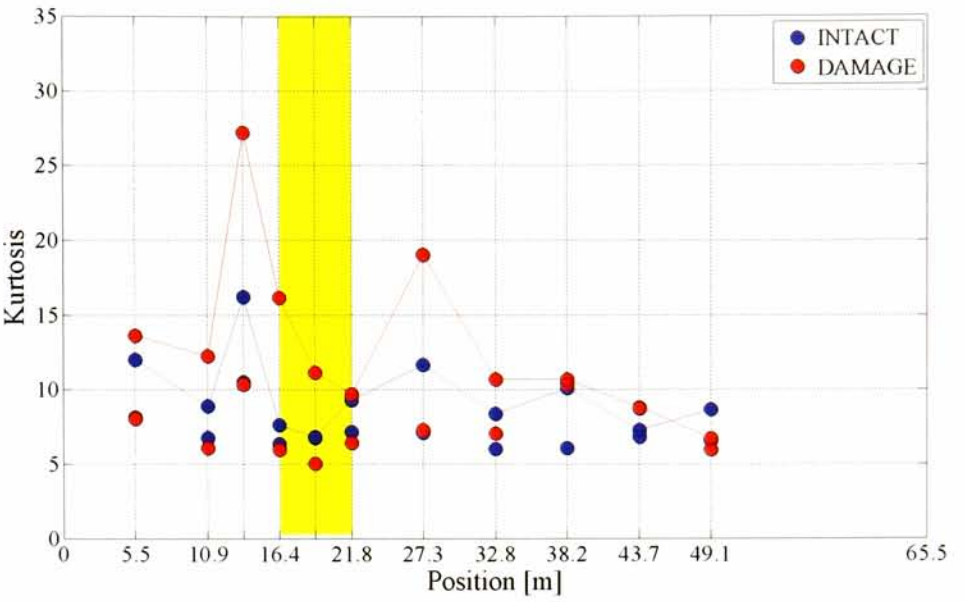

(a) 20 (km/h)

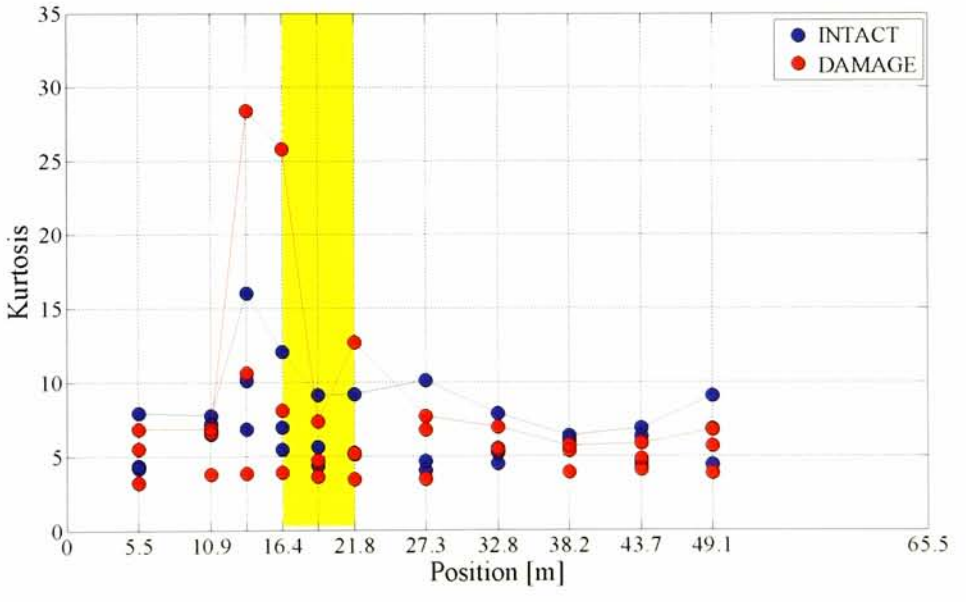

(b) 40 (km/h)

Fig. C.2.2 Kurtosis of independent components of the bridge responses at each sensors position in the cases where the heavy vehicle runs

Reference

[1] Brinker, R., Zhang, L. and Andersen, P.: Modal identification of output-only systems using frequency domain decomposition, Smart Materials and Structures, Vol.10, pp.441-445, 2001.

[2] Nagae, N., Watase, M. and Tamaki, T.: Operational modal analysis using cross correlation function, Journal of Structural Engineering. A, JSCE, Vol.57A, pp.232-241, 2011.

[3] Chakrabarti, A. and Hamsapriye: Derivation of the errors involved in interpolation and their application to numerical quadrature formulae, Journal of Computational and Applied Mathematics, Vol.98, pp.59-68, 1998.

[4] Kawatani, M., Kobayashi, Y. and Takamori, K.: Nonstationary random analysis with coupling vibration of bending and torsion of simple girder bridges under moving vehicles, Proc. of JSCE, Vol.570, pp.231-238, 1997.

[5] Yamamoto, K., Isemoto, R., Oshima, Y., Kim, C.W. and Sugiura, K.: Evaluation of acceleration responses in a steel truss bridge and passing vehicle before and after member's breakage, Journal of Structural Engineering, JSCE, Vol.58A, pp.180-193, 2012.